NAVAL POSTGRADUATE SCHOOL

MONTEREY, CALIFORNIA

THESIS

FORCE PROTECTION VIA UGV-UAV COLLABORATION: DEVELOPMENT OF CONTROL LAW FOR VISION BASED TARGET TRACKING ON SUAV

by

Lee Shay Liang

December 2007

Thesis Co-Advisors: Vladimir N. Dobrokhodov
                             Richard Harkins

Approved for public release; distribution is unlimited

THIS PAGE INTENTIONALLY LEFT BLANK

REPORT DOCUMENTATION PAGE		*Form Approved OMB No. 0704-0188*
Public reporting burden for this collection of information is estimated to average 1 hour per response, including the time for reviewing instruction, searching existing data sources, gathering and maintaining the data needed, and completing and reviewing the collection of information. Send comments regarding this burden estimate or any other aspect of this collection of information, including suggestions for reducing this burden, to Washington headquarters Services, Directorate for Information Operations and Reports, 1215 Jefferson Davis Highway, Suite 1204, Arlington, VA 22202-4302, and to the Office of Management and Budget, Paperwork Reduction Project (0704-0188) Washington DC 20503.		
1. AGENCY USE ONLY *(Leave blank)*	**2. REPORT DATE** December 2007	**3. REPORT TYPE AND DATES COVERED** Master's Thesis
4. TITLE AND SUBTITLE Force Protection via UGV-UAV Collaboration: Development of Control Law for Vision Based Target Tracking on SUAV		**5. FUNDING NUMBERS**
6. AUTHOR(S) Lee Shay Liang		
7. PERFORMING ORGANIZATION NAME(S) AND ADDRESS(ES) Naval Postgraduate School Monterey, CA 93943-5000		**8. PERFORMING ORGANIZATION REPORT NUMBER**
9. SPONSORING /MONITORING AGENCY NAME(S) AND ADDRESS(ES) N/A		**10. SPONSORING/MONITORING AGENCY REPORT NUMBER**
11. SUPPLEMENTARY NOTES The views expressed in this thesis are those of the author and do not reflect the official policy or position of the Department of Defense or the U.S. Government.		
12a. DISTRIBUTION / AVAILABILITY STATEMENT Approved for public release; distribution is unlimited		**12b. DISTRIBUTION CODE**

13. ABSTRACT (maximum 200 words)

The Naval Postgraduate School UAV Laboratory developed a Small Unmanned Aerial Vehicle (SUAV) equipped with a Vision Based Target Tracking (VBTT) system as part of its Tactical Network Topology field experimentation program. The VBTT system includes a miniaturized gimbaled camera that allows autonomous target tracking while providing concurrent estimates of target motion including its position, velocity and heading. Using the current control law, the speed of convergence and the range-holding performance have been found to deteriorate as target speed increases. The aim of this thesis is to elaborate on the existing control law in order to achieve better performance. Employing a new and novel algorithm from the Lyapunov Stability Analysis, for the purpose of adjusting the feedback gain, is proposed in this thesis; to that end a control law with adjustable gain can be easily implemented based on UAV-Target kinematics to optimize UAV performance. The performance of the newly adjustable gain control law is tested in both SIMULINK model and Hardware-In-the-Loop simulations to verify any improvement in performance over the constant gain control law. Principal results offer improved SUAV target-tracking performance with no additional hardware costs.

14. SUBJECT TERMS SUAV, Lyapunov stability, Control, Vision Based Target Tracking, Hardware-In-Loop, Piccolo, UAV, Unmanned Aerial Vehicle		**15. NUMBER OF PAGES** 107
		16. PRICE CODE
17. SECURITY CLASSIFICATION OF REPORT Unclassified	**18. SECURITY CLASSIFICATION OF THIS PAGE** Unclassified	**19. SECURITY CLASSIFICATION OF ABSTRACT** Unclassified	**20. LIMITATION OF ABSTRACT** UU

THIS PAGE INTENTIONALLY LEFT BLANK

Approved for public release; distribution is unlimited

FORCE PROTECTION VIA UGV-UAV COLLABORATION: DEVELOPMENT OF CONTROL LAW FOR VISION BASED TARGET TRACKING ON SUAV

Shay Liang, Lee
Defence Science and Technology Agency (Singapore)
B.Eng (Mechanical Engineering), National University of Singapore, 2001

Submitted in partial fulfillment of the
requirements for the degree of

MASTER OF SCIENCE IN MECHANICAL ENGINEERING
and
MASTER OF SCIENCE IN APPLIED PHYSICS

from the

NAVAL POSTGRADUATE SCHOOL
December 2007

Author: Lee Shay Liang

Approved by: Professor Vladimir N. Dobrokhodov
                 Thesis Advisor

                 Professor Richard Harkins
                 Thesis Co-Advisor

                 Professor Anthony Healy
                 Chairman, Department of Mechanical and Astronautical
                 Engineering

                 Professor James Luscombe
                 Chairman, Department of Physics

THIS PAGE INTENTIONALLY LEFT BLANK

ABSTRACT

The Naval Postgraduate School UAV Laboratory developed a Small Unmanned Aerial Vehicle (SUAV) equipped with a Vision Based Target Tracking (VBTT) system as part of its Tactical Network Topology field experimentation program. The VBTT system includes a miniaturized gimbaled camera that allows autonomous target tracking while providing concurrent estimates of target motion including its position, velocity and heading. Using the current control law, the speed of convergence and the range-holding performance have been found to deteriorate as target speed increases. The aim of this thesis is to elaborate on the existing control law in order to achieve better performance. Employing a new and novel algorithm from the Lyapunov Stability Analysis, for the purpose of adjusting the feedback gain, is proposed in this thesis; to that end a control law with adjustable gain can be easily implemented based on UAV-Target kinematics to optimize UAV performance. The performance of the newly adjustable gain control law is tested in both SIMULINK model and Hardware-In-the-Loop simulations to verify any improvement in performance over the constant gain control law. Principal results offer improved SUAV target-tracking performance with no additional hardware costs.

THIS PAGE INTENTIONALLY LEFT BLANK

TABLE OF CONTENTS

THIS PAGE INTENTIONALLY LEFT BLANK

LIST OF FIGURES

LIST OF TABLES

THIS PAGE INTENTIONALLY LEFT BLANK

ACKNOWLEDGMENTS

THIS PAGE INTENTIONALLY LEFT BLANK

I.   INTRODUCTION

A.   BACKGROUND

The proliferation of unmanned system technology in military and homeland security applications has accelerated in the past decade. The success of UAV and UGV use in every theatre of operations further cements the significance of an unmanned system technology application in modern warfare. During the 1991 Gulf War, Unmanned Aerial Vehicles (UAV) were deployed as reconnaissance units which sought targets for naval guns. The War on Terror in Afghanistan and Iraq has seen the role of the UAV transition from a reconnaissance vehicle to an Unmanned Combat Air Vehicle where the UAV is armed with Hellfire missile [1].

Unmanned Ground Vehicles (UGV), capable of combating against Improvised Explosive Devices (IEDs), are also increasingly deployed in Iraq [2]. These remote-controlled ground vehicles have the ability to probe dubious objects and detonate any suspected IEDs. Unmanned aerial vehicles and unmanned ground vehicles are, therefore, critical assets and effective force multipliers in today's battlefield and future network-centric warfare. Due to the complementary capabilities of the UAV and UGV, collaboration of both unmanned systems expands the tactical capabilities of the integrated system in order to execute complex missions.

The UGV has a limited Field-Of-View (FOV) and this leads to the UGV being less responsive to threats beyond its FOV; however with its aerial superiority, the UAV has a superior FOV. By incorporating wireless communication between the UAV and UGV, the UGV is able to utilize the reconnaissance information provided by the UAV to speed up the UGV's response to approaching targets. One key application of the integration of both unmanned platforms is the ability to have unmanned force protection for ground troops operating in Iraq and Afghanistan [3]. Ongoing research at the Naval

Postgraduate School's (NPS) Physics Department arms the UGV with shaped charges that can incapacitate soft skin vehicles and detonate suspected IEDs. Via aerial reconnaissance with onboard sensors, the UAV would be able to detect threats such as armored vehicles or anomalies such as suspected insurgent movements, minefields or suspected IEDs. The UAV would then dispatch the UGV to the area in order to neutralize the threat.

B.   PROBLEM STATEMENT

Many large-scale tactical UAVs have evolved towards multi-role and multi-mission platforms. However due to the high acquisition cost, a limited number of UAVs are made available to support day-to-day troop operations in Iraq. Driven by technological advancements in miniature autopilots, networking and robotics, a low-cost Small UAV (SUAV) may be constructed using low cost Commercial-Off-the-Shelf (COTS) components to achieve the same capabilities. Therefore, the collaboration of SUAV and UGV offers unmanned force protection at a lower cost, yet provides an equally effective solution.

The NPS UAV laboratory has developed a SUAV equipped with a COTS Vision Based Target Tracking (VBTT) system as part of the Tactical Network Topology field experiment program. The VBTT onboard the SUAV includes a miniaturized gimbaled camera that is capable of autonomous target tracking. The control concept of the SUAV is illustrated in Figure 1 below. The developed control guarantees that the SUAV is autonomously guided such that the target remains constantly in the FOV of the gimbaled camera [4]. This results in two coordinated motions: SUAV motion relative to target and motion of gimbaled camera relative to the target. Previous research has already addressed the issue of devising a coordinated camera and a UAV controlled law. The control algorithm for both gimbaled camera and UAV was developed, and preliminary results on the robustness of the control were obtained [5]. This thesis concentrates on further analysis of the stability bounds for the case of actively moving targets.
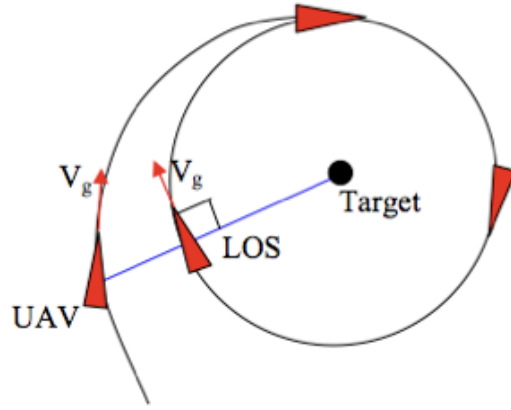
Figure 1.   Illustration of Control Algorithm [From 4]

C.   SCOPE

Previous thesis research showed that the control law stated below in equation (1) showed improved robustness and efficiency. However for constant feedback gain, the speed of convergence and the range holding performance deteriorate as v_t/v_g increases. Therefore, the objective of the research efforts in this thesis is to elaborate on the existing control law in order to improve the performance of the control law when v_t/v_g increases.

$$\dot{\psi} = \frac{v_g}{\rho_d}\cos\eta - k_1\eta \qquad\qquad (1)$$

$$\dot{\psi}_h = k_1\eta + k_2\varepsilon$$

$\eta = $ Navigation angle error $\dot{\psi} = $ UAV turn rate in inertial frame

$\varepsilon = $ Line-of-sight error $\dot{\psi}_h = $ Camera turn rate in UAV frame

$v_g = $ SUAV ground speed $\rho_d = $ Desired range

$k_1, k_2 = $ Gain constants

3

Since constant value for Gain parameters has performance limitations, this thesis aims to improve the performance of the control law by using an adjustable gain that factors UAV and target kinematics into the control law. The scope of work in this thesis includes testing the performance of adjustable gain over constant gain.

D.   THESIS OUTLINE

In Chapter II, it is shown how the feedback control gain is derived from the Lyapunov Stability analysis that guarantees a bounded solution. It is also shown how adjustable gain v_{adj} for the UAV guidance varies with UAV and target kinematics, namely v_g, v_t and ρ_d. The adjustable gain can be chosen to extend the region of attraction. Consequently the dynamics of v_{adj} as a function of v_g, v_t and ρ_d are analyzed.

Chapter III illustrates the implementation of the control algorithm with adjustable gain in both the SIMULINK model of the SUAV and the Hardware-In-the-Loop (HIL) simulation. The objective of running the SIMULINK model is to predict the performance of the newly developed control law while HIL simulation validates the results of SIMULINK model for physical SUAV. The performance of the modified control algorithm is then compared with the previous control algorithm and initial results of 5. An analysis of the results is presented in this chapter.

Chapter IV presents the conclusion of the research efforts in this thesis and recommendations for future research.

II. DEVELOPMENT OF CONTROL LAW

A. SUAV CONTROL SYSTEM MODEL

Assuming that the autopilot module is capable of maintaining the UAV at level flight, the kinematics model for the UAV and target may be simplified into a two-dimensional problem. The two-dimensional kinematics model is shown in Figure 2 below.
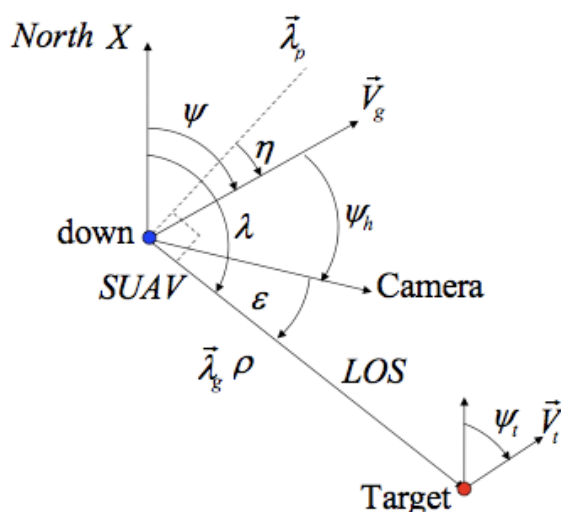
η	= navigation error	ψ	= UAV heading in inertia frame
ε	= camera LOS Pan error	ψ_t	= Target heading in inertia frame
λ	= LOS angle in inertia frame	ψ_h	= Camera angle in UAV body frame
$\vec{\lambda}_g$	= LOS vector	$\vec{V}_g$	= SUAV ground speed in inertia frame
$\vec{\lambda}_p$	= Normal to LOS vector	$\vec{V}_t$	= Target ground speed in inertia frame

Figure 2.   Simplified 2-D UAV-target kinematics model [From 5]

It is shown in [4] that the kinematics of the tracking problem is given by equation [2]. The angles η and ε denote the UAV guidance error and Gimbaled camera control errors; therefore, the control objective is to drive η and ε using the UAV turn rate $\dot{\psi}$ and $\dot{\psi}_h$ as control inputs.

$$\dot{\eta} = -\frac{V_g \cos \eta - V_t \cos\left(\psi_t - (\psi - \eta)\right)}{\rho} + \dot{\psi} \tag{2}$$

$$\dot{\varepsilon} = \frac{v_g \cos \eta - v_t \cos\left(\psi_t - (\psi - \eta)\right)}{\rho} - \dot{\psi} - \dot{\psi}_h$$

$$\dot{\rho} = -v_g \sin \eta + v_t \sin\left(\dot{\psi} - (\psi - \eta)\right)$$

By applying feedback control as described in equation (1) to the two-d kinematics model, the control system equations are given in equation (3)[1].

$$\dot{\hat{\eta}} = -v_g \rho_e \cos\left(\hat{\eta}\rho_d\right)/\rho_d - k_1 \hat{\eta}\rho_d + v_t \bar{\rho} \cos\left(\hat{\eta}\rho_d - \psi_r\right)/\rho_d \tag{3}$$

$$\dot{\rho}_e = \bar{\rho}^2 v_g \sin\left(\hat{\eta}\rho_d\right) - v_t \sin\left(\hat{\eta}\rho_d - \psi_r\right)\bar{\rho}^2$$

$$\dot{\varepsilon} = v_g \rho_e \cos\left(\hat{\eta}\rho_d\right) - k_2 \varepsilon - v_t \cos\left(\hat{\eta}\rho_d - \psi_r\right)\bar{\rho}$$

where ψ_r represents the relative heading $\psi - \psi_t$ with respect to the target.

It is noted [4] that Equation (2) may be separated into two sub-systems.

<u>Sub-system I:</u>

$$\dot{x} = \begin{bmatrix} \dot{\hat{\eta}} \\ \dot{\rho}_e \end{bmatrix} = \begin{bmatrix} -v_g \rho_e \cos\left(\hat{\eta}\rho_d\right)/\rho_d - k_1 \hat{\eta}\rho_d + v_t \bar{\rho} \cos\left(\hat{\eta}\rho_d - \psi_r\right)/\rho_d \\ \bar{\rho}^2 v_g \sin\left(\hat{\eta}\rho_d\right) - v_t \sin\left(\hat{\eta}\rho_d - \psi_r\right)\bar{\rho}^2 \end{bmatrix} \tag{4}$$

<u>Subsystem II:</u>

$$\dot{\varepsilon} = v_g \rho_e \cos\left(\hat{\eta}\rho_d\right) - k_2 \varepsilon - v_t \cos\left(\hat{\eta}\rho_d - \psi_r\right)\bar{\rho}$$

Sub-system I depicts the system dynamics that drive the UAV such that the ground speed vector v_g of the UAV is perpendicular to the Line of Sight, i.e. $\hat{\eta} = 0$ and $\rho_e = 0$. Thus ensuring the stability of sub-system I guarantees that the UAV orbits above the target, as illustrated in Figure 1.

---

[1] The derivation of the control system equations is given from equation (3) and equation (4) in Reference 5.

B. LYAPUNOV STABILITY ANALYSIS

1. Stability Analysis for Stationary Target

From equation (3), it is obvious that sub-system I is a highly non-linear system. The Lyapunov function for the non-linear system may be derived from the linearization of Sub-system I. Using Taylor Expansion, the linearized model is:

$$\dot{x} = \begin{bmatrix} -k_1 & -v_g / \rho_d \\ v_g / \rho_d & 0 \end{bmatrix} x = A_o x \tag{5}$$

Solving for P from the algebraic Lyapunov Stability criterion[2],

$$P = \begin{bmatrix} \dfrac{1}{k_1} & \dfrac{\rho_d}{2v_g} \\ \dfrac{\rho_d}{2v_g} & \dfrac{k_1^2 \rho_d^2 + 2v_g^2}{2k_1 v_g^2} \end{bmatrix} \tag{6}$$

A candidate Lyapunov function [6] is given by $V = x^T P x$.

Re-expressing Subsystem I in terms of the linearized model,

$$\dot{x} = A_o x + \Delta f(x) \quad \text{where} \quad \Delta f(x) = f(x) - A_o x \tag{7}$$

By substituting equation (7) into V and taking time derivative,

$$\dot{V}(x) = -x^T x + 2\Delta f^T(x) P x$$

By substituting equation (3) into $\Delta f(x)$ yields:

$$\Delta f(x) = \begin{bmatrix} v_g \rho_e \left(1 - \cos(\hat{\eta}\rho_d)\right) / \rho_d + v_t \bar{\rho} \cos(\hat{\eta}\rho_d - \psi_r) / \rho_d \\ v_g \bar{\rho}^2 \sin(\hat{\eta}\rho_d) - v_t \sin(\hat{\eta}\rho_d - \psi_r) \bar{\rho}^2 - \dfrac{v_g}{\rho_d}\hat{\eta} \end{bmatrix} \tag{8}$$

---

2 Algebraic Lyapunov Stability Criterion is given by $A_o^T P + P A_o = -I$

Define a compact set $\Omega_c = \left\{ \xi : \xi^T P \xi \leq c^2 ; c = \dfrac{c_\rho^2}{\rho_d^2} \lambda_{\min}(P) \text{ for } 0 < c_\rho < 1 \right\}$

From matrix property, $\lambda_{\min}(P)\|x\|^2 \leq x^T P x \leq \lambda_{\max}(P)\|x\|^2$

$$\|x\| \leq \left(\frac{c_\rho}{\rho_d}\right)$$

$$\|\rho_e\| = \left\|\frac{1}{\rho} - \frac{1}{\rho_d}\right\| \leq \left(\frac{c_\rho}{\rho_d}\right)$$

$$\left(\frac{1-c_\rho}{\rho_d}\right)^2 \leq \bar{\rho}^2 \leq \left(\frac{1+c_\rho}{\rho_d}\right)^2 \tag{9}$$

The target is assumed to be stationary $(v_t = 0)$,

$$\Delta f(x) = \begin{bmatrix} v_g \rho_e (1-\cos(\eta))/\rho_d \\ v_g \bar{\rho}^2 \sin(\eta) - \dfrac{v_g}{\rho_d^2}\eta \end{bmatrix} = \begin{bmatrix} \dfrac{2 v_g \rho_e \sin^2\left(\dfrac{\eta}{2}\right)}{\rho_d} \\ v_g \bar{\rho}^2 \sin(\eta) - \dfrac{v_g}{\rho_d^2}\eta \end{bmatrix}$$

$$\|\Delta f(x)\|^2 = \left(\frac{v_g}{\rho_d^2}\right)^2 \left[\left(2\rho_d \rho_e \sin^2\left(\frac{\eta}{2}\right)\right)^2 + \left(\rho_d^2 \bar{\rho}^2 \sin\eta - \eta\right)^2 \right] \tag{10}$$

Using small angle approximation and equation (9),

$$\|\Delta f(x)\|^2 \leq \left(\frac{v_g}{\rho_d^2}\right)^2 \left[c_\rho^2 \left(\frac{\eta^2}{2}\right)^2 + \left(c_\rho\left(2+c_\rho\right)\eta + |\sin\eta - \eta|\right)^2 \right] \tag{11}$$

For small η, $|\sin\eta - \eta| \leq \dfrac{|\eta|^3}{6}$ \qquad (12)

From $\|x\| \leq \left(\dfrac{c_\rho}{\rho_d}\right)$, $\eta^2 \leq c_\rho^2$ \qquad (13)

Substituting equation (13) & (12) into (11) and after simplification,

$$\left\|\Delta f(x)\right\|^2 \le c_\rho^2 \left(\frac{v_g}{\rho_d}\right)^2 \left[\left(\frac{c_\rho^2}{4}\right) + \left(2 + c_\rho + \frac{c_\rho}{6}\right)^2\right]\hat{\eta}^2$$

$$\left\|\Delta f(x)\right\| \le c_\rho \left(\frac{v_g}{\rho_d}\right)\sqrt{\left(\frac{c_\rho^2}{4}\right) + \left(2 + c_\rho + \frac{c_\rho}{6}\right)^2}\ \|x\| \tag{14}$$

$$\left\|\Delta f(x)\right\| \le \gamma \left(\frac{v_g}{\rho_d}\right)\|x\| \tag{15}$$

Substituting equation (15) into $\dot{V}(x)$

$$\dot{V}(x) \le -x^T x + 2\left\|\Delta f(x)\right\|\|P\|\|x\|$$

$$\dot{V}(x) \le -\left[1 - 2\gamma\left(\frac{v_g}{\rho_d}\right)\|P\|\right]\|x\|^2 \tag{16}$$

From the Lyapunov Stability Criterion, $\dot{V}(x) < 0$ only if $\|P\| < \dfrac{\rho_d}{2\gamma v_g}$

$$\therefore \lambda_{\max}(P) < \frac{\rho_d}{2\gamma v_g} \tag{17}$$

2.   Stability Analysis for Moving Target

The stability of Subsystem I for a moving target can be analyzed in an approach similar to that of a stationary target. For most ground moving targets, it can be reasonably assumed that the target speed is bounded such that the least upper bound of target velocity is lower than $v_{t,\max}$.

Re-arranging equation (8),

$$\Delta f(x) = \begin{bmatrix} v_g \rho_e \left(1 - \cos\left(\hat{\eta}\rho_d\right)\right)/\rho_d \\ v_g \bar{\rho}^2 \sin\left(\hat{\eta}\rho_d\right) - \dfrac{v_g}{\rho_d}\hat{\eta} \end{bmatrix} + \begin{bmatrix} v_t \bar{\rho} \cos\left(\hat{\eta}\rho_d - \psi_r\right)/\rho_d \\ -v_t \sin\left(\hat{\eta}\rho_d - \psi_r\right)\bar{\rho}^2 \end{bmatrix} \tag{18}$$

Substituting equation (15) into equation (18),

9

$$\left\|\Delta f\left(x\right)\right\| \leq \gamma \left(\frac{v_g}{\rho_d}\right)\left\|x\right\| + \sqrt{\frac{\left(v_t\bar{\rho}\cos\left(\hat{\eta}\rho_d - \psi_r\right)\right)^2}{\rho_d^2} + \left(v_t\sin\left(\hat{\eta}\rho_d - \psi_r\right)\bar{\rho}^2\right)^2}$$

Since $\left|\cos\left(\hat{\eta}\rho_d - \psi_r\right)\right| \leq 1$ and $\left|\sin\left(\hat{\eta}\rho_d - \psi_r\right)\right| \leq 1$

$$\left\|\Delta f\left(x\right)\right\| \leq \gamma \left(\frac{v_g}{\rho_d}\right)\left\|x\right\| + \bar{\rho}\sqrt{\left(\frac{v_t}{\rho_d}\right)^2 + \left(v_t\right)^2}$$

From equation (9), $\bar{\rho} \leq \left(\frac{1+c_\rho}{\rho_d}\right)$

$$\left\|\Delta f\left(x\right)\right\| \leq \gamma \left(\frac{v_g}{\rho_d}\right)\left\|x\right\| + v_{t,\max}\left(\frac{1+c_\rho}{\rho_d^2}\right)\sqrt{1 + \rho_d^2\bar{\rho}^2}$$

$$\left\|\Delta f\left(x\right)\right\| \leq \gamma \left(\frac{v_g}{\rho_d}\right)\left\|x\right\| + v_{t,\max}\left(\frac{1+c_\rho}{\rho_d^2}\right)\sqrt{1 + \left(1 + c_\rho\right)^2} \tag{19}$$

Substituting equation (19) into $\dot{V}\left(x\right)$

$$\dot{v}\left(x\right) \leq -x^T x + 2\left\|\Delta f\left(x\right)\right\|\left\|P\right\|\left\|x\right\|$$

$$\dot{v}\left(x\right) \leq -\left[1 - 2\gamma\left\|P\right\|\left(\frac{v_g}{\rho_d}\right)\right]\left\|x\right\|^2 + \frac{2v_{t,\max}\left(1+c_\rho\right)}{\rho_d^2}\sqrt{1 + \left(1 + c_\rho\right)^2}\left\|P\right\|\left\|x\right\|$$

$$\dot{v}\left(x\right) \leq -\left\|x\right\|\left\{\left[1 - 2\gamma\left\|P\right\|\left(\frac{v_g}{\rho_d}\right)\right]\left\|x\right\| - \frac{2v_{t,\max}\left(1+c_\rho\right)}{\rho_d^2}\sqrt{1 + \left(1 + c_\rho\right)^2}\left\|P\right\|\right\}$$

The Lyapunov stability criteria requires $\dot{V}\left(x\right) < 0$ for asymptotic stability.

$$\left\{\left[1 - 2\gamma\left\|P\right\|\left(\frac{v_g}{\rho_d}\right)\right]\left\|x\right\| - \frac{2v_{t,\max}\left(1+c_\rho\right)}{\rho_d^2}\sqrt{1 + \left(1 + c_\rho\right)^2}\left\|P\right\|\right\} \geq 0$$

$$\|x\| \geq \frac{\dfrac{2v_{t,\max}\left(1+c_\rho\right)}{\rho_d^2}\sqrt{1+\left(1+c_\rho\right)^2}\,\|P\|}{1-2\gamma\|P\|\left(\dfrac{v_g}{\rho_d}\right)}$$

From stability analysis for a stationary target (Page 7), $\|x\| \leq \left(\dfrac{c_\rho}{\rho_d}\right)$

$$c_\rho - \frac{2v_{t,\max}\left(1+c_\rho\right)\sqrt{1+\left(1+c_\rho\right)^2}\,\|P\|}{\rho_d - 2\gamma v_g \|P\|} \geq 0 \qquad (20)$$

Suppose the condition given by equation (20) is valid for all $V_t : \sup\limits_{t\geq 0}|V_t| \leq V_{t,\max}$, $v_g \in \left[v_{g,\min}, v_{g,\max}\right]$ and $\rho_d \in \left[\rho_{d,\min}, \rho_{d,\max}\right]$, Subsystem 1 is ultimately bounded for any $x(0) \ni \Omega_c$. Therefore Ω_c defines the region of attraction (R_A) for subsystem I and c_ρ is a measure for R_A . The larger the region of attraction R_A , the larger is the space that would allow a SUAV to converge to the stable solution.

C.   DERIVING OPTIMAL GAIN FROM STABILITY CRITERION

Two new parameters e_1 and e_2 are introduced below in equation (21) and equation (22) to determine the appropriate values of gain k_1 for both stationary target and moving target cases. From the previous stability analysis, it is evident that the regions where $e_1 > 0$ and $e_2 > 0$ are the regions of stability. Figure 3 and Figure 4 illustrate the dependency of e_1 on k_1 and c_ρ for known UAV-Target kinematics

$$e_1 = \frac{\rho_d}{2\gamma v_g} - \lambda_{\max}(P) \qquad (21)$$

$$e_2 = c_\rho - \frac{2v_{t,\max}\left(1+c_\rho\right)\sqrt{1+\left(1+c_\rho\right)^2}\,\|P\|}{\rho_d - 2\gamma v_g \|P\|} \qquad (22)$$
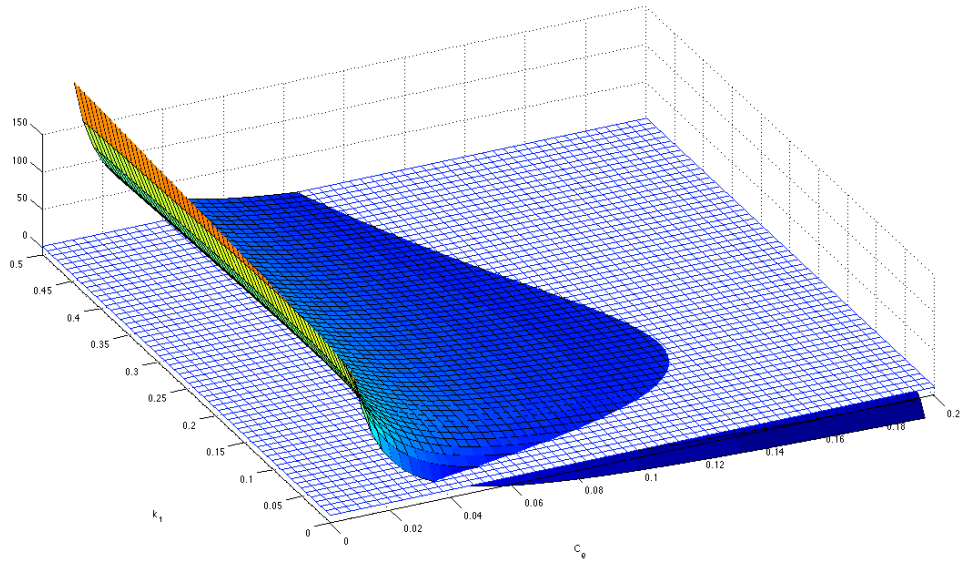
Figure 3. Stationary Target case, $e_1 = f(k_1, c_\rho)$ for $v_g = 10$, $\rho_d = 100$
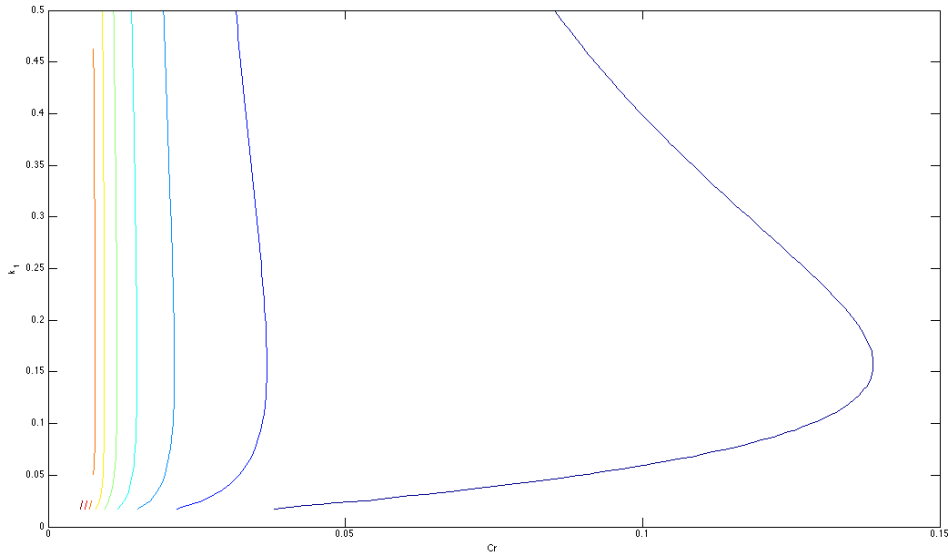
Figure 4. Stationary Target contour, $e_1 = f(k_1, c_\rho)$ for $v_g = 10$, $\rho_d = 100$

One observation from Figure 3 is the intersection of surface e_1 with the plane $e_1 \approx 0$, within the stable region ($e_1 > 0$) yields an optimal choice of k_1 that

12

maximizes c_ρ, i.e., maximizes the region of attraction R_A. A second observation from Figure 4 suggests that the optimal choice of k_1 remains unchanged when the surface e_1 intersects with any plane $e_1 = \text{constant}$. From both observations, it is postulated that an optimal k_1 exists from the Lyapunov stability analysis. Successive runs of e_1 with varying speeds of UAV further confirm the existence of optimal k_1.

In many practical military missions, foe targets more consistently keep maneuvering or evading than remaining stationary. An optimal feedback gain k_1 is defined by analyzing the numerical results derived from the Lyapunov Stability Analysis as applied to the moving target scenario. The optimality of the feedback gain is defined by the extension R_A. Figure 5 and Figure 6 below illustrate the dependency of e_2 on k_1 and c_ρ based on equation (22) for known UAV-Target kinematics. The e_2 surface figures are obtained for the following parameters: $v_g = 10$, $\rho_d = 100$ and $v_t = 10$.
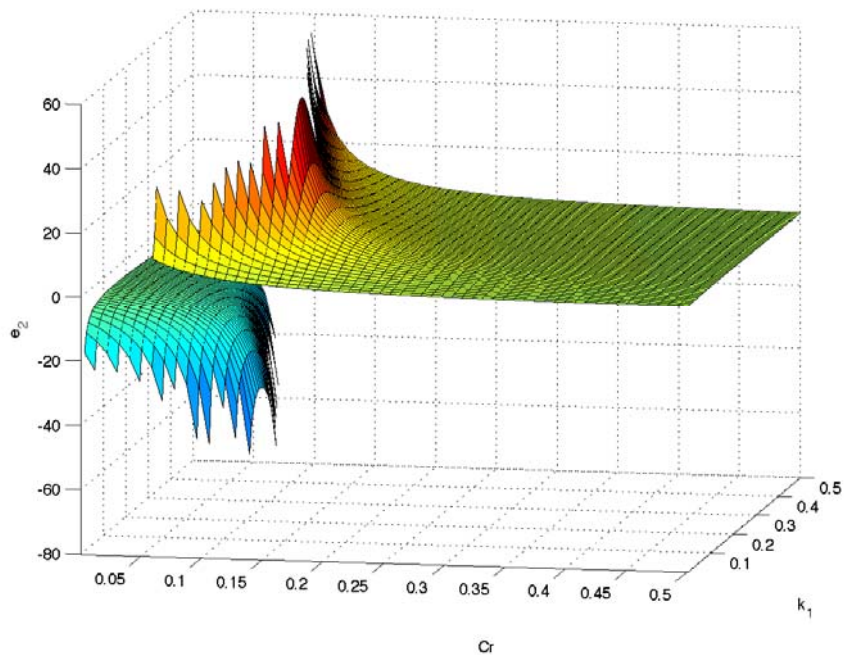
Figure 5.   Moving Target case, $e_2 = f(k_1, c_\rho)$ for $v_g = 10$, $v_g = 10$, $\rho_d = 100$
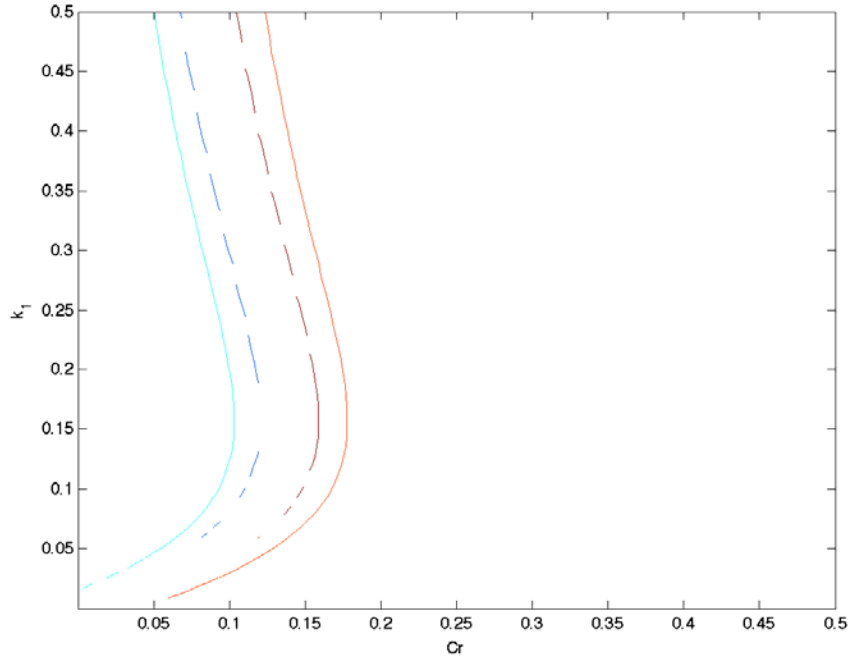
Figure 6.   Moving Target contour, $e_2 = f(k_1, c_\rho)$ for $v_g = 10$, $v_t = 10$, $\rho_d = 100$

Similar to the stationary target case, Figure 5 and Figure 6 suggest that optimal k_1 may be defined from the Lyapunov Stability function for the moving target scenario. From Figure 5, it is observed that e_2 is also a critical parameter. The optimal k_1 is obtained only when a suitably defined e_2 plane intersects with the e_2 surface. Successive runs of e_2 with varying UAV speed and target speed in Appendix II likewise reinforced the existence of optimal k_1. Hence from the Lyapunov Stability Analysis for the control law implemented, it is deduced that an optimal k_1 exists that maximizes the performance of the control law by extending R_A. The concept of Region of Attraction R_A is illustrated in Figure 7 on the following page. From the kinematics, it is shown earlier that the states of the system are given by range error, navigation error and line-of-sight error. Once the phase trajectory enters R_A, the state of the dynamic system automatically converges to a stable solution. From a system-stability viewpoint, larger R_A is desired so that the stability of the system is insensitive to disturbances.

14
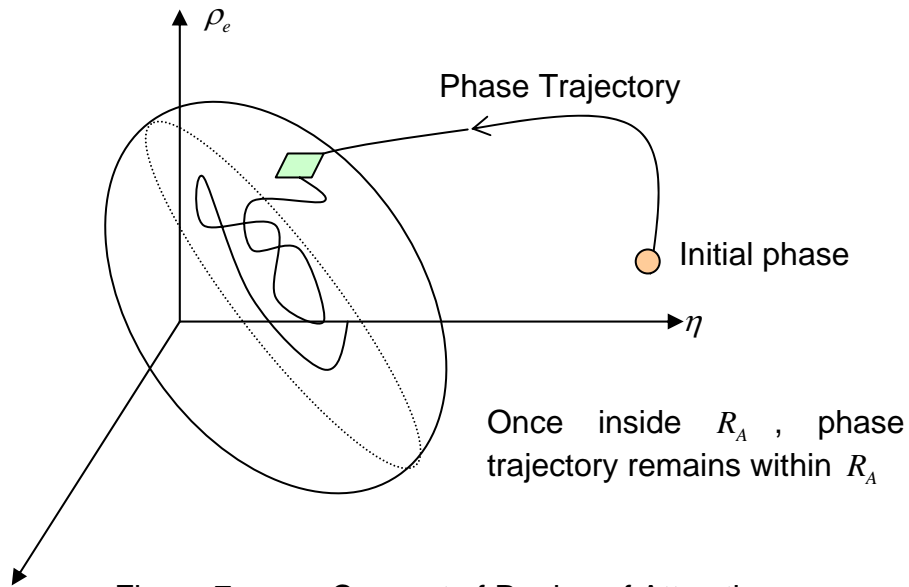
Figure 7.   Concept of Region of Attraction

It is evident that the stable solution has a smaller error magnitude for the smaller R_A. The larger the R_A, the higher the likelihood that the stabilized solution will be displaced much further from the origin. Figure 8 below depicts the changes in the region of attraction with increasing k_1. The increase in k_1 drives the reduction in the size of R_A.
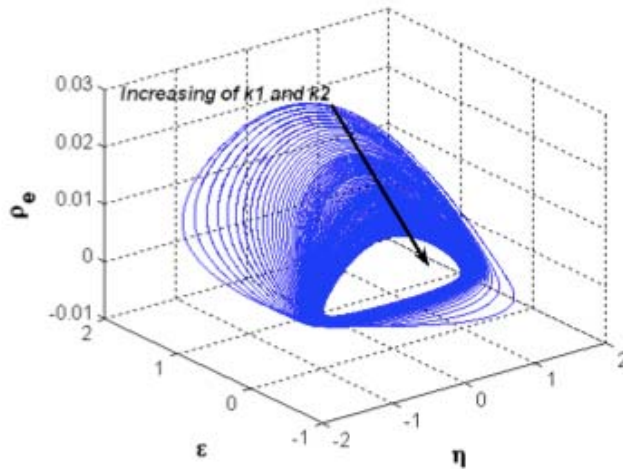
Figure 8.   Steady-State Trajectory showing Region of Attraction

The desired phase trajectory first selects a smaller k_1 so that the phase trajectory begins converging to a stabilized solution in the shortest time. Once the phase trajectory begins converging to a stabilized solution, it is desirable to increase k_1 to drive the error of the stabilized solution to a minimum. Therefore the optimal k_1 as defined by the Lyapunov Stability Analysis seeks the optimal tradeoff between the steady state error and speed at which phase trajectory arrives at R_A. The dependency of optimal k_1 upon v_g, v_t, and ρ_d is studied in greater detail in the next section so that adjusted gain may be implemented in the control law for the SUAV.

D.   DEPENDENCE OF OPTIMAL GAIN ON TARGET SPEED v_t

Deriving the analytical expression for optimal k_1 from equation (22) is mathematically complicated. To circumvent the mathematical challenges, the optimal k_1 is established by computing the optimal gain as target speed v_t varies. The SUAV speed is constant at 10 m/s at a desired range of 50m. Figure 9 shows a variation of surface e_2 as target speed v_t increases from 1 m/s to 10 m/s.
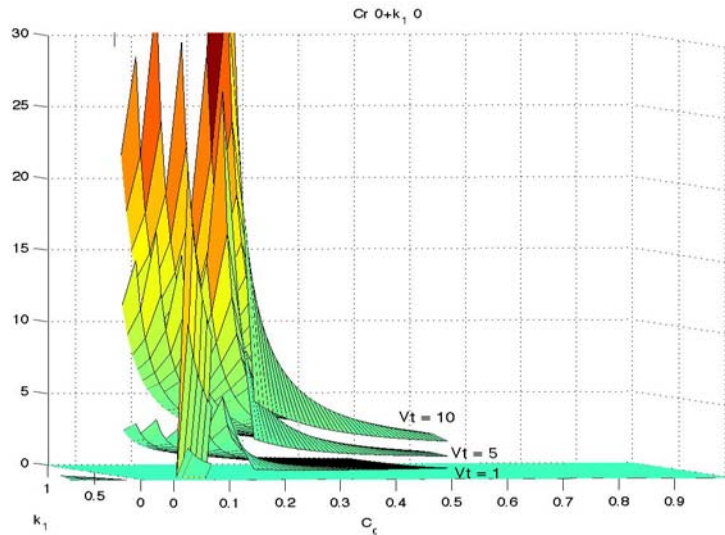
Figure 9.   Changes in Surface e_2 as v_t increases

From Figure 9, it is observed that increments in target speed shift the e_2 surface toward higher values of e_2. A fixed plane of e_2 is thus not practicable because the intersection of the fixed plane with e_2 surface does not guarantee the required contour. However by defining the intersecting plane $e_2 = v_t$, desired contours to compute optimal k_1 can be obtained for each v_t. The effect of increasing target speed on the shape of e_2 surface is more obvious from the contour plot instead. The series of contours is depicted in Figure 10 below.
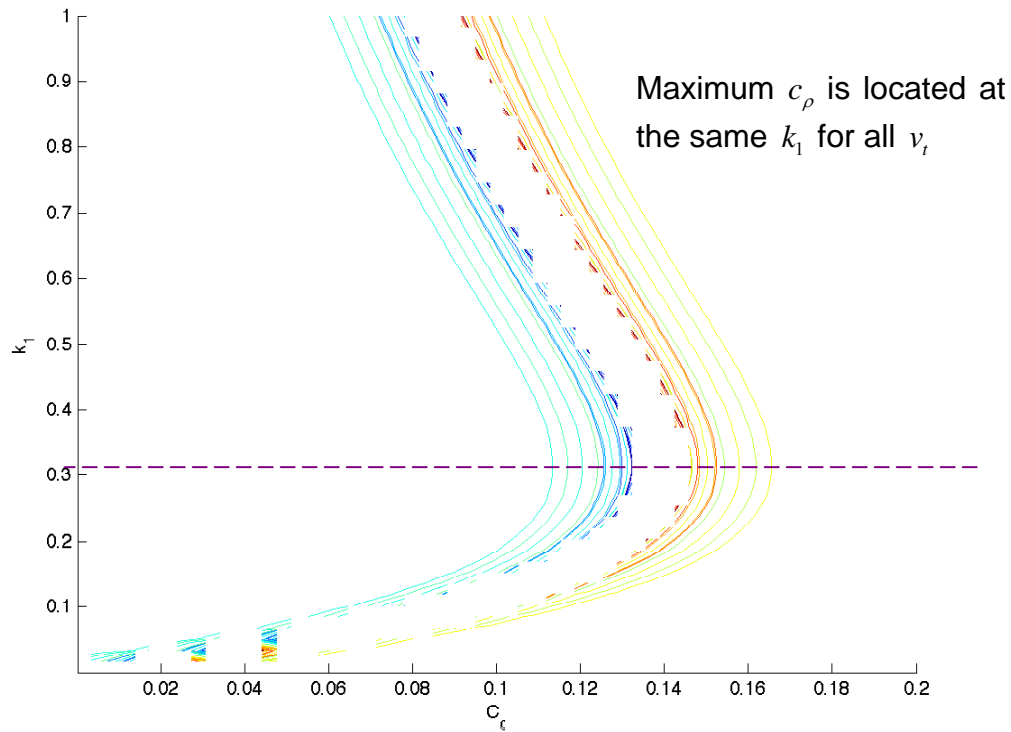
Figure 10.   Contours for intersection of e_2 plane with e_2 surface

From the contour lines, the optimal k_1 at different v_t are computed, and the dependency of optimal k_1 on v_t is plotted in Figure 11 below. The results obtained show that optimal k_1 (where c_ρ is maximum) is independent of target velocity, i.e. *optimal* $k_1 = f\left(v_g, \rho_d\right)$ only. The independence relationship between optimal k_1 and v_t remains valid for different values of SUAV speed and desired

distance. Since the optimal k_1 for each target speed is obtained via different values for the e_2 plane, a comparison of c_ρ for each optimal k_1 does not draw any meaningful conclusion.
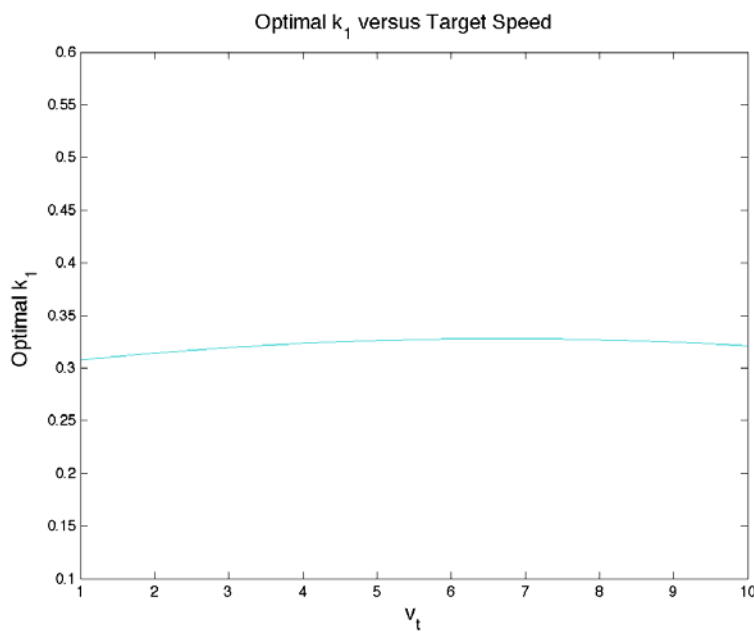
Figure 11.   Optimal k_1 versus Target Speed

The dynamics of subsystem I drive the UAV to orbit around the target at a desired distance. From the control law implemented, the value of gain k_1 drives the heading of the UAV to achieve its desired orbit. Since the turn rate of the UAV is limited by its orbital angular momentum, the optimal gain k_1 depends on v_g and ρ_d only.

E.   DEPENDENCE OF OPTIMAL GAIN ON v_g & ρ_d

A similar approach is undertaken to investigate the dependence of optimal gain on ρ_d. To demonstrate the changes in e_2 surface as ρ_d increases from 100m to 500m, the SUAV speed is maintained at 10 m/s and the target speed is kept constant at 5 m/s. The e_2 surfaces in Figure 12 below indicate that the effect

of increasing ρ_d shifts the e_2 surfaces closed towards the k_1 axis (lower c_ρ values for the same gain k_1). The absence of vertical shifts for the e_2 surfaces in Figure 12 allows a fixed level of e_2 plane to intersect with changing e_2 surfaces. The contour plot in Figure 13 below depicts the shape change in e_2 surface due to ρ_d.
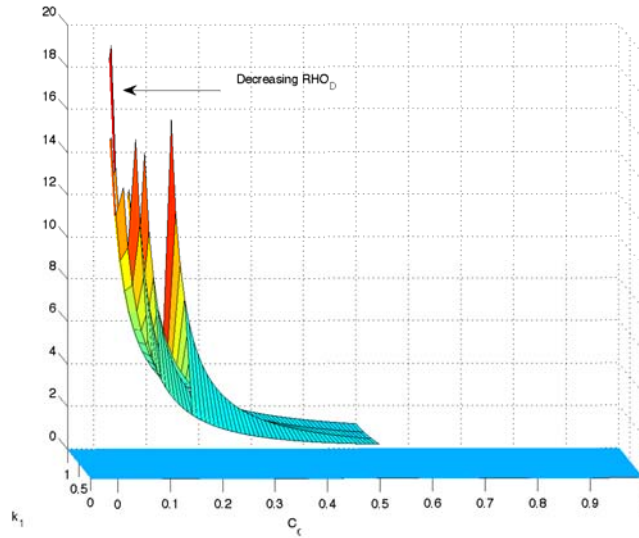
Figure 12.　　Changes in e_2 surfaces as ρ_d decreases
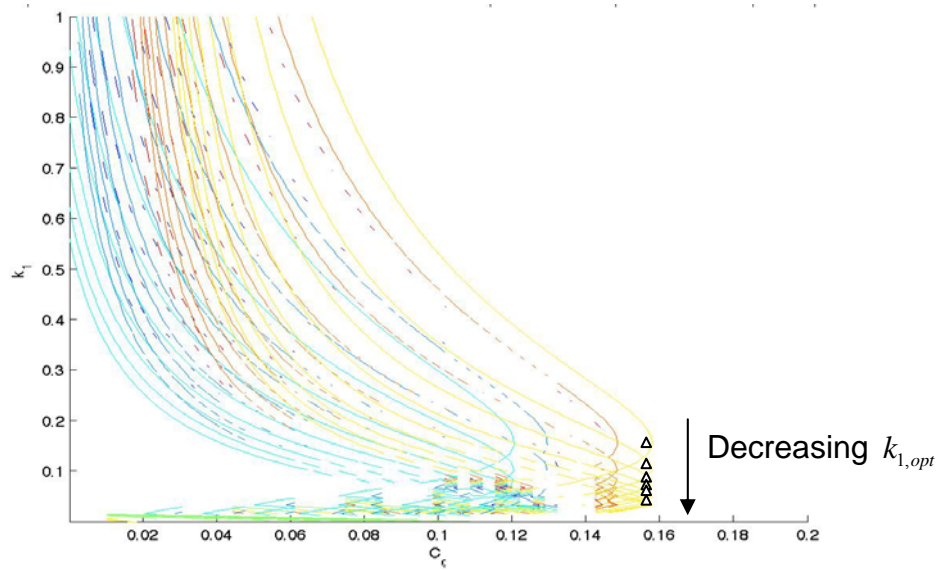
Figure 13.　　Contours for intersection of e_2 plane with e_2 surface

19

The contour plot in Figure 13 suggests that optimal gain decreases as ρ_d increases. From kinematics, a larger value of ρ_d is expected to reduce the turn rate expected of SUAV. The SUAV thus requires a smaller rate of change in bearing, and this leads to a smaller value for optimal gain. A similar argument can also be extended for the relationship between the optimal gain and varying v_g for a constant desired range ρ_d. The larger the SUAV speed, the larger the turn rate expected from the SUAV in order to maintain the desired range. This SUAV thus requires a faster rate of bearing change, and this leads to a larger value for optimal gain.

For implementation of the proposed adjustable gain control law, it is assumed that the SUAV has a constant operating speed of 10 m/s to 50 m/s, and the desired tactical range is from 100m to 500m. The optimal gain k_1 for the assumed range of operating conditions is tabulated in Table 1 below, and Figure 14 illustrates the dependence of the optimal gain on SUAV speed and desired range to target. Henceforth for an SUAV operating within the assumed tactical operating conditions, an adjusted gain control law can be implemented in SIMULINK model and HIL simulations. In the following chapter, the performance of the adjustable gain control law is evaluated in both Simulink model testing and hardware simulation testing.

k_1 opt	ρ_d								
V_g	100m	150m	200m	250m	300m	350m	400m	450m	500m
10 m/s	0.165	0.115	0.09	0.075	0.065	0.055	0.045	0.035	0.035
20 m/s	0.32	0.215	0.16	0.13	0.1050	0.09	0.08	0.075	0.065
30 m/s	0.42	0.285	0.21	0.17	0.14	0.12	0.105	0.095	0.085
40 m/s	0.55	0.38	0.285	0.23	0.19	0.165	0.145	0.125	0.115
50 m/s	0.73	0.51	0.38	0.3050	0.255	0.215	0.190	0.17	0.155

Table 1.   Optimal Gain for Tactical Operating Condition assumed
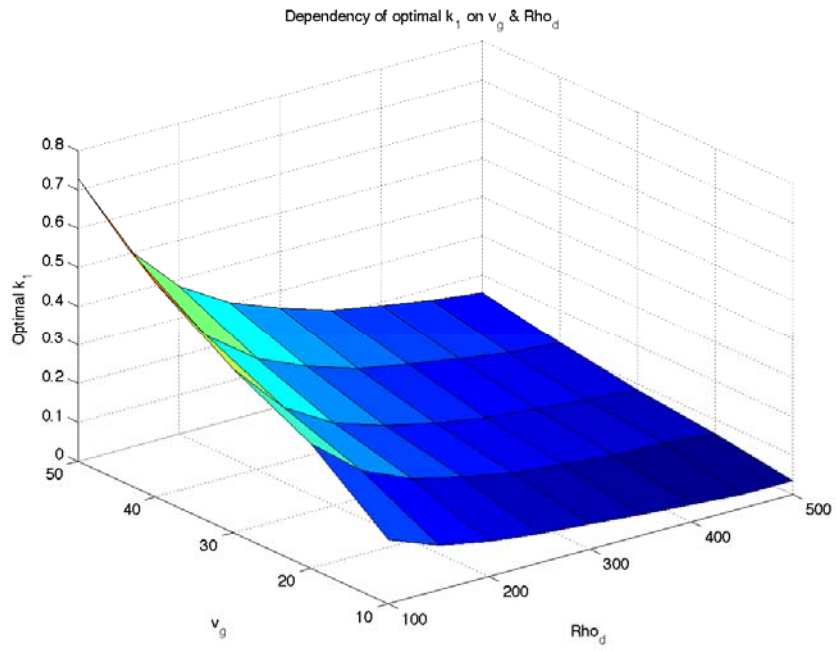
Figure 14.   Dependence of the optimal gain on v_g and ρ_d

21

THIS PAGE INTENTIONALLY LEFT BLANK

III. ADJUSTABLE GAIN IMPLEMENTATION

A. MODIFICATION OF SIMULINK DIAGRAM FOR ADJUSTED GAIN

With the implementation of an adjustable gain in the control law in equation (1), the modified control law is given by:

$$\dot{\psi} = \frac{v_g}{\rho_d}\cos\eta - k_{1,\text{opt}}\ \eta \tag{23}$$

$$\dot{\psi}_h = k_{1,\text{opt}}\eta + k_2\varepsilon$$

Where $k_{1,\text{opt}} = f\left(v_g, \rho_d\right)$

The control system architecture as depicted in Figure 15 below implements the control law given by equation (23). The adjustable gain control law is implemented within the VB Control block. It consists of an autopilot and a gimbaled camera driven by the control inputs $\dot{\psi}$ and $\dot{\psi}_h$. The onboard camera provides real-time video to the imagery target-tracking software. This software computes the tracking error ε when the target is engaged. The onboard GPS and inertial navigation systems measure the navigation error η for the SUAV. The Control System Architecture is modeled in SIMULINK to predict the target-tracking performance of the SUAV with the amended control law.
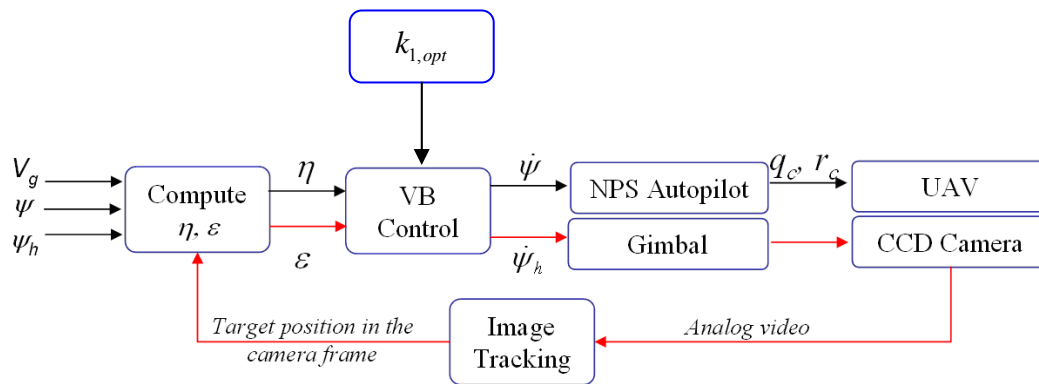
Figure 15.   Control System Architecture

23

B. SIMULATION RESULTS FROM SIMULINK MODEL

The performance and the system response to the newly developed adjustable gain control law are predicted for the following target scenarios: (1) stationary target scenario, (2) non-maneuvering moving target scenario, and (3) maneuvering target scenario. Since the system response of most control systems can be modeled either as a first order or a second order system [7], two measures of performance (MOP-1 and MOP-2) are defined as follows:

- MOP-1 is defined as the percentage of maximum steady-state range deviation as compared to the desired range. MOP-1 thus measures the SUAV range-holding capability after converging to the steady-state flight path. This is similar to the measurement of performance used in [5].

- MOP-2 is defined as the convergence speed, computed by the ratio of desired range to convergence time. Unlike in [5], convergence time is defined such that the response is contained within MOP-1. This allows MOP-2 to be a well-defined parameter even if the response is similar to that of an over-damped second-order system.

1. Simulation Results for Stationary Target

The adjustable gain control law is developed from the Lyapunov Stability Analysis for a moving target. The analysis of parameter e_2 in Chapter II shows that optimal gain is independent of target speed. It is thus deduced that the optimal gain in Table 1 remains valid even when the target is stationary. For the stationary target scenario, simulations are conducted to achieve the following objectives:

- To investigate the system response of the adjustable gain in control law

- To investigate the performance obtained by utilizing the adjustable gain control law over the previous control law

The initial conditions for this simulation run are: (1) SUAV velocity = 28 m/s, (2) SUAV location = [0, -1000, 300], (3) Target location = [0, 0, 0], (4) $k_2 = 0.25$ and (5) $\rho_d = 300$. The results are illustrated in Figure 16 on the following page.
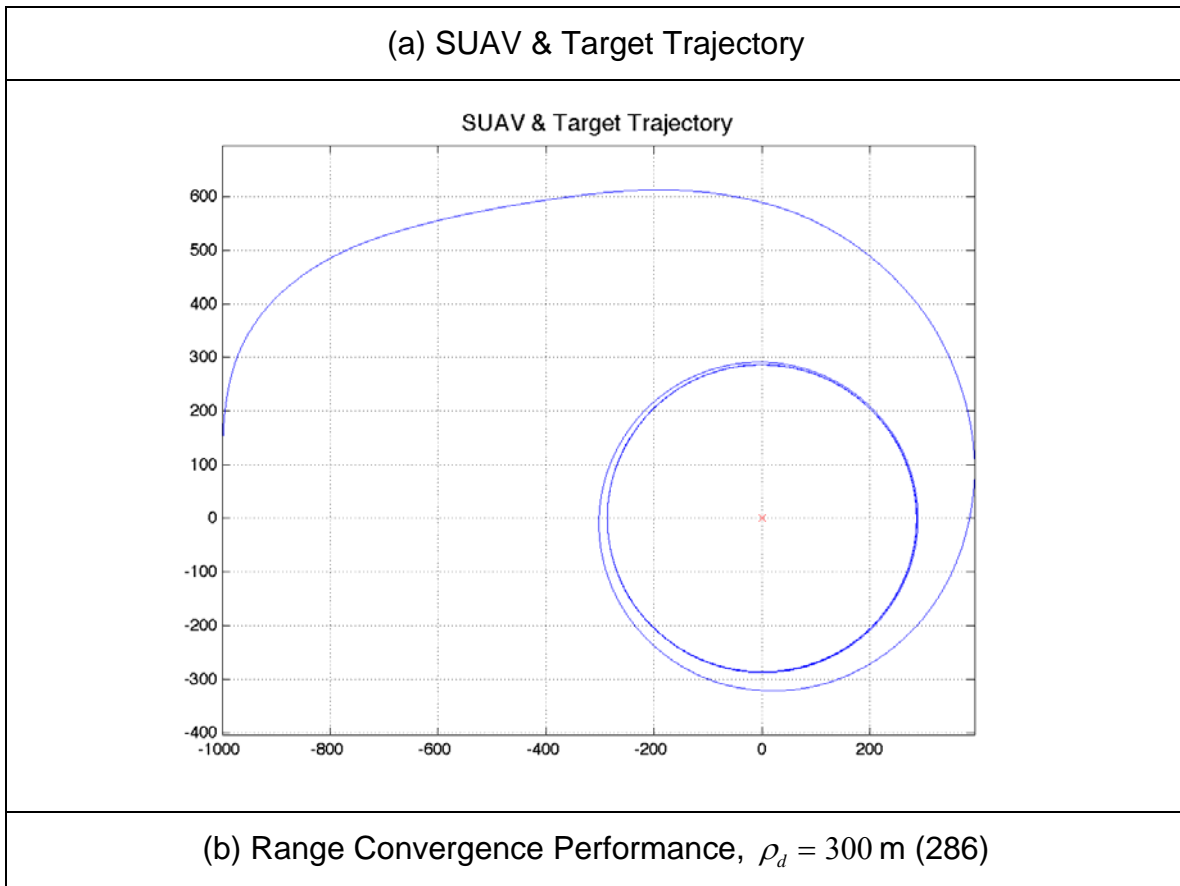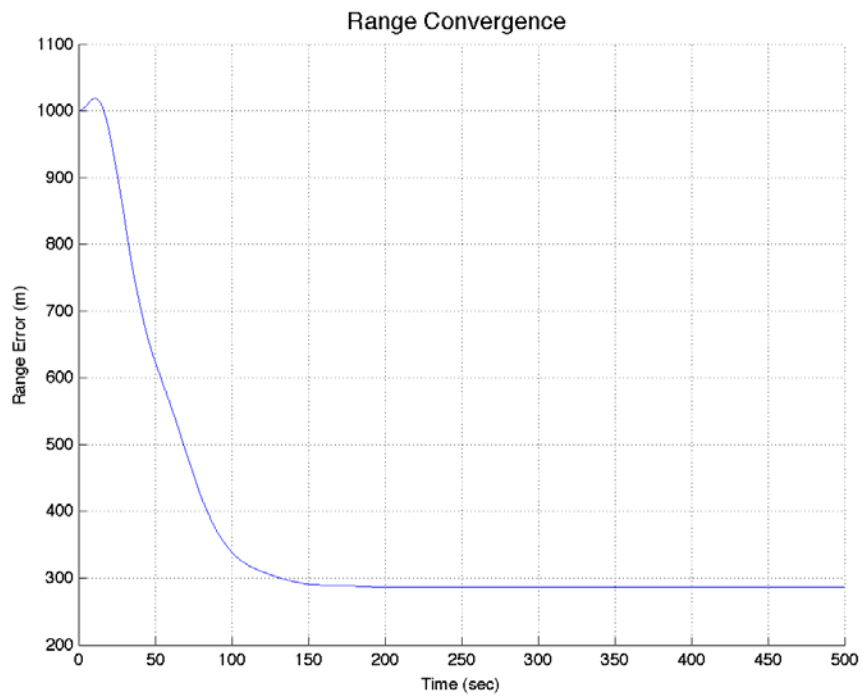
(a) SUAV & Target Trajectory

(b) Range Convergence Performance, $\rho_d = 300$ m (286)

(c) Navigation bearing error Convergence Performance
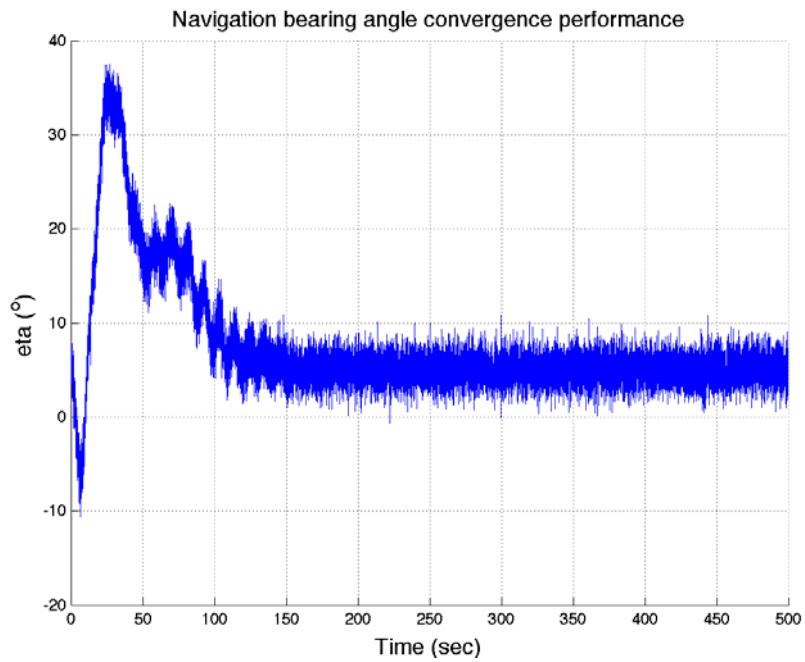
(d) Adjustable Gain versus Time
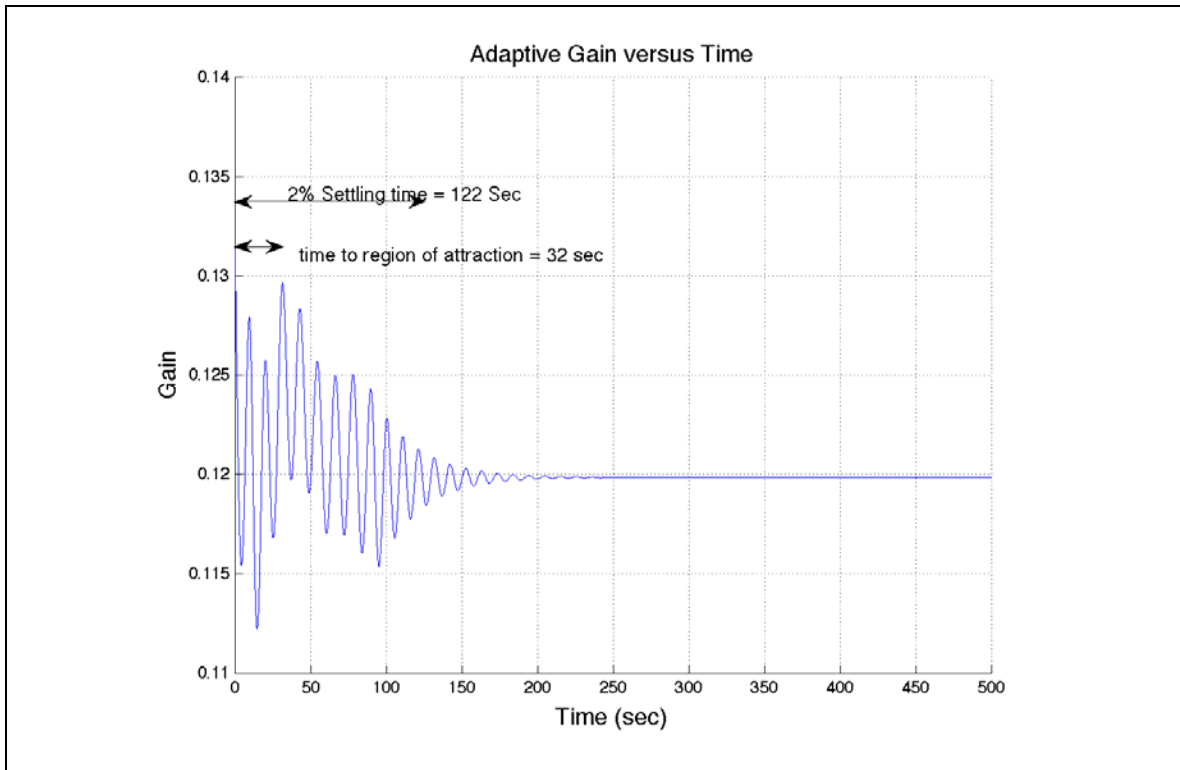
Figure 16.   SUAV Performance in Tracking Stationary Target

The performance of the adjustable gain control law for this simulation run is described as follows:

a) From Figure 16b, the SUAV converges to a steady-state range of 284m from the stationary target and the steady-state range error is 16m. MOP-1 is evaluated to be 5.33%.

b) The 2% settling time for the SUAV range is measured to be 122 seconds from Figure 16b. Comparing the response of Figure 16b to Figure 14c and Figure 16d, all three figures have identical values for 2% settling time. MOP-2 is thus evaluated to be 4.098 m/s.

c) From Figure 16c and 16d, it is evident that the navigation bearing error and gain parameters begin to converge only after 32 seconds. It is deduced that the SUAV take 32 seconds to arrive at the region of attraction R_A and the convergence time within R_A to the stable solution is approximately 90 seconds.

27

The aim of the first simulation run is to investigate the improvement in performance. The previous simulation is repeated with the same set of initial conditions with a different constant gain ranging from $k_1 = 0.1$ to $k_1 = 0.4$. The improvement in performance is assessed by the MOP-1 and MOP-2 comparison obtained for each case. The performance obtained for each case is appended in Appendix II and summarized in Table 2 below.

Gain	MOP-1	MOP-2
0.1	6.67%	3.62 m/s
0.2	5.68%	2.18 m/s
0.3	19.3%	1.72 m/s
0.4	32.0%	1.09 m/s
Adjustable	5.33%	4.10 m/s

Table 2.   Performance Comparison between Adjustable Gain versus Constant Gain

A comparison of MOP-1 suggests that there is a constant gain of 0.1 to 0.3 that reduces the steady-state error to a minimum. However as the gain increases from 0.1 to 0.3, a comparison of MOP-2 shows that the speed of convergence decreases. Thus from the performance of the adjustable gain control law, it is concluded that the implementation of an adjustable gain seeks the optimal balance between MOP-1 and MOP-2, i.e. seeking the lowest steady-state range error while optimizing the speed of convergence.

2.   Simulation Results for Non-Maneuvering Target

The objectives in the series of simulations conducted for a non-maneuvering target are similar to that of the stationary target. The first objective is to investigate the performance of the adjustable control law when the target is

moving in a constant velocity. For the stationary target scenario, the adjustable gain gives optimal performance by the optimal tradeoff between MOP-1 and MOP-2. The second objective is, therefore, to investigate whether optimized performance of an adjustable control law remains valid for the moving target scenario. The parameters for the series of simulations conducted are identical to the stationary target scenario, except that the target is now moving in an easterly direction with a speed of 5 m/s. The initial conditions for this simulation run are: (1) SUAV velocity = 28 m/s, (2) SUAV location = [0, -1000, 300], (3) Target location = [0, 0, 0], (4) $k_2 = 0.25$ and (5) $\rho_d = 300$. (6) Target velocity = 5 m/s. The results obtained are illustrated in Figure 17 on the following page.
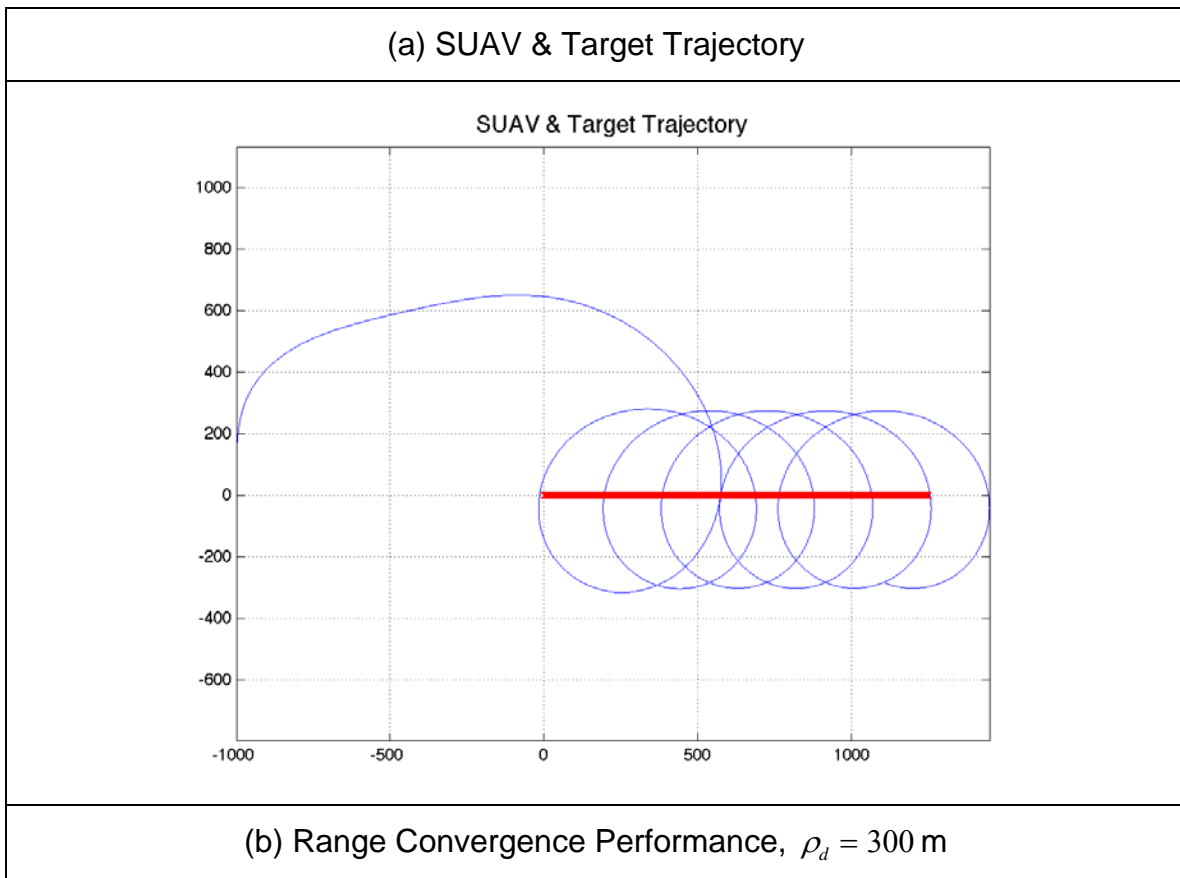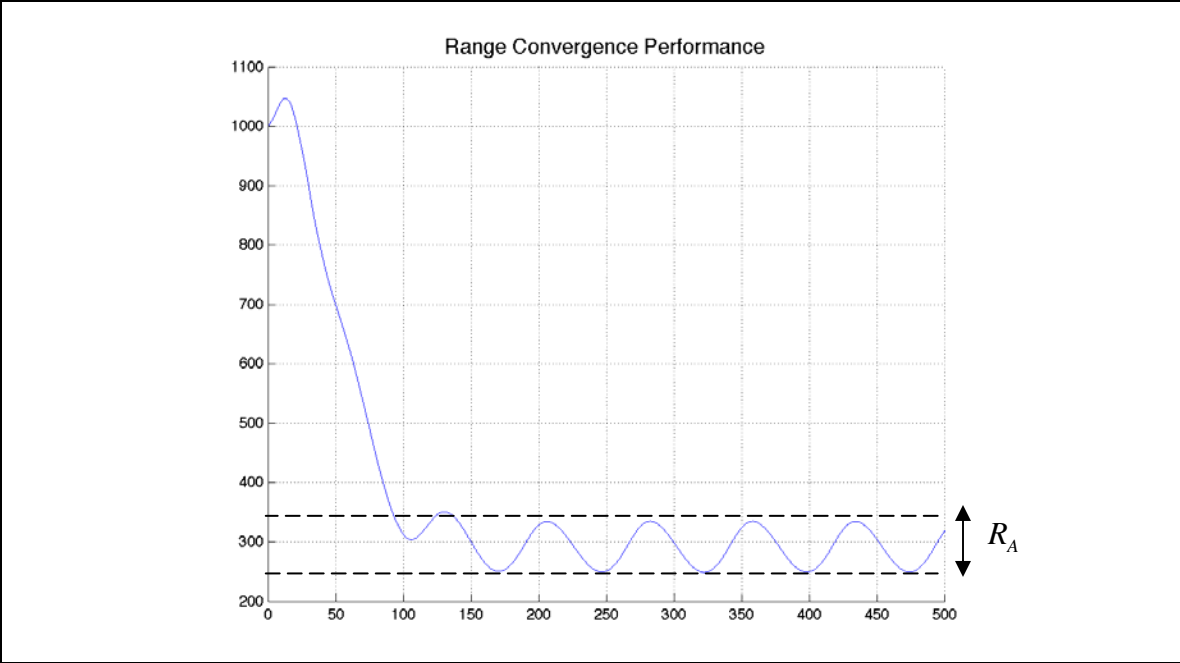
(a) SUAV & Target Trajectory

(b) Range Convergence Performance, $\rho_d = 300\,\text{m}$

Range Convergence Performance

(c) Navigation bearing error Convergence Performance

Navigation bearing angle convergence performance

(d) Adjustable Gain versus Time

30
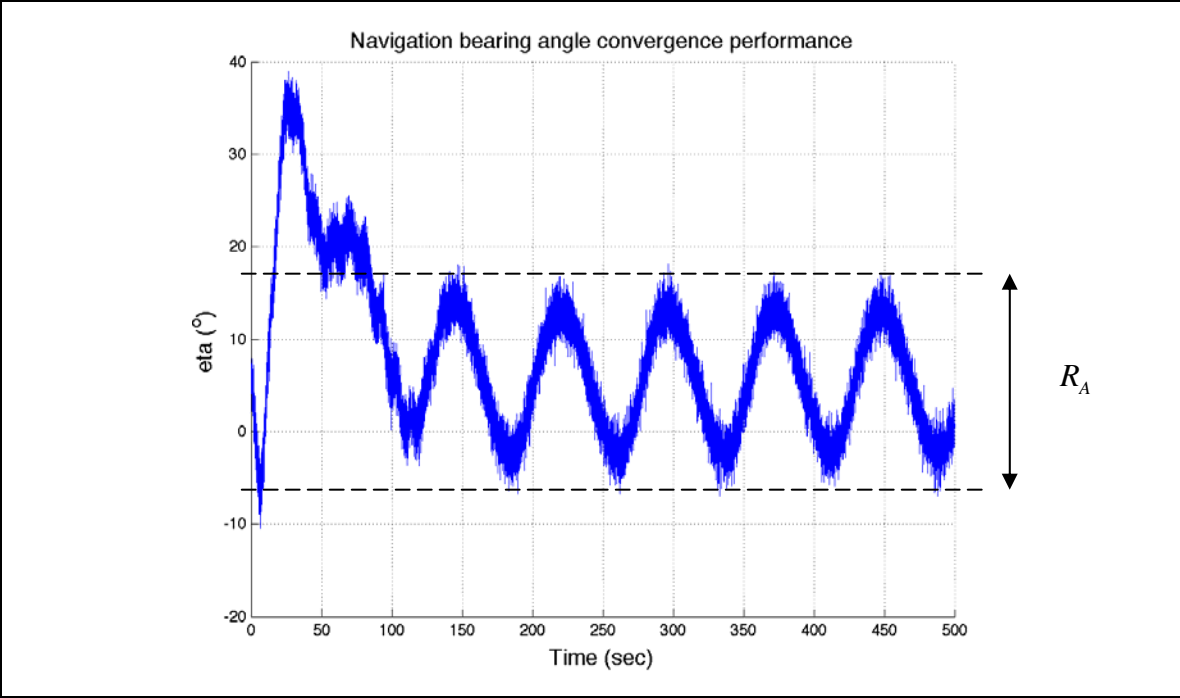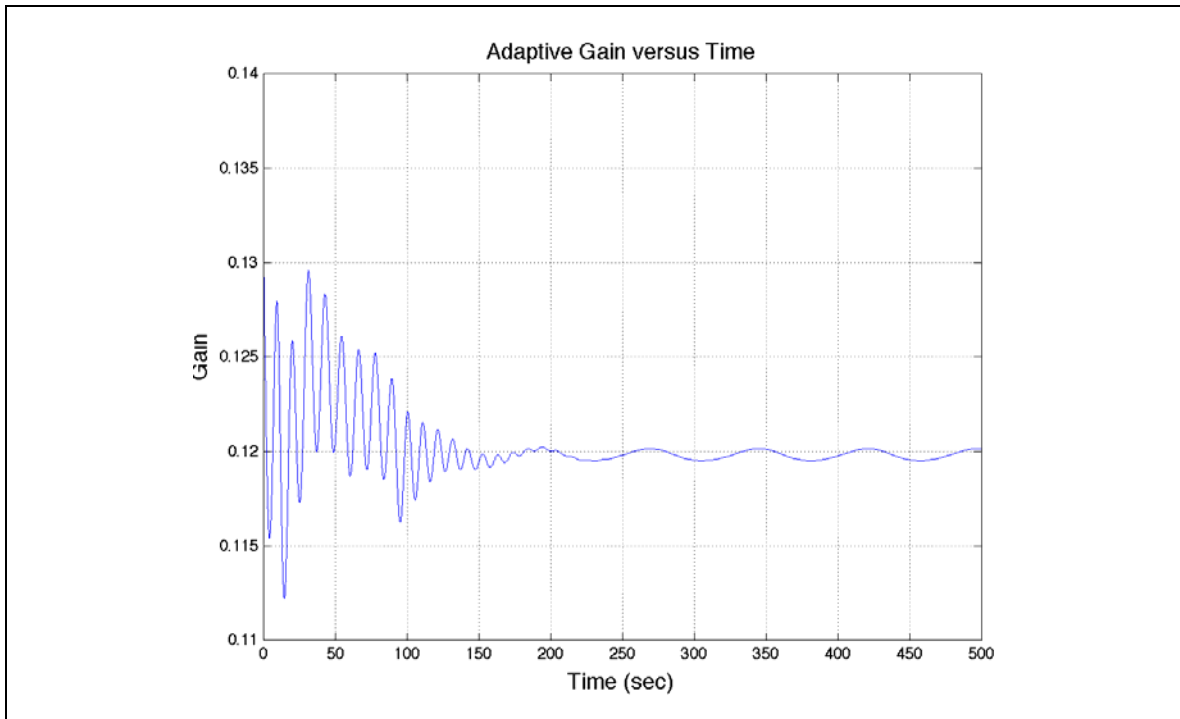
Figure 17.   SUAV Performance in Tracking Non-maneuvering Targets

The observations of the simulated SUAV performance for tracking a non-maneuvering target are summarized as follows:

a) Figure 17b indicates that the SUAV range does not converge to a fixed value. Instead the SUAV range continuously oscillates within bounds as suggested by the results of the Lyapunov stability analysis.

It is observed that the steady state response of range oscillates between 334.5 m and 249.5 m, and the mean value is 292 m. The previous performance measure for MOP-1 is an inadequate measure for range convergence. For a moving target, an alternative performance measure for range convergence is devised, MOP-3. MOP-3 computes the percentage error between the desired range and the mean value for the steady-state function; thus, MOP-3 is calculated to be 2.67%.

b) Likewise the convergence time defined previously is not applicable in the case of a non-maneuvering target. Instead of utilizing the 2% settling time as a measure, the convergence time is re-defined as the time taken for a response to reach steady state function. From Figure 17b the convergence time is 140 seconds. MOP-2 is thus evaluated to be 3.57 m/s.

c) From Figure 17c and Figure 17d, the SUAV takes 31.2 seconds to be within the region of attraction R_A (as shown in Figure 15). Likewise, the convergence time within R_A is dependent upon the initial position of the SUAV from the target. It is also observed that the steady state response for feedback gain is an oscillatory waveform instead of a fixed value.

d) Since the steady state response for range error and navigation oscillates within bounds, the region of attraction can be estimated from the magnitude of the bounds, as shown in Figure 17c and Figure 17d.

In the second series of simulation runs, the aim is to investigate the improvement in performance of the adjustable gain control law over the constant gain control law for non-maneuvering targets. The initial conditions for this simulation run are: (1) SUAV velocity = 28 m/s, (2) SUAV location = [0, -1000, 300], (3) Target location = [0, 0, 0], (4) $k_2 = 0.25$ and (5) $\rho_d = 300$. (6) Target velocity = 5 m/s. The previous simulation is repeated with different constant gains ranging from $k_1 = 0.05$ to $k_1 = 0.4$. The performance obtained for each case is appended in Appendix III and summarized in Table 3 below.

Gain	MOP-3	MOP-2
0.05	9.00%	1.97 m/s
0.1	4.50%	3.03 m/s
0.2	6.27%	2.66 m/s
0.3	20.32%	2.18 m/s
0.4	32.92%	1.37 m/s
Adjustable	2.67%	3.57 m/s

Table 3.   Performance comparison for Non-maneuvering Target at 5m/s

A comparison of MOP-3 in Table 3 suggests gain $k_1 = 0.1$, reducing the steady-state error to a minimum. The same value of k_1 also increases the convergence speed to maximum and gain $k_1 = 0.1$ appears to be the optimum gain. However, it is evident that the adjusted gain shows a much improved performance over the constant gain control law. Therefore, optimized performance for the adjustable gain control law remains valid for a constant speed non-maneuvering target scenario.

Previously in 5, it has been demonstrated that for the constant gain control law, SUAV target-tracking performance degrades, i.e. an increase in range error and a decrease in convergence speed is created. This motivates the need for a more rigorous analysis to determine the sensitivity of an adjustable gain control to target speed. The simulation is repeated with target speeds varying from 5 m/s to 20 m/s; the performance for each target speed is appended in Appendix III. The initial conditions are: (1) SUAV velocity = 28 m/s, (2) SUAV location = [0, -1000, 300], (3) Target location = [0, 0, 0], (4) $k_2 = 0.25$ and (5) $\rho_d = 300$. The sensitivity of the adjustable gain control law to target speed is summarized in Table 4.

Target Speed	MOP-3	MOP-2
20 m/s	18.80%	5.00 m/s
15 m/s	9.8%	5.35 m/s
10 m/s	3.00%	3.45 m/s
5 m/s	2.67%	3.57 m/s

Table 4.   Performance comparison for varying Target Speed

As observed from Table 4, an increase in target speed leads to degradation in the range holding for the adjusted gain control law. The closer the target speed approaches the SUAV speed, the more severe the degradation in range holding becomes. This may be noted by the comparison of MOP-3. Intuitively the sudden increase in MOP-2 for target speed at 15 m/s is due to the larger range error. The larger the range error, the larger the SUAV orbit radius is expected to become, resulting in a faster convergence speed.

The conclusion derived from the series of simulations conducted for non-maneuvering targets include:

a) The adjustable gain control law improves performance as compared to the constant gain control law. The use of the adjustable gain in the control law optimizes range convergence performance and convergence speed.

b) Range-holding performance degrades with increased target speed. As target speed approaches the SUAV speed, the more severe the degradation in range holding performance. However, convergence speed improves with target speed increase.

3. Simulation Result for Maneuvering Target

The initial conditions for this simulation run are: (1) SUAV velocity = 28 m/s, (2) SUAV location = [0, -1000, 300], (3) Target location = [0, 0, 0], (4) $k_2 = 0.25$ and (5) $\rho_d = 300$. (6) Target velocity = 10 m/s.
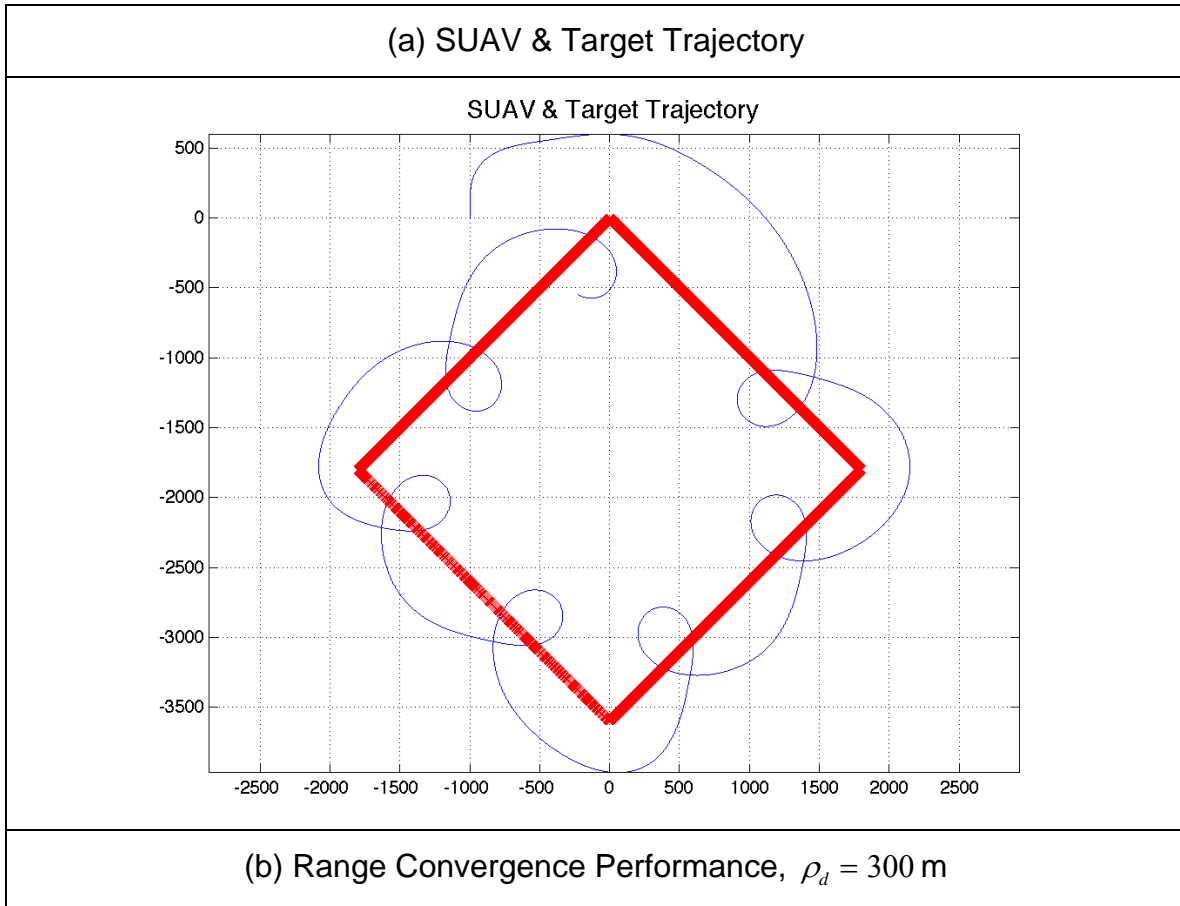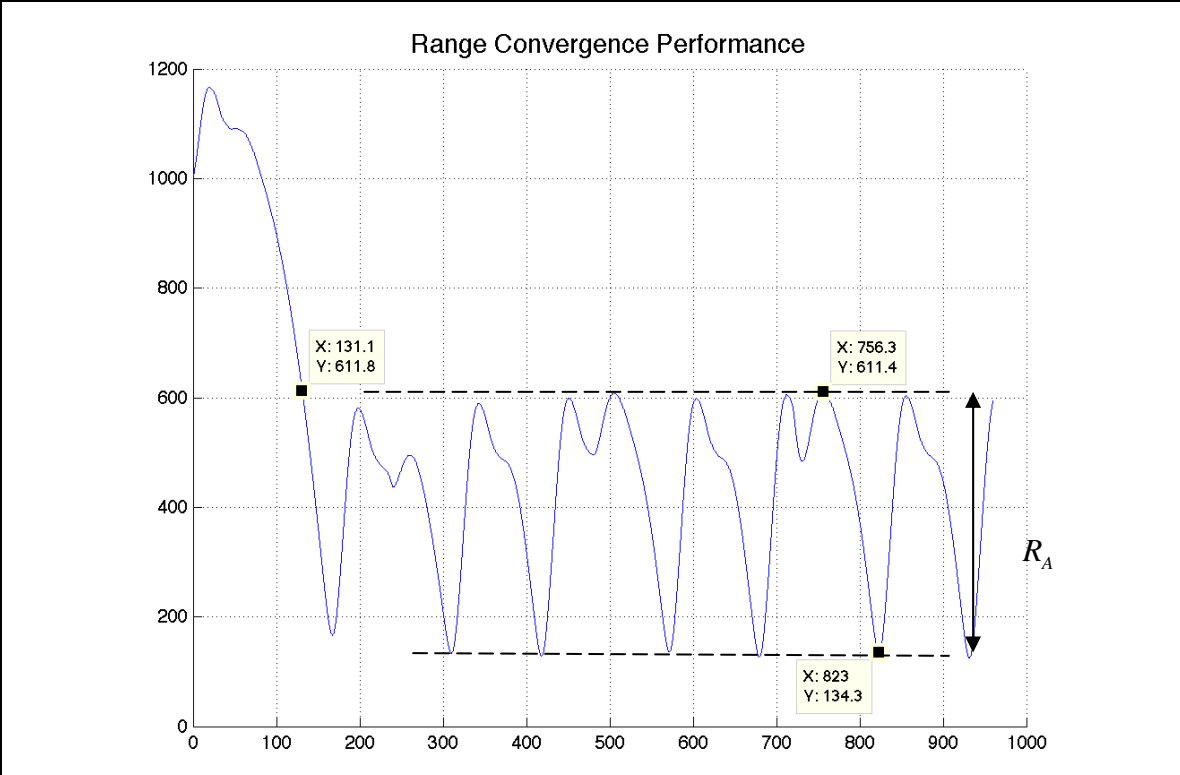
(a) SUAV & Target Trajectory
(b) Range Convergence Performance, $\rho_d = 300$ m

(c) Navigation bearing error Convergence Performance
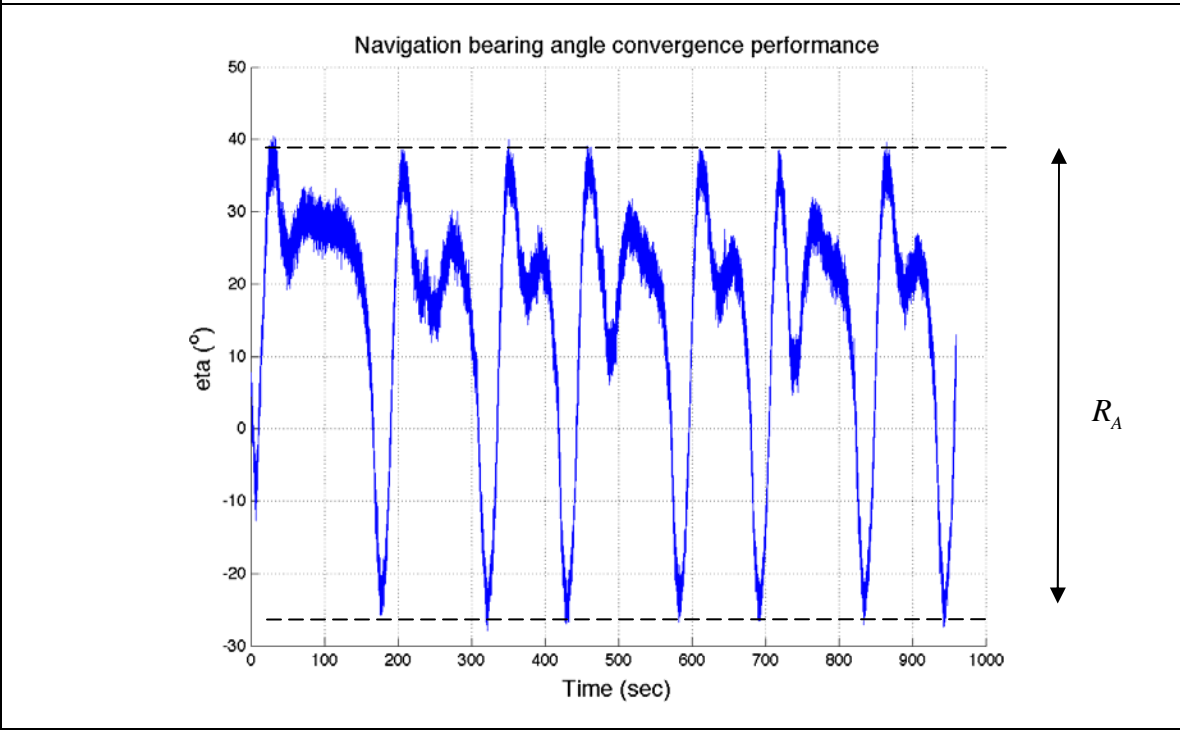
(d) Adjustable Gain versus Time
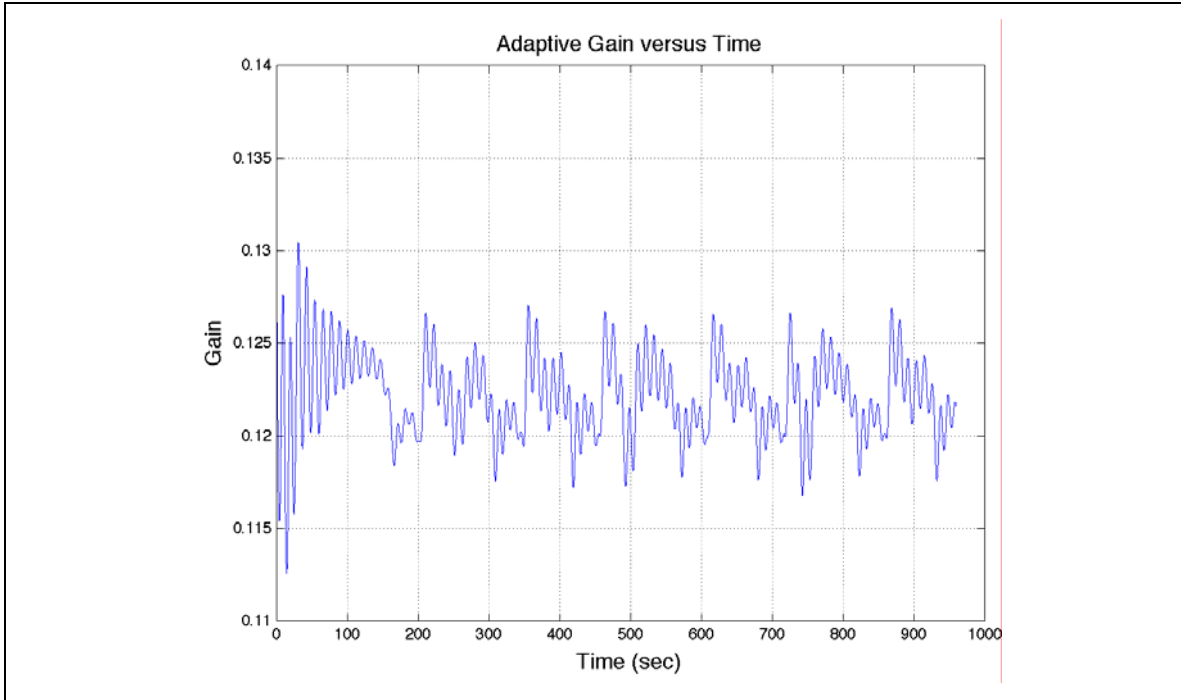
Figure 18.   SUAV Performance in Tracking Maneuvering Target

In Figure 18b, the measure of performance for the maneuvering targets are given by (1) MOP-3 = 24.28 % and (2) MOP-2 = 3.81 m/s. In comparing the results obtained in Table 4, it is evident that when a target changes its course of direction, the range holding capability of the SUAV deteriorates significantly. The navigation error η is much larger compared to that of a non-maneuvering target, and speed of convergence is reduced significantly. However the SUAV continues to track the target, as shown by the SUAV trajectory in Figure 18a, with a larger region of attraction. Hence it is concluded that the adjustable gain control law as proposed in equation (23) is capable of tracking a maneuvering target.

C.   HARDWARE-IN-LOOP SIMULATION

The intention of HIL simulation is to validate the performance improvement concluded previously from the SIMULINK model. The simulated SUAV model has demonstrated improved performance by the adjustable gain control law in equation (23) over the previous control law. In practical implementation of an SUAV collaborating with the UGV, the SUAV actual response differs from the

SIMULINK model of the SUAV. Hardware-In-The-Loop (HIL) simulation has been carried out to ensure the robustness of the modified control law. The SUAV used for the HIL simulation is the Senior Telemaster SUAV shown in Figure 19 below. The HIL setup and the results obtained are described in a later part of this section.

Figure 19.   Senior Telemaster SUAV [From 4]

1.   Hardware-In-Loop Setup

Cloud Cap Technology has developed an integrated avionics system control (Piccolo) for small-unmanned aircraft that allow HIL testing of SUAV performance. Piccolo consists mainly of four parts: an avionics control system onboard SUAV, a Ground Control Station (GCS), a PC for manned operations, and manual flight control via a modified Futaba radio controller. The HIL hardware setup is identical to that performed in 5. The HIL setup in the SUAV is depicted in Figure 20 below:
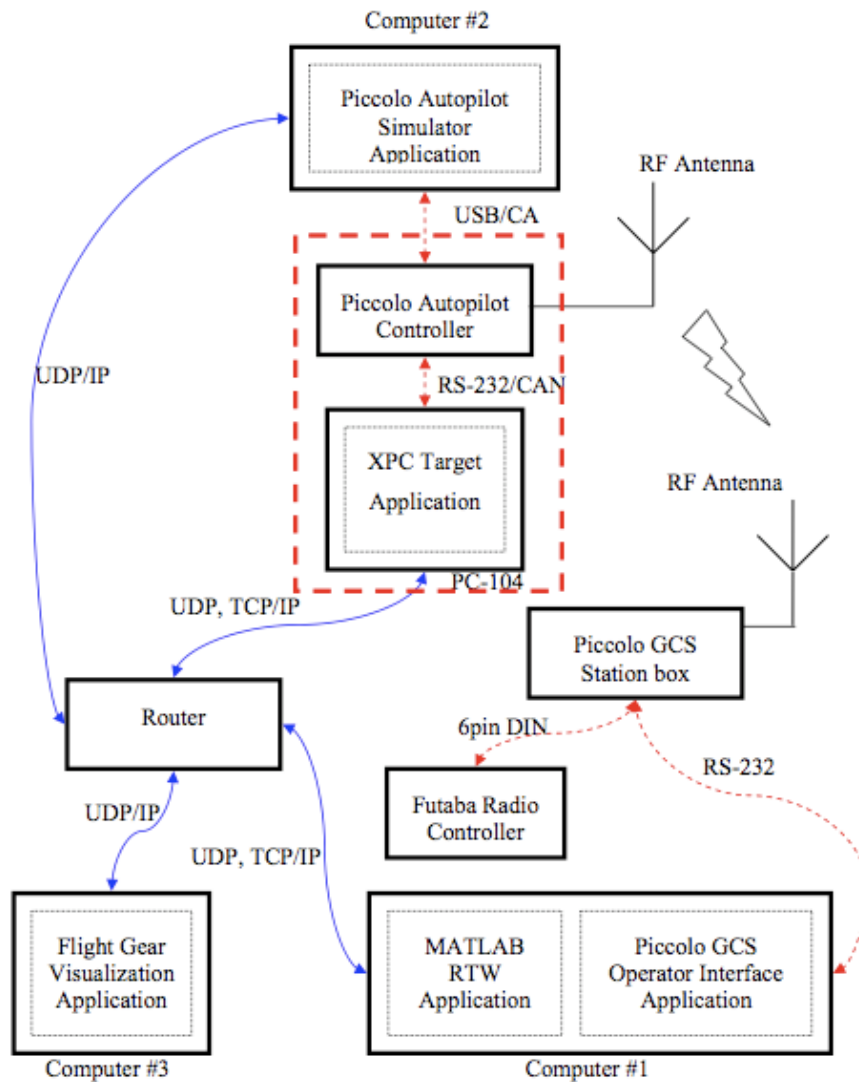
Figure 20.　　　Schematic of HIL Setup [From 5]

　　　The Piccolo system has several control loops. The slower outer loop computes the desired turn rate reference command for circular guidance and sends the command turn rate to the faster inner loop. The faster inner loop then controls the actuators so as to follow the reference commands and therefore maintain stable dynamics of the aircraft. In the HIL setup and simulation environment, the autopilot is connected to the second computer via the USB-CAN data exchange cable. The simulator, which runs in the second computer, tests the aircraft control laws in a software environment with the servo and

sensor data which is received from the CAN bus. Since the simulator communicates with the avionics in real time, the second computer is isolated for simulator software only. The GCS is of similar hardware configuration as the avionics system onboard the SUAV. The GCS manages the communication link to the avionics system to interface with the autopilot in the loop console. It also provides a command and control stream to the operator's PC via a standard ninepin serial cable. The third computer runs the Flight Gear application that provides visualization of the effect of the control law on flight performance and stability of the aircraft. More detailed information regarding the HIL setup may be obtained from Ref 5, Ref 8, Ref 9 and Ref 10.

By employing an XPC Target within the SIMULINK Real-Time Workshop (RTW) environment, HIL simulation may be executed by the PC-104 board onboard the SUAV. The simulation model in SIMULINK is compiled on the Host PC into 'C' code that runs on the Target PC. The real-time capability of the system executes the code at a regular interval for optimal control. From the previous SIMULINK model, the AP controller block and the 6-DOF aircraft model block are replaced with the actual Piccolo AP controller hardware. The simulator software provides the sensor input that is required to compute the simulated flight parameters of the aircraft. The SIMULINK model schematic for the XPC Target model is identical to that in Tay's work except for the gain input to the control law. The SIMULINK model schematic for the HIL simulation is depicted in Figure 21 on the following page. The procedure for running the XPC HIL simulation is documented in Appendix V.
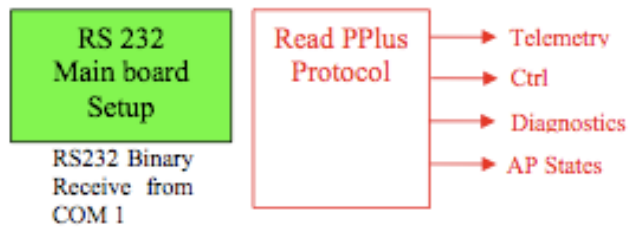
READ BLOCK of Simulink RTW communication interface program
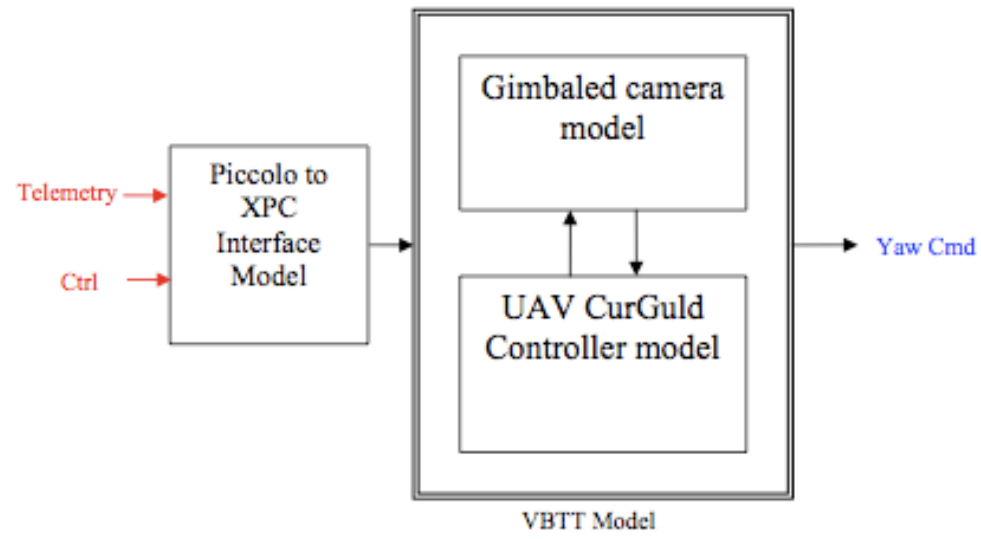
WRITE BLOCK of Simulink RTW communication interface program
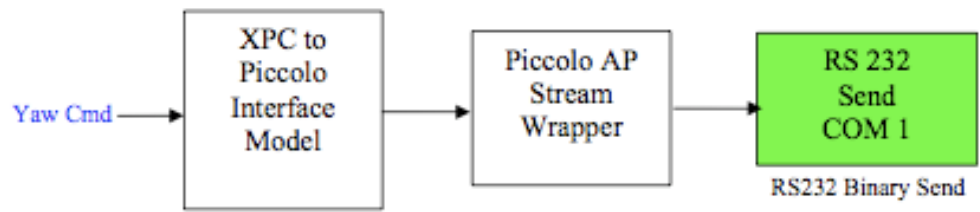
Figure 21.   XPC Target Model Schematic

2. HIL Simulation Results

The objectives in the series of simulations that were conducted for a stationary target are identical to those performed for the SIMULINK model of the SUAV. The first objective is to investigate if implementation of the adjustable gain control law in physical hardware offers improved performance over the constant gain control law. The first series of simulations repeats the HIL simulation with a different constant gain, ranging from $k_1 = 0.05$ to $k_1 = 0.4$ for the adjustable gain case. The second objective is to investigate the sensitivity of the adjustable gain control law to target speed. In the second series of HIL simulations, target velocity varies from 5 m/s to 20 m/s. The initial conditions for this simulation run are: (1) SUAV velocity = 28 m/s, (2) SUAV location = [0, -1000, 500], (3) Target location = [0, 0, 0], (4) $k_2 = 0.25$ and (5) $\rho_d = 300$. Figure 22 below shows the HIL simulation result obtained for stationary target scenario.
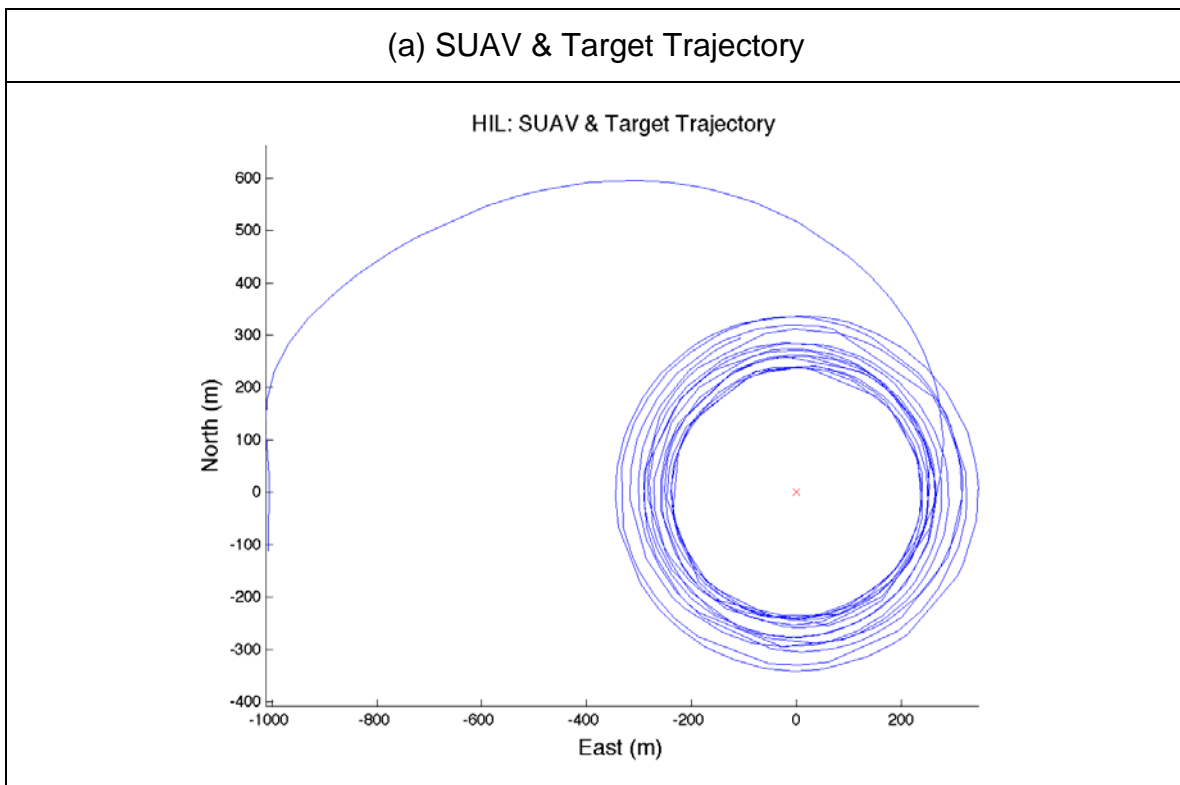
(a) SUAV & Target Trajectory

(b) Range Convergence Performance, $\rho_d = 300$

Range Convergence Performance

X: 498.5
Y: 47.01

X: 80.95
Y: -63.2

X: 714
Y: -63.53

R_A

(c) Navigation bearing error Convergence Performance

Navigation bearing angle convergence performance

X: 866
Y: 0.7256

X: 394.9
Y: -4.912

R_A
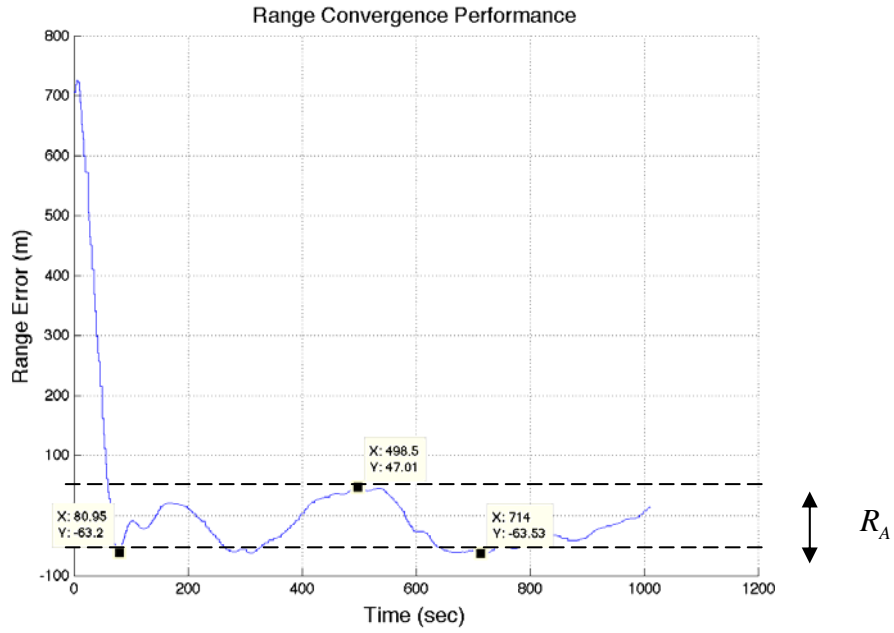
(d) Adjustable Gain versus Time
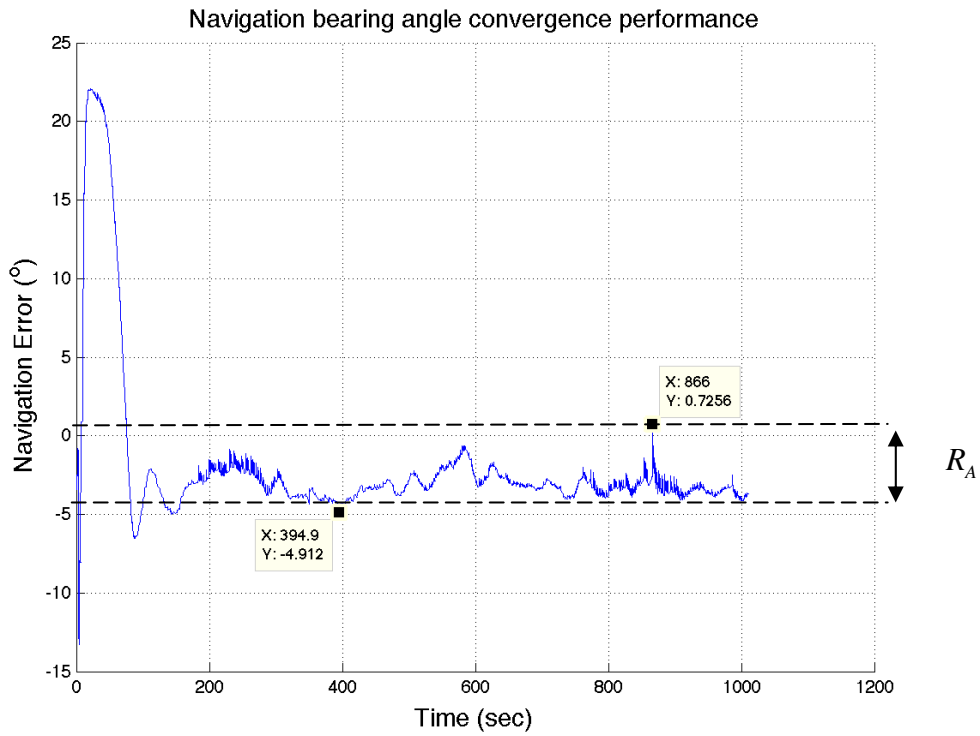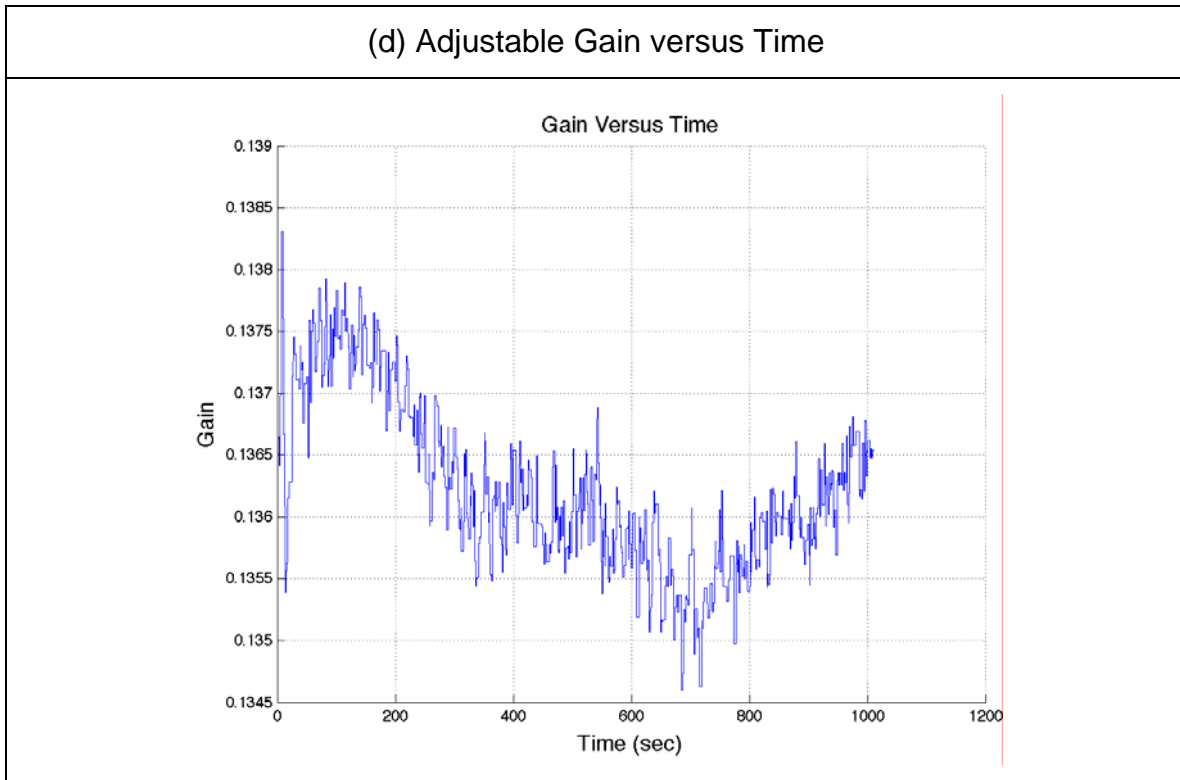
Figure 22.   SUAV HIL Performance in Tracking Stationary Target

Unlike the SIMULINK model, the trajectory of an SUAV does not converge to a fixed range from the target. However the response of the HIL simulation is similar to that obtained for maneuvering targets where steady-state responses of the SUAV are within bounds. Through comparisons of Figure 20b to Figure 14b, it is evident that the HIL simulation introduces more disturbances to the steady-state response. This is because the SIMULINK model in simulation does not reflect the actual hardware response. Instead the SIMULINK model is an approximation to the behavior of the actual hardware. A similar response to the adjustable gain control law is expected. As such, MOP-3 is a more suitable performance measure than the MOP-1 is. Similarly MOP-2 defined for moving targets is used as the performance measure for speed of convergence. MOP-3 is measured to be - 8.01 m, and MOP-2 is measured to be 3.71 m/s. The performance of constant gain control law in HIL simulations are appended in Appendix IV and summarized in Table 5 on the following page.

Gain	MOP-3	MOP-2
0.05	4.68%	1.44 m/s
0.1	2.95%	3.53 m/s
0.2	4.62%	3.13 m/s
0.3	11.87%	2.56 m/s
0.4	16.12%	2.41 m/s
Adjustable	2.67%	3.71 m/s

Table 5.   HIL Performance comparison for Stationary Target

Although the HIL simulation outcome varies significantly from the SIMULINK model, the flight characteristics and control law behavior are identical to that of the SIMULINK model. Similar to the SIMULINK, Table 5 suggests that at gain $k_1 = 0.1$ the average steady state range error is at its minimum. For the same value of k_1 convergence speed is at its maximum, and gain $k_1 = 0.1$ appears to be the optimum gain for the constant gain control law. However Table 5 also demonstrates that the adjustable gain control law has improved performance over the constant gain control law. Hence from the first series of HIL simulations, optimal performance for the adjustable gain control law is validated in an HIL Simulation environment.

Target Speed	MOP-3	MOP-2
20 m/s	48.67%	6.96 m/s
15 m/s	22.86%	6.13 m/s
10 m/s	8.63%	4.23 m/s
5 m/s	1.36%	6.38 m/s

Table 6.   HIL Performance comparison for Non-Maneuvering Target Speed

Table 6 validates the previous SIMULINK hypothesis that the increase in target speed leads to degradation in the range holding for the adjustable gain control law. The closer the target speed approaches the SUAV speed, the more severe the degradation in range holding becomes. This may be noted by the comparison of the MOP-3. Similar to the results for the SIMULINK model, the larger SUAV orbit radius is expected for larger range error and thus faster convergence speeds. Since the results from the SIMULINK model simulation and the XPC Target simulation are identical, the improved performance for adjustable gain control law has been verified.

IV. CONCLUSION AND RECOMMENDATIONS

In comparison with the constant gain control law as defined by equation (1), the newly modified control law selects an optimal gain by taking the desired range and SUAV speed. The condition for optimal gain is derived from the Lyapunov Stability analysis, based on the kinematics of target tracking, thus ensuring the robustness of the control system. The performance improvement provided by the adjustable gain control law developed in equation (23) seeks the optimal tradeoff between speed of convergence and range holding capability.

The results obtained from the implementation of the adjustable gain control law in both software simulation and Hardware-In-Loop simulations showed identical improvement in performance over the previous control law.

Recommendations for future research:

a) Since the modified control law offers improved performance without incurring hardware costs, it is recommended that actual flight trials should be conducted to test the robustness of performance gain where the SUAV is subjected to unwanted aerodynamic disturbances in a practical environment.

b) It is also recommended that future work should seek further refinement of the control law, particularly the dependence on continuous varying target speed and direction.

THIS PAGE INTENTIONALLY LEFT BLANK

LIST OF REFERENCES

[1]   J.C.Wong *et al.,* DSTA Horizon 2005: "Unmanned Aerial vehicle: Development Trends & Technology Forecast," Internet 21 Aug 2007, Available at http://www.dsta.gov.sg/index.php/DSTA-2005-Chapter-2/ .

[2]   United States President's Office of Management and Budget, "Budget of United States Government FY 2007"; Internet 5 Sep 2007, Available at http://www.whitehouse.gov/omb/budget/fy2007/defense.html .

[3]   David M. Carroll, Jerry L. Harbour, Scott G. Bauer, David J. Bruemmer *et a*l., "Enabling Technologies for Unmanned Protection Systems," SPIE Proc 5804: Unmanned Ground Vehicle Technology, 29-31 Mar 2005.

[4]   Dobrokhodov V.N, Kaminer I, Jones K.D, Ghabcheloo R, "Vision-based tracking and motion estimation for moving targets using small UAVs," American Control Conference 14-16 June 2006.

[5]   B.Tay," Development and implementation of New Control Law for Vision Based Target Tracking system onboard small unmanned aerial vehicles," Master's Thesis, Naval Postgraduate School, Monterey CA, 2006.

[6]   H.K. Khalil, "Nonlinear systems," Prentice Hall, 3rd edition 2001.

[7]   Ogata Katsuhiko, "Modern Control Engineering," Fourth edition, New Jersey. Prentice Hall, 2002.

[8]   Bill Vagilienti, and Ross Hoag, "Piccolo System User Guide." Cloud Cap Technologies, 2004, from http://www.cloudcaptech.com (10 Nov 2007).

[9]   "Introduction to PC 104 Setup, Building XPC Model for Target PC," from http://lims.mech.northwestern.edu/students/stephens/me333/main.html (11 Nov 2007).

[10]   "PC 104 Embedded System FAQ," http://www.controlled.com/pc104faq/ (14 Nov 2007).

THIS PAGE INTENTIONALLY LEFT BLANK

Figure 23.   SIMULINK MODEL

Figure 24.   XPC HIL MODEL

APPENDIX II: STATIONARY TARGET TRACKING

Stationary Target Tracking: Case 2: $k_1 = 0.1$

(a) SUAV & Target Trajectory
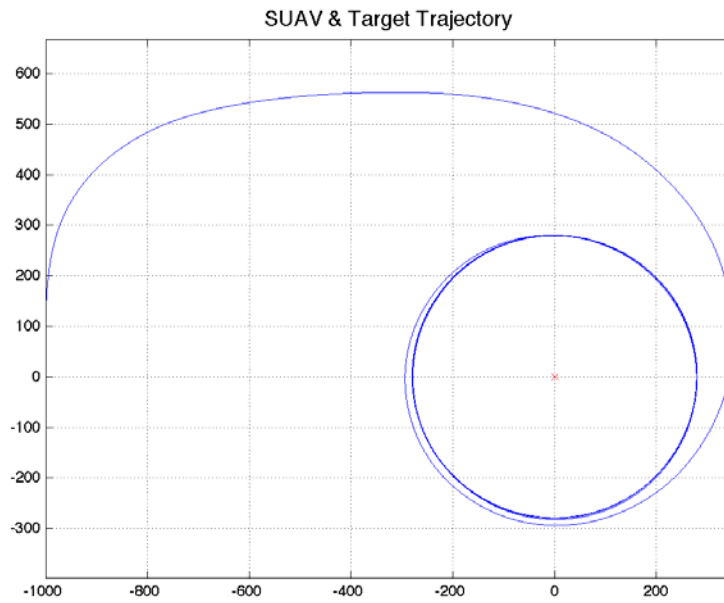
(b) Range Convergence Performance, $\rho_d = 300$ m, (280m 138sec)
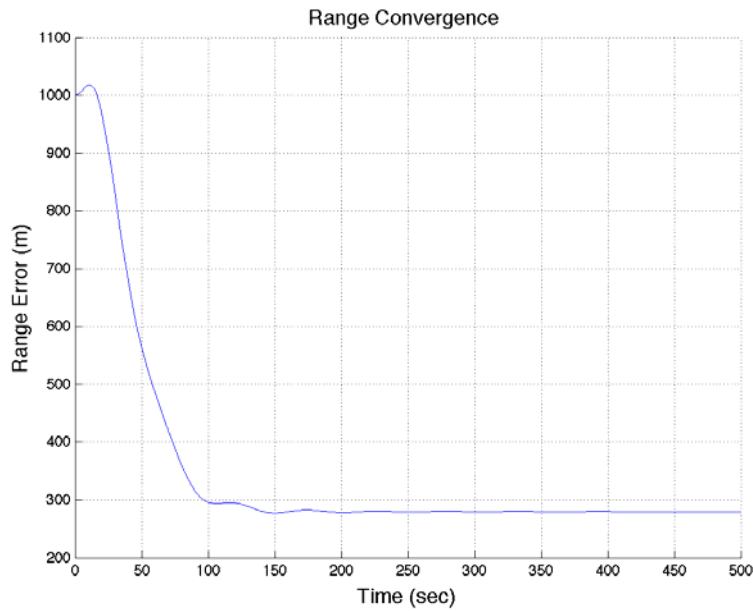
(c) Navigation bearing error Convergence Performance
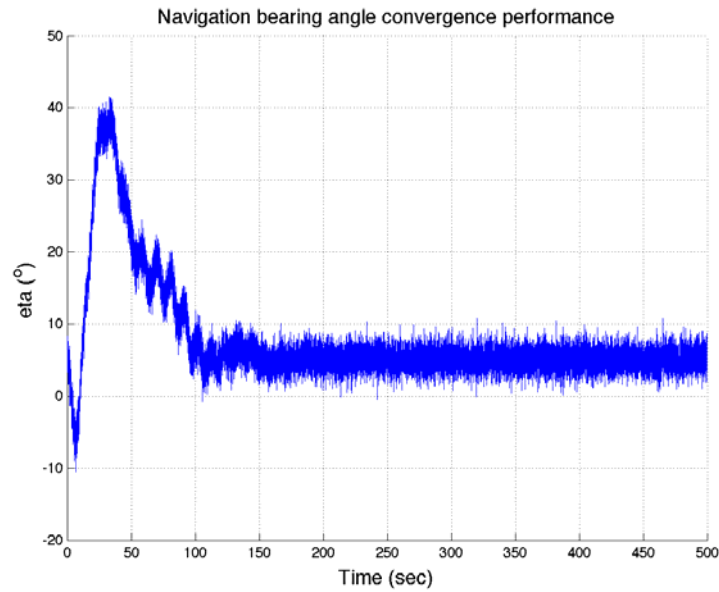
Figure 25.　　SUAV Target Tracking Performance with Gain $k_1 = 0.1$

Stationary Target Tracking Case 3: $k_1 = 0.2$

(a) SUAV & Target Trajectory
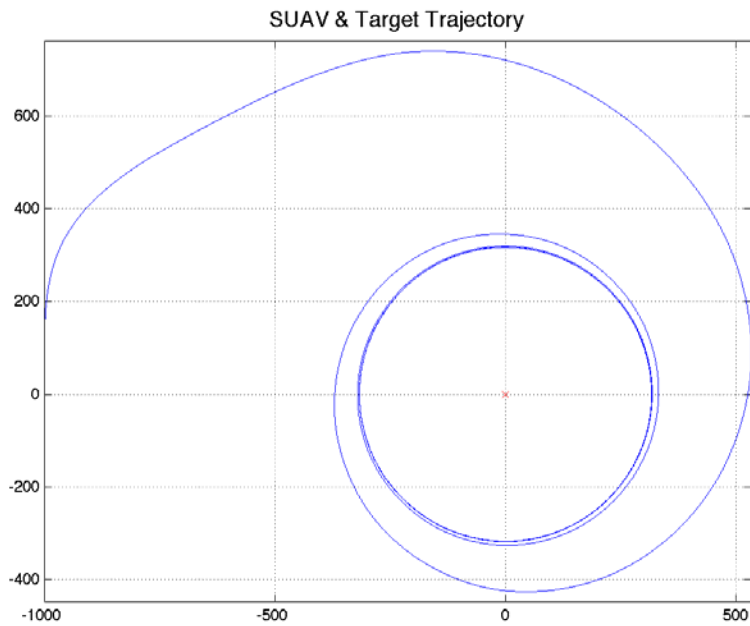
(b) Range Convergence Performance, $\rho_d = 300$ m (229s, 317m)
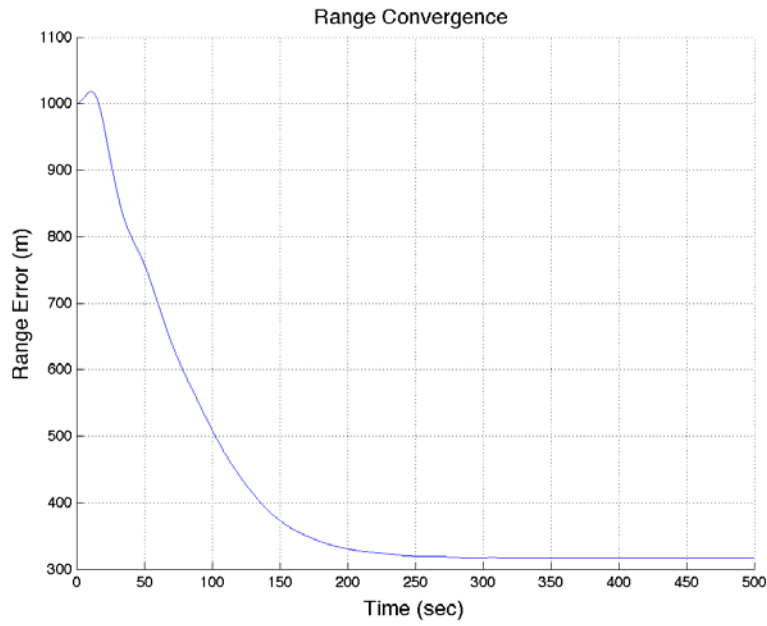
(c) Navigation bearing error Convergence Performance
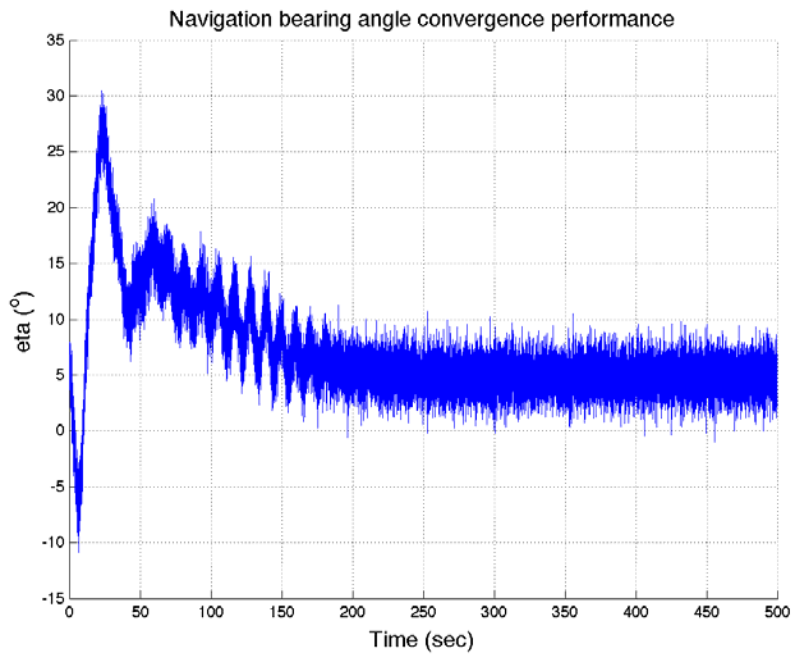
Figure 26.   SUAV Target Tracking Performance with Gain $k_1 = 0.2$

Stationary Target Tracking Case 4: $k_1 = 0.3$
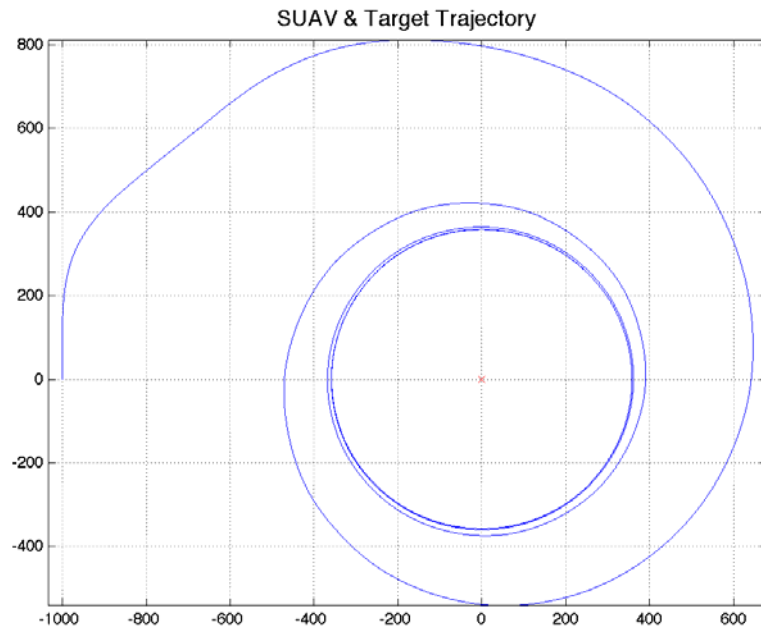
(a) SUAV & Target Trajectory
(b) Range Convergence Performance, $\rho_d = 300$ m (291s, 358m)
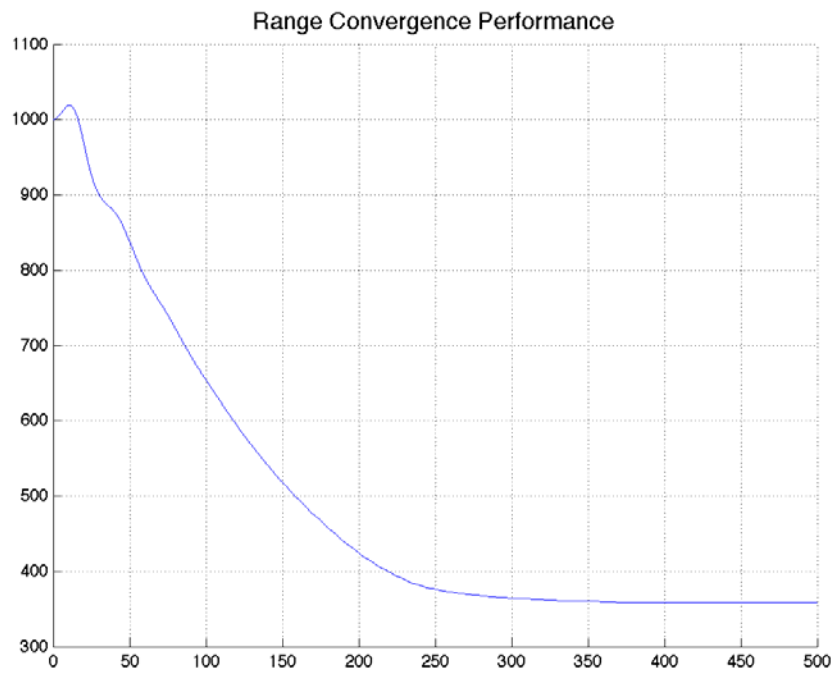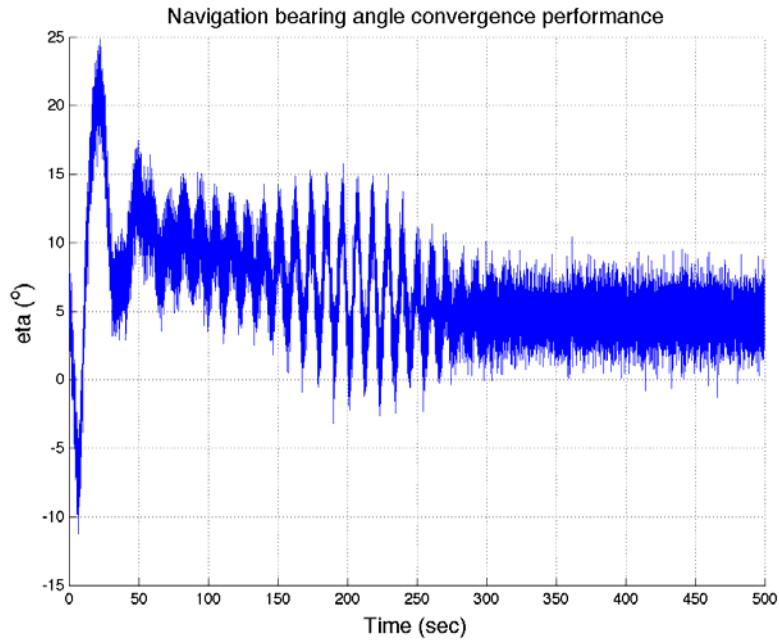
Figure 27.   SUAV Target Tracking Performance with Gain $k_1 = 0.3$

Stationary Target Tracking Case 5: $k_1 = 0.4$

(a) SUAV & Target Trajectory (460s, 396m)
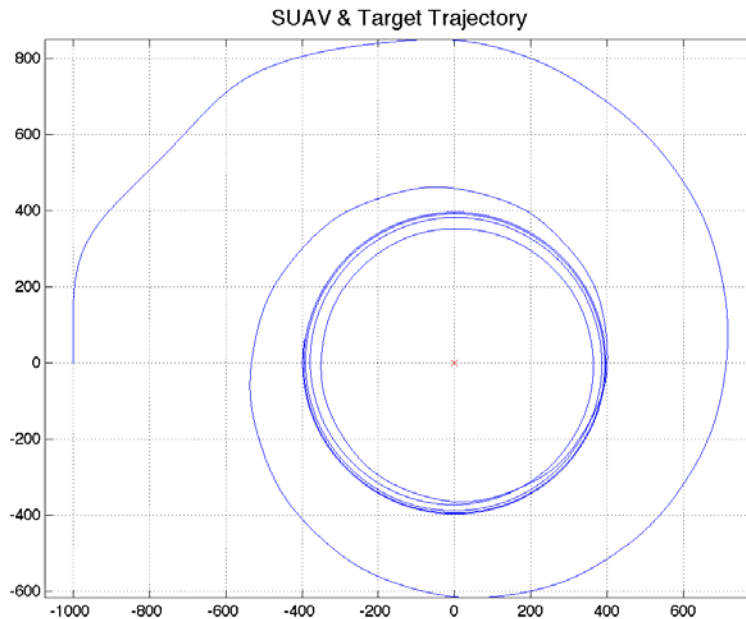
57
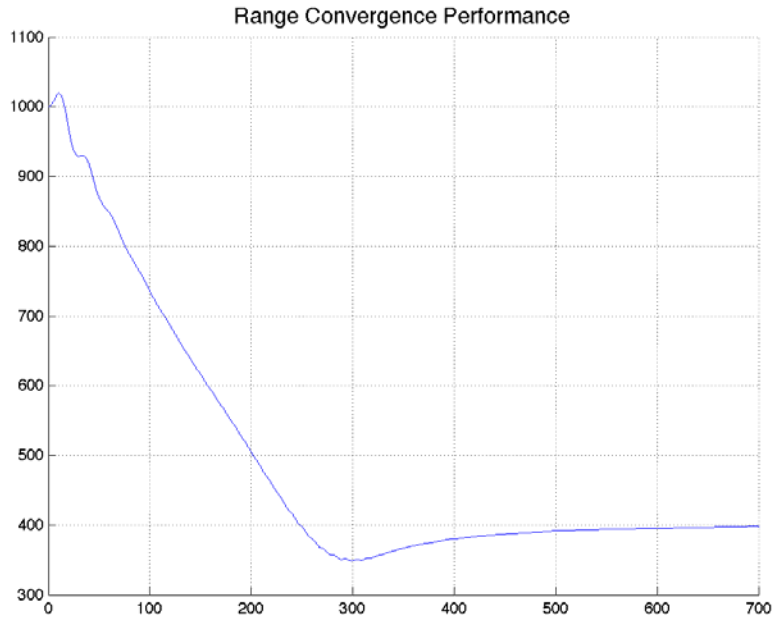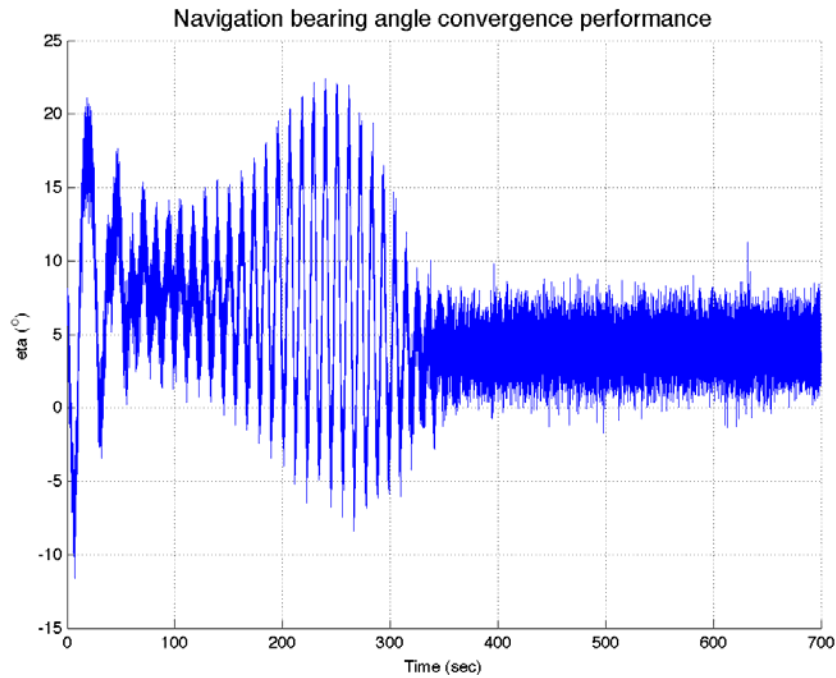
Figure 28. SUAV Target Tracking Performance with Gain $k_1 = 0.4$

APPENDIX III: NON-MANEUVERING TARGET TRACKING

Performance Benchmark Case 1: $k_1 = 0.4$

(a) SUAV & Target Trajectory
(b) Range Convergence Performance, $\rho_d = 300$ m, (280m 138sec)
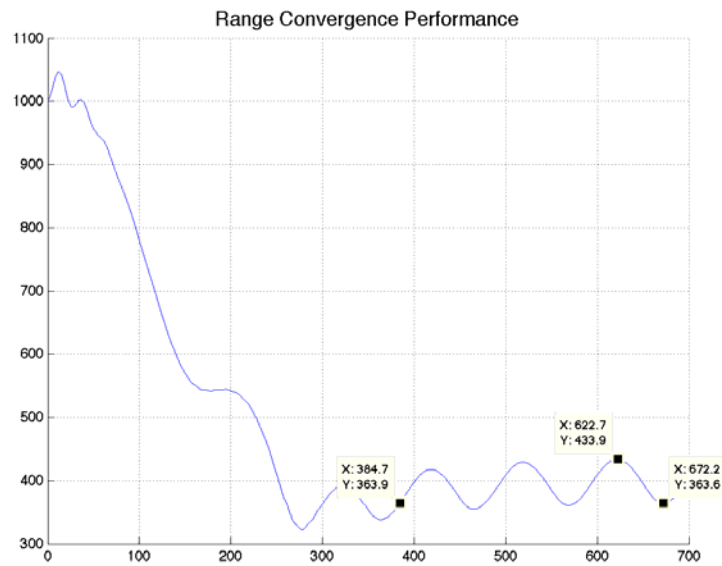
Figure 29.   Non-Maneuvering Target Tracking Performance with Gain $k_1 = 0.4$

Performance Benchmark Case 2: $k_1 = 0.3$

(a) SUAV & Target Trajectory
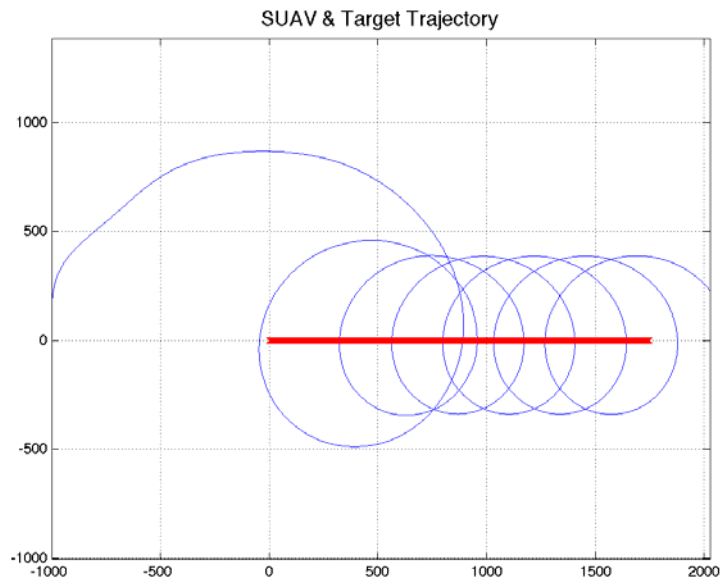
(b) Range Convergence Performance, $\rho_d = 300$ m
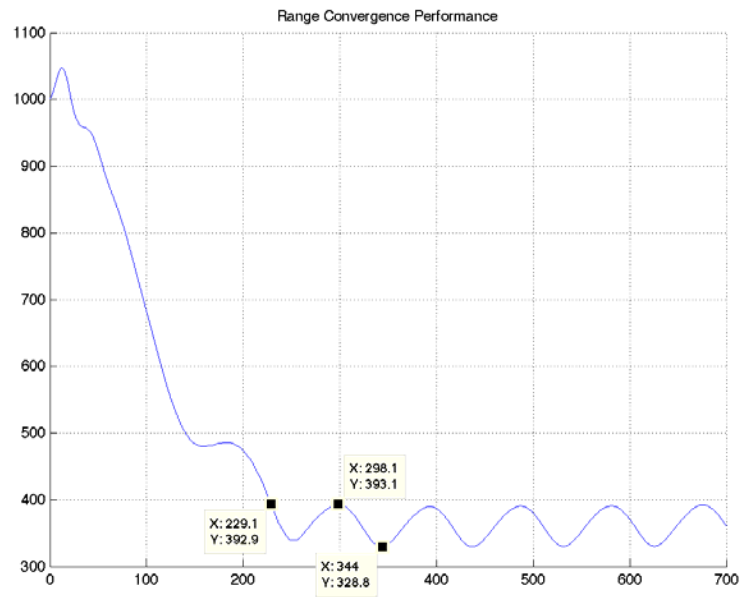
(c) Navigation bearing error Convergence Performance
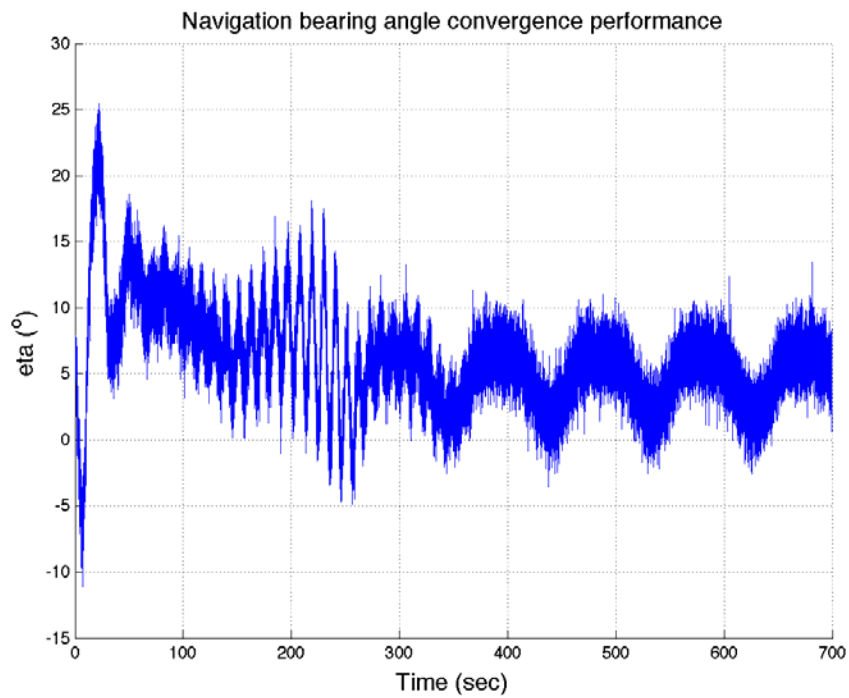
Figure 30.   Non-Maneuvering Target Tracking Performance with Gain $k_1 = 0.3$

Performance Benchmark Case 3: $k_1 = 0.2$

(a) SUAV & Target Trajectory

(b) Range Convergence Performance, $\rho_d = 300$
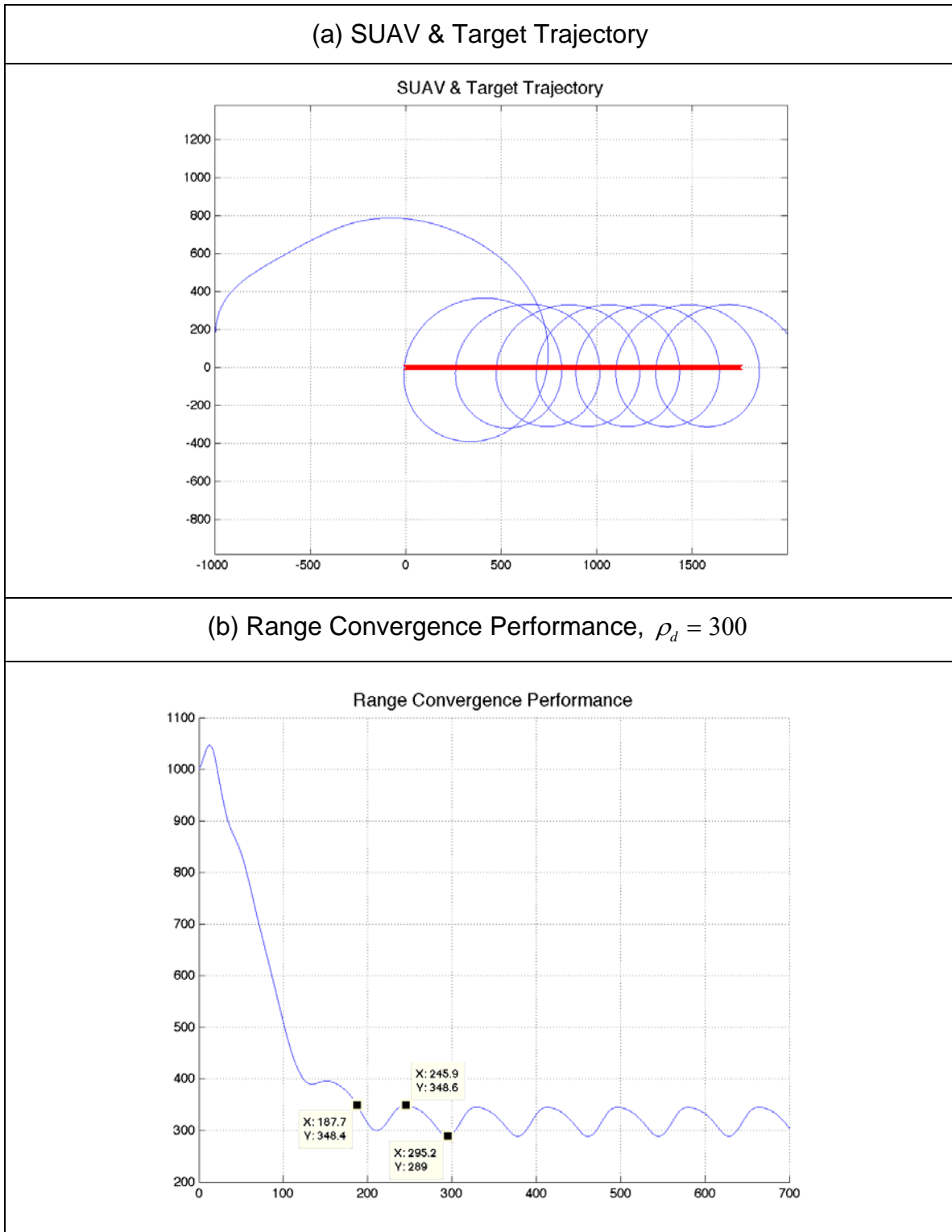
Figure 31.　　Non-Maneuvering Target Tracking Performance with Gain $k_1 = 0.2$

Performance Benchmark Case 4: $k_1 = 0.1$

(a) SUAV & Target Trajectory
(b) Range Convergence Performance, $\rho_d = 300$
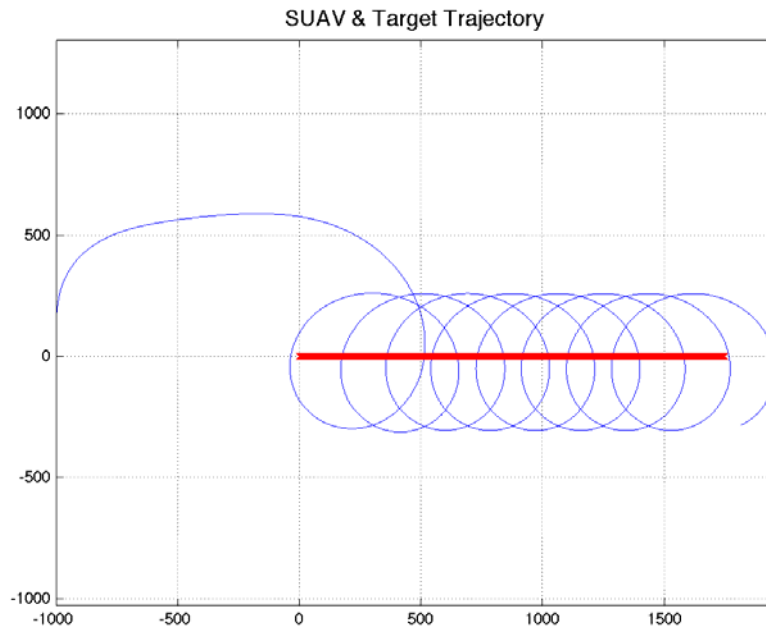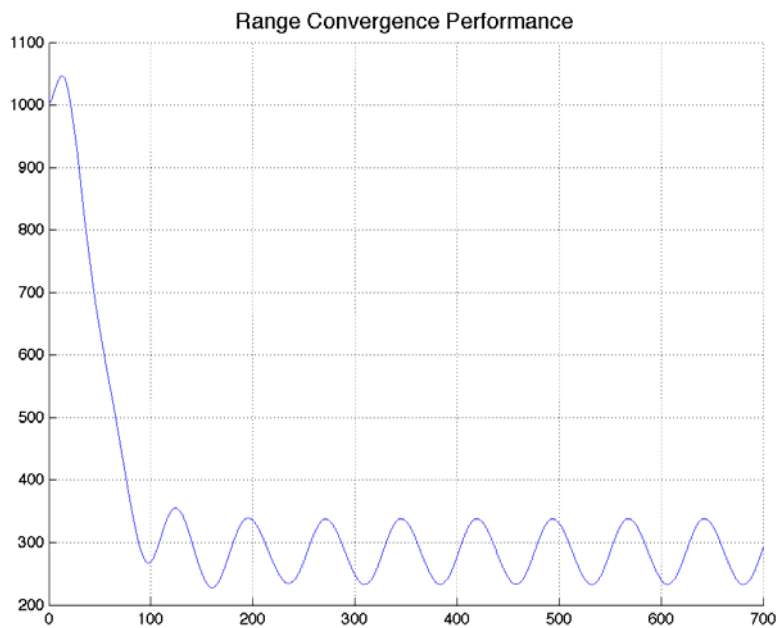
(c) Navigation bearing error Convergence Performance
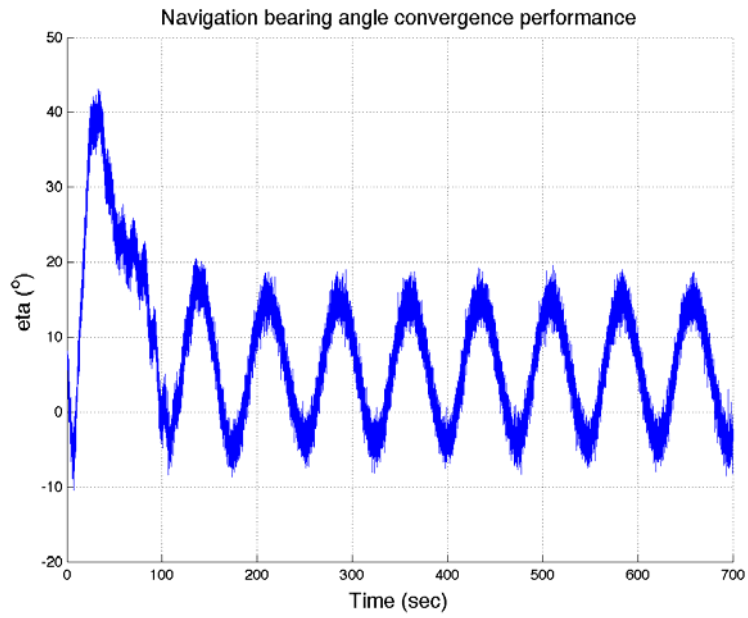
Figure 32.　　Non-Maneuvering Target Tracking Performance with Gain $k_1 = 0.1$

Performance Benchmark Case 4: $k_1 = 0.05$

(a) SUAV & Target Trajectory
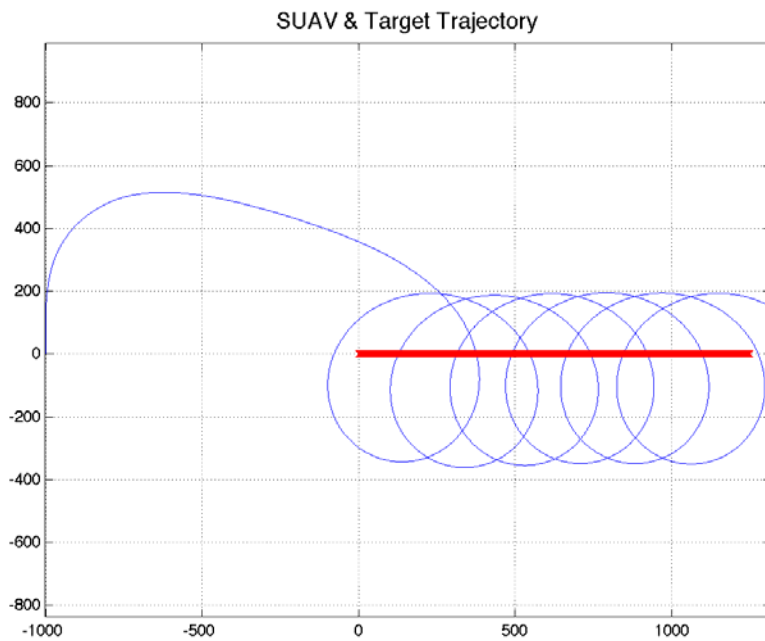
(b) Range Convergence Performance, $\rho_d = 300$
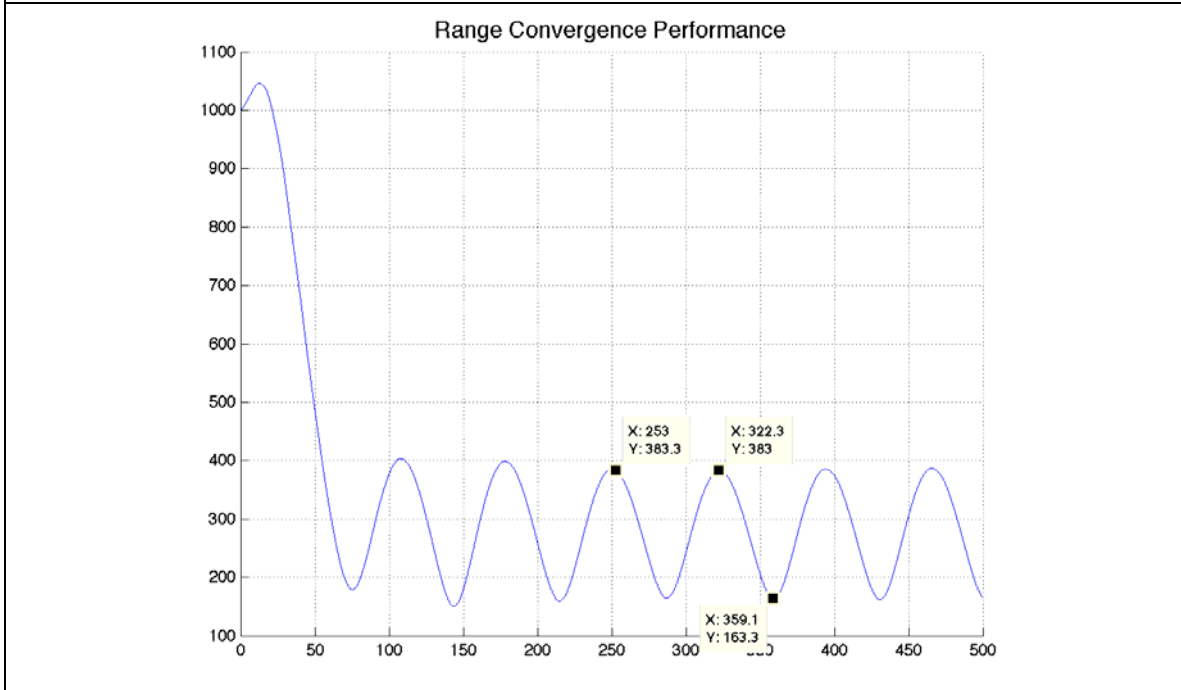
(c) Navigation bearing error Convergence Performance
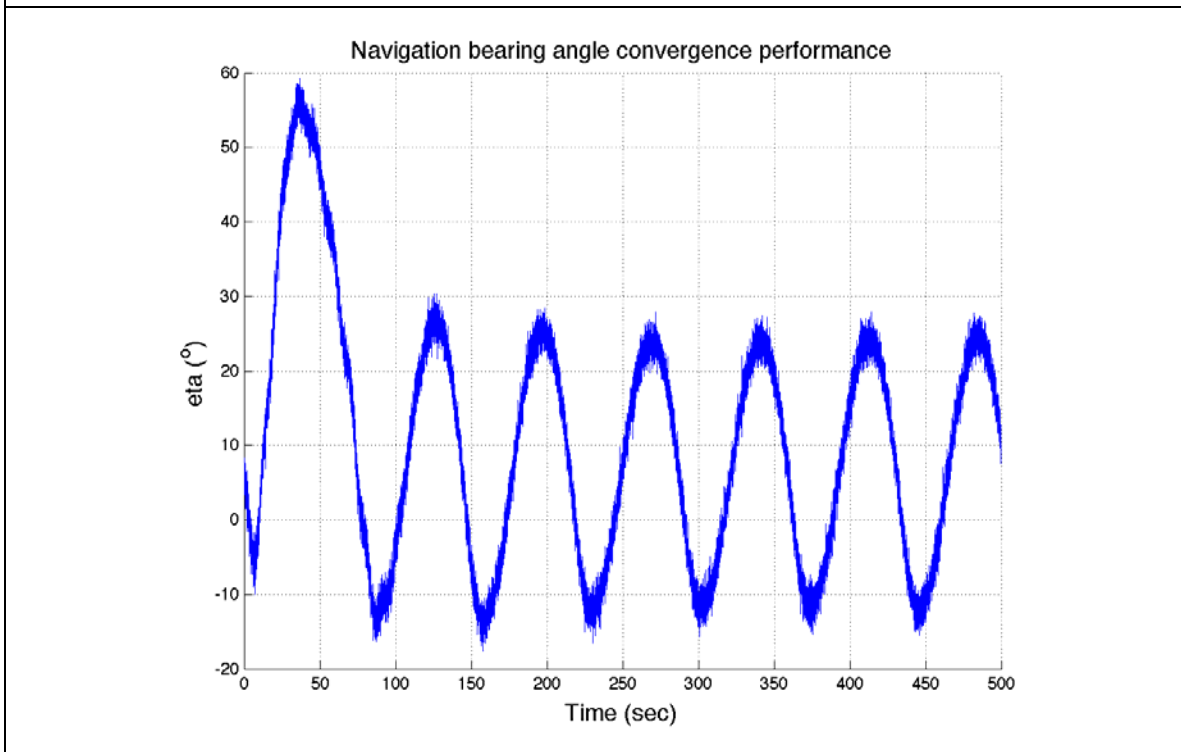
Figure 33.   Non-Maneuvering Target Tracking Performance with Gain $k_1 = 0.05$

Target Speed Sensitivity Case 1: $v_t = 10$ m/s

(a) SUAV & Target Trajectory
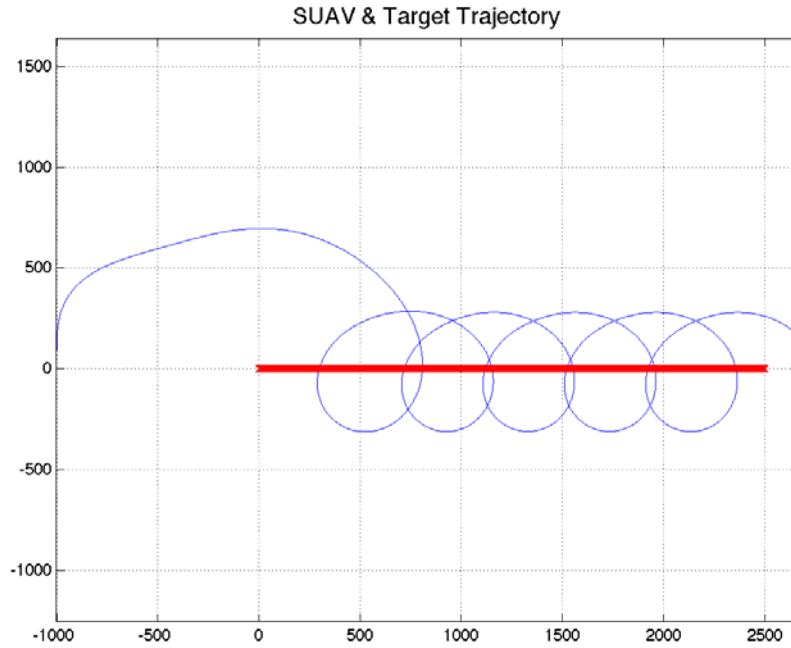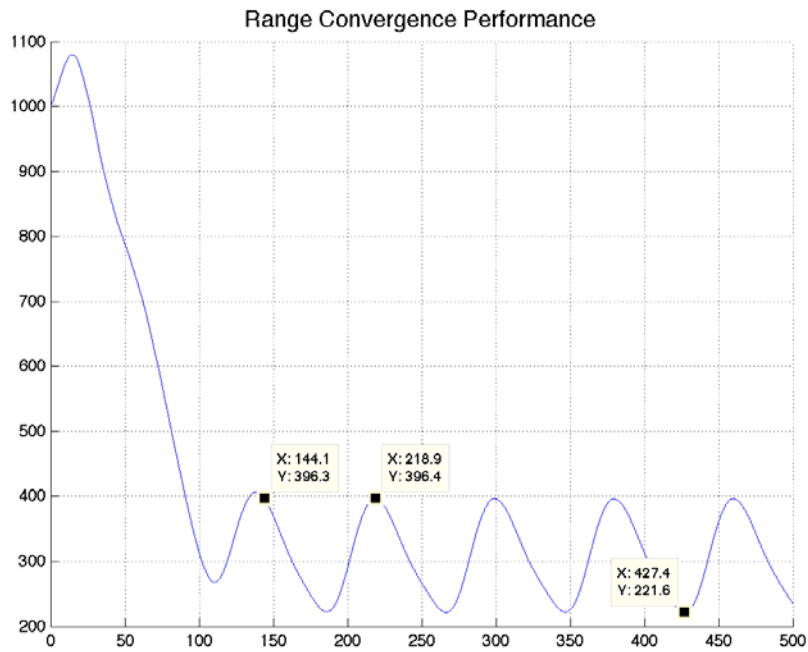
(b) Range Convergence Performance, $\rho_d = 300$
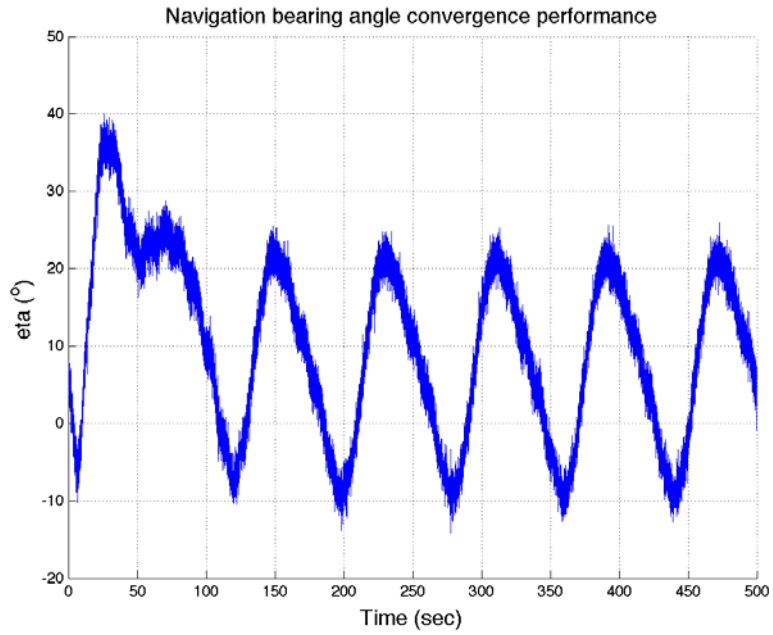
(c) Navigation bearing error Convergence Performance
(d) Adjustable Gain versus Time
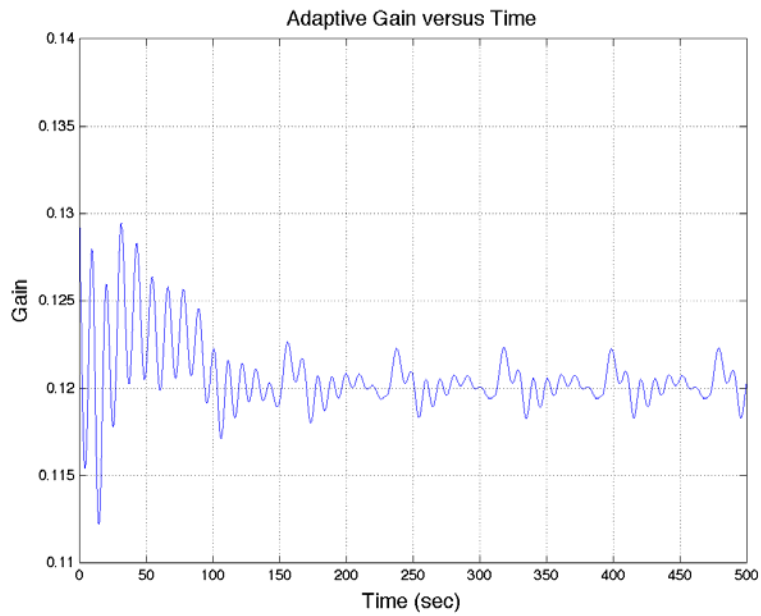
Figure 34.　　Adjustable Gain Control Law Performance $v_t = 10$ m/s

Target Speed Sensitivity Case 2: $v_t = 15$ m/s

(a) SUAV & Target Trajectory
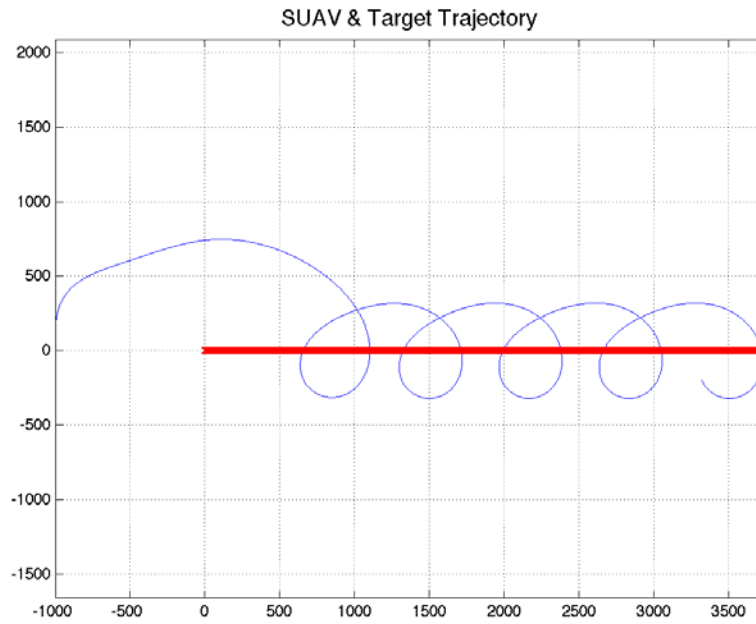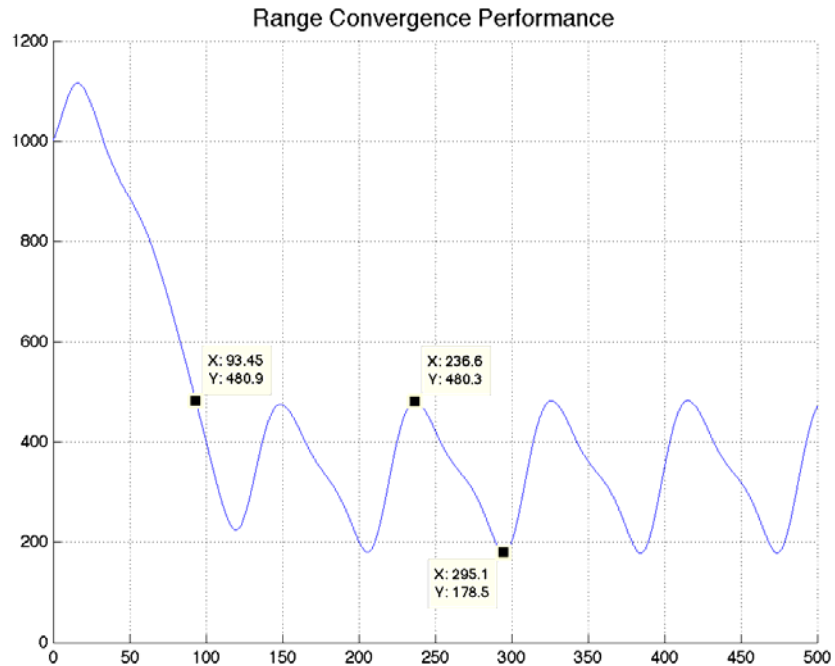
(b) Range Convergence Performance, $\rho_d = 300$
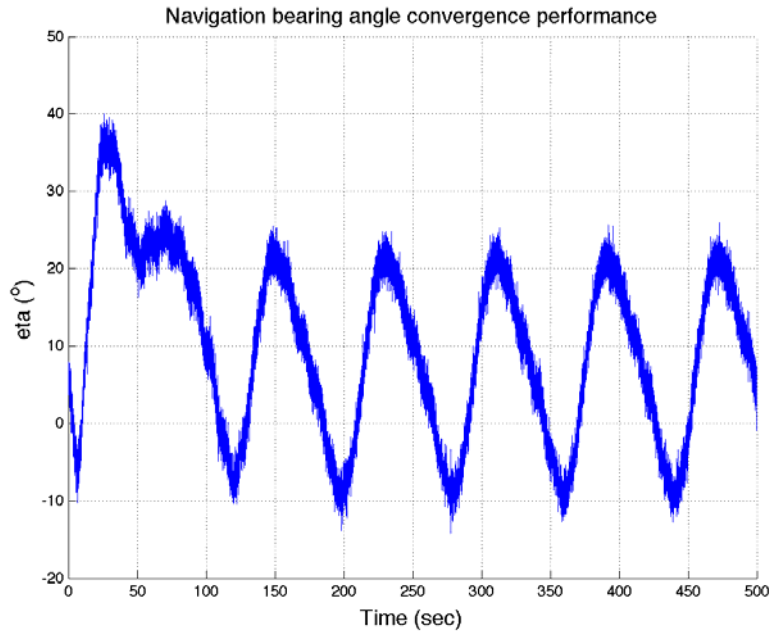
| (c) Navigation bearing error Convergence Performance |
|---|
| |
| (d) Adjustable Gain versus Time |
| |
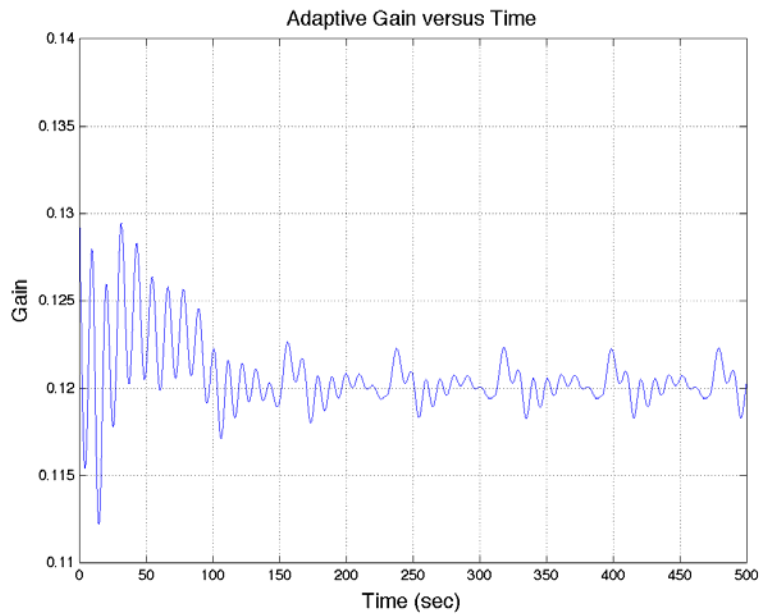
Figure 35.   Adjustable Gain Control Law Performance $v_t = 10\,\text{m/s}$

Target Speed Sensitivity Case 2: $v_t = 20 \, \text{m/s}$

(a) SUAV & Target Trajectory
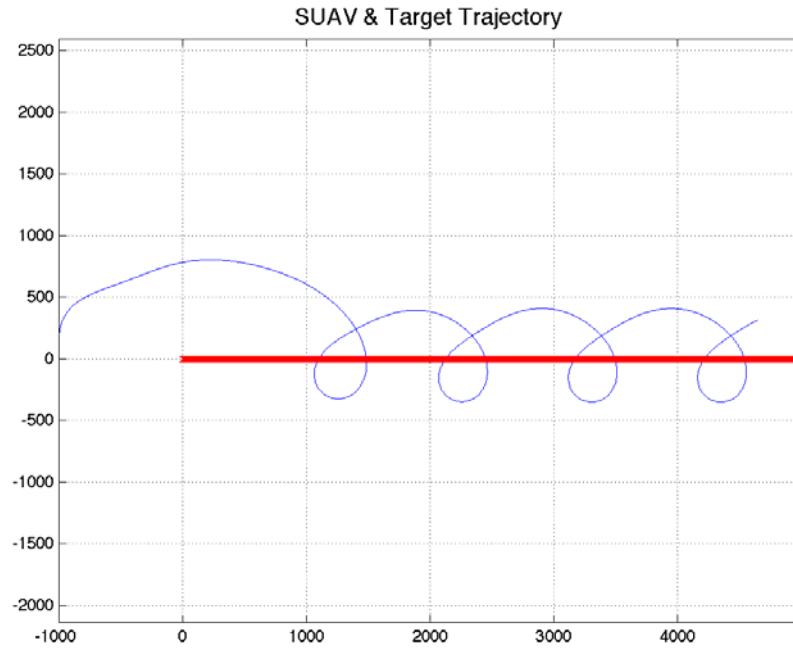
(b) Range Convergence Performance, $\rho_d = 300 \, (18.80\%)$
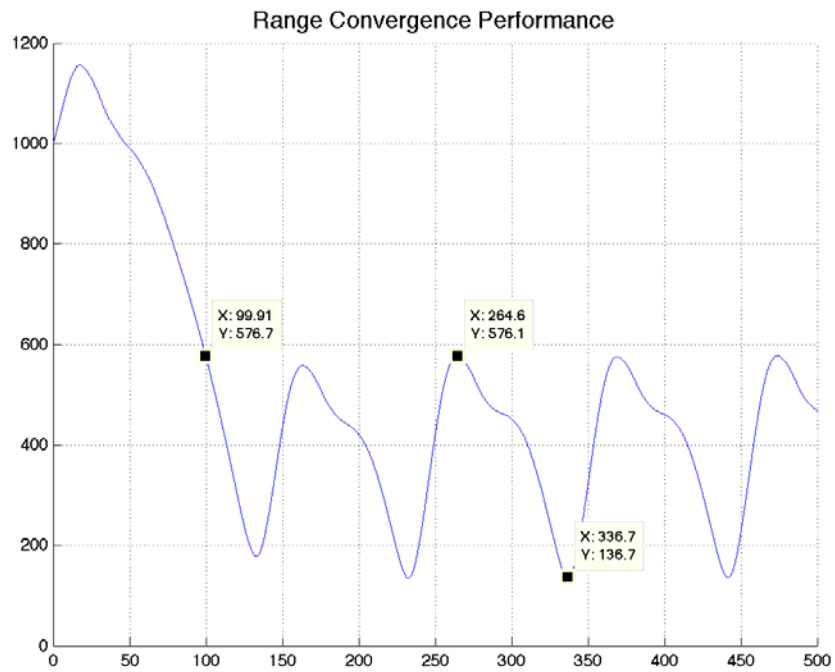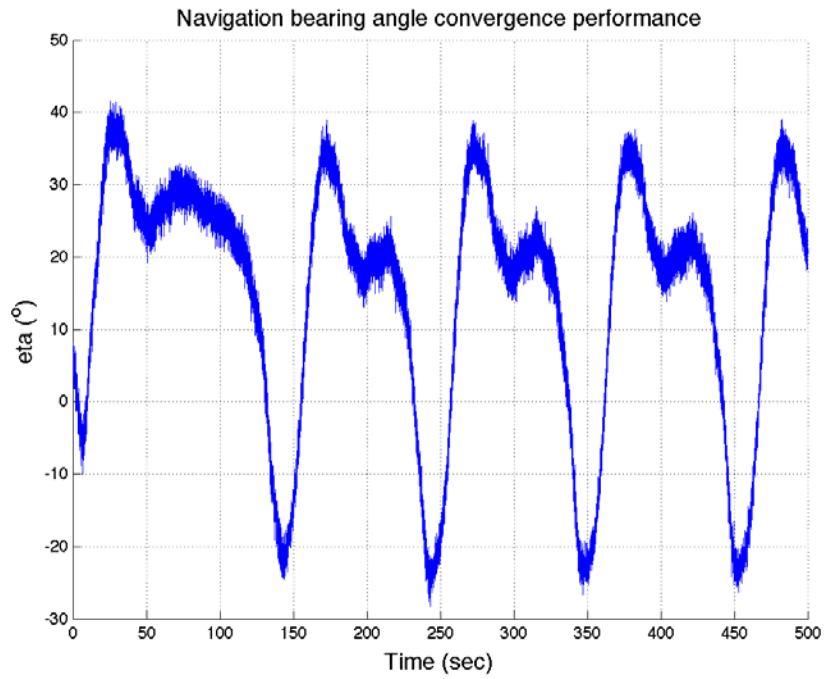
(c) Navigation bearing error Convergence Performance
Navigation bearing angle convergence performance
(d) Adjustable Gain versus Time
Adaptive Gain versus Time
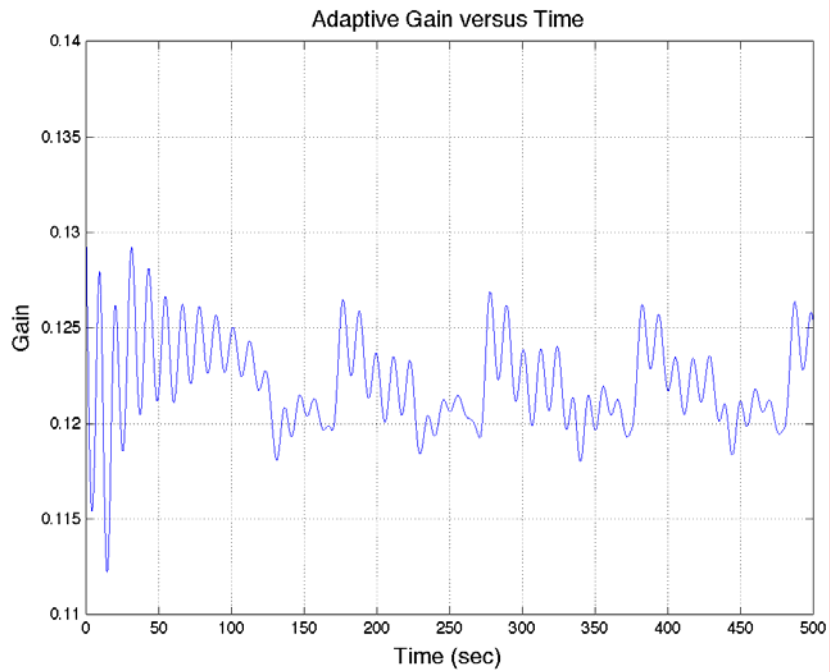
Figure 36.   Adjustable Gain Control Law Performance $v_t = 20$ m/s

THIS PAGE INTENTIONALLY LEFT BLANK

APPENDIX IV HIL SIMULATION RESULTS

Stationary Target Case 1: $k_1 = 0.1$

(a) SUAV & Target Trajectory
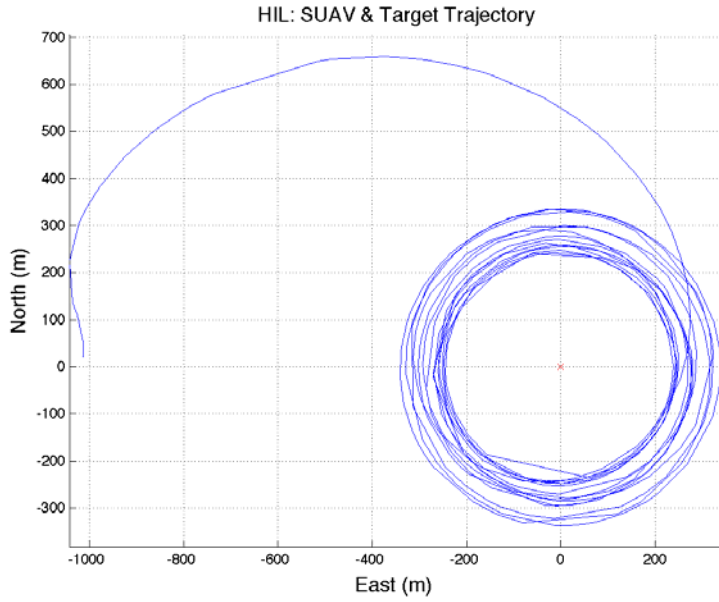
(b) Range Convergence Performance, $\rho_d = 300$
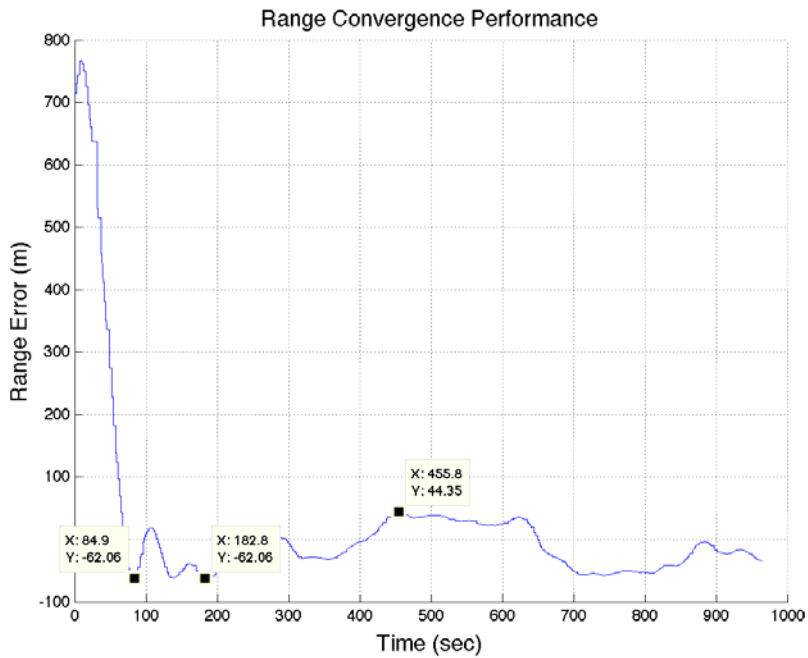
| (c) Navigation bearing error Convergence Performance |
|---|
| |
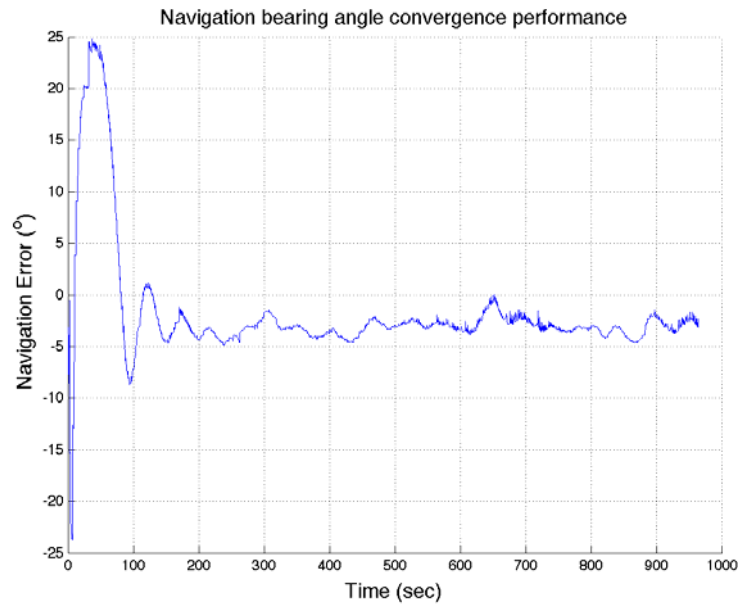
Figure 37.   Constant Gain Control Law HIL Performance $k_1 = 0.1$

Stationary Target Case 2: $k_1 = 0.2$

(a) SUAV & Target Trajectory
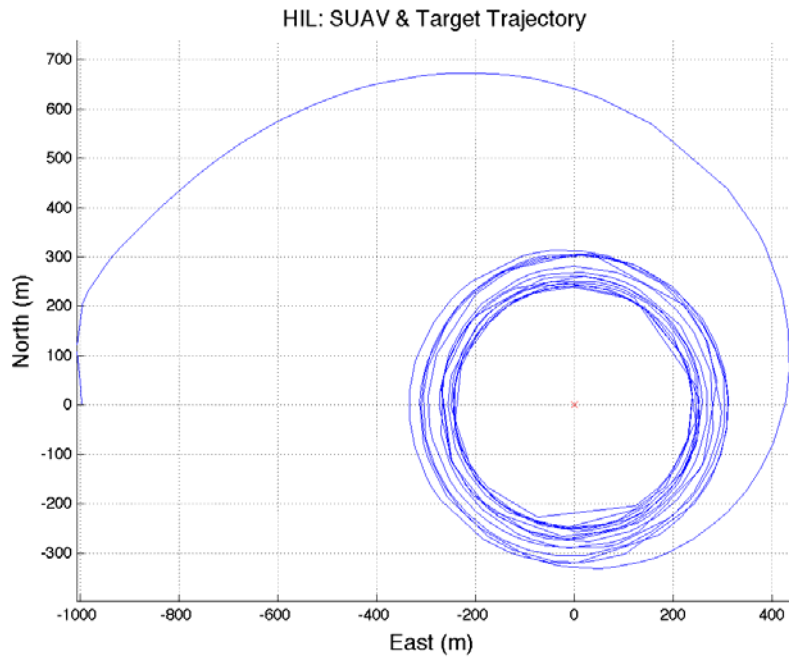
(b) Range Convergence Performance, $\rho_d = 300$
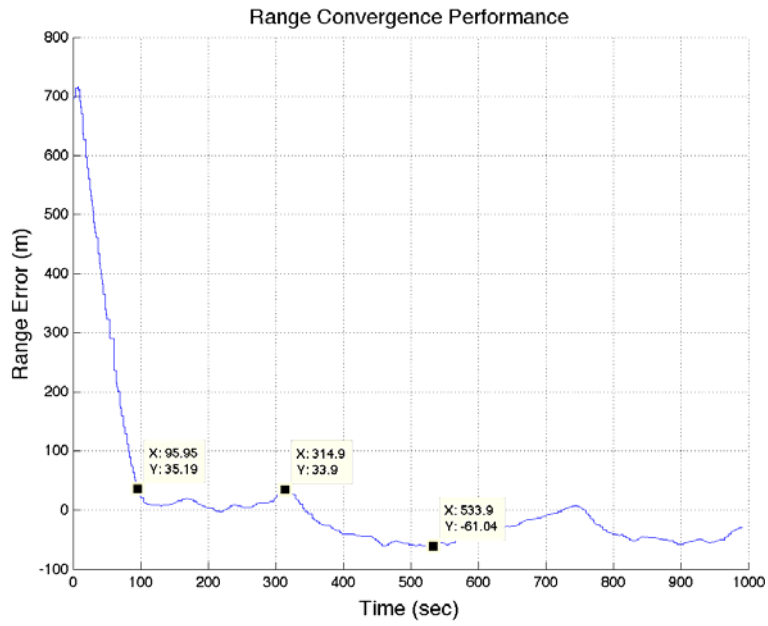

(c) Navigation bearing error Convergence Performance
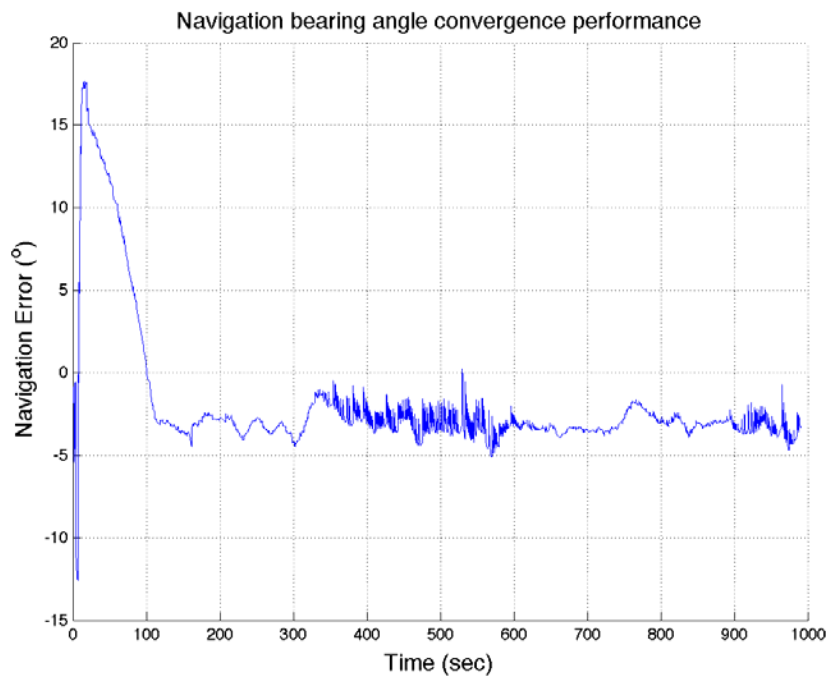
Figure 38.   Constant Gain Control Law HIL Performance $k_1 = 0.2$

Stationary Target Case 3: $k_1 = 0.3$

(a) SUAV & Target Trajectory
(b) Range Convergence Performance, $\rho_d = 300$
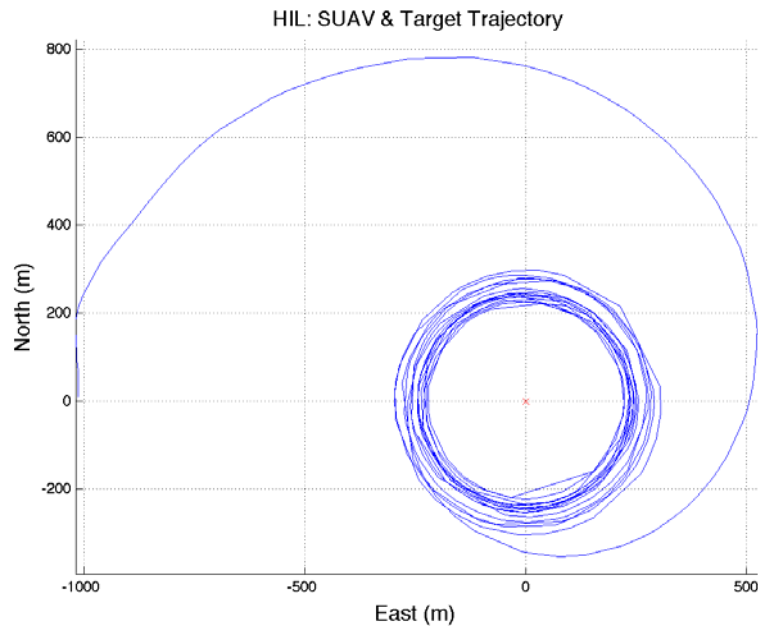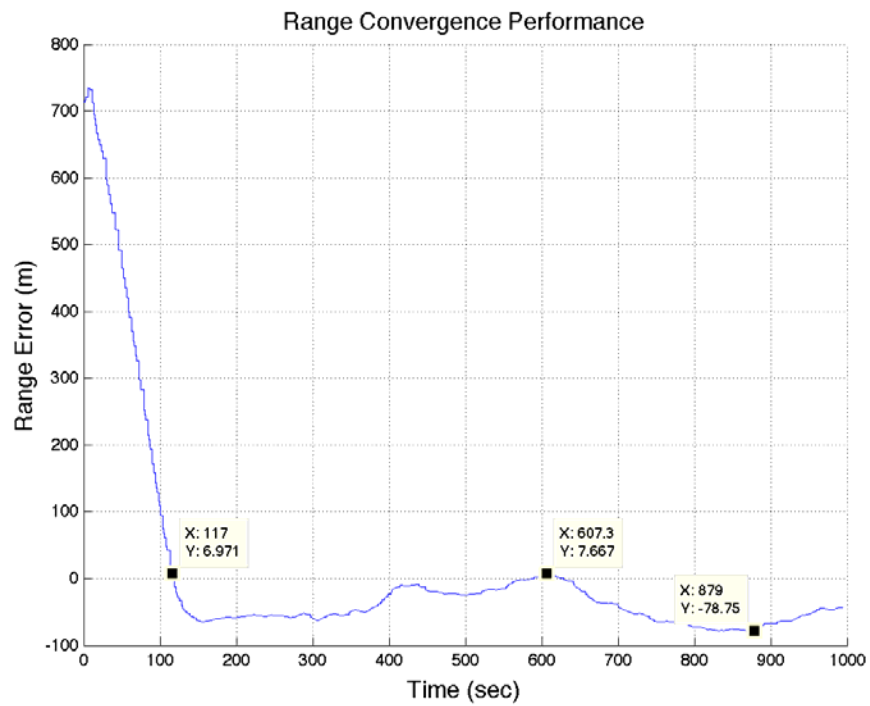
(c) Navigation bearing error Convergence Performance
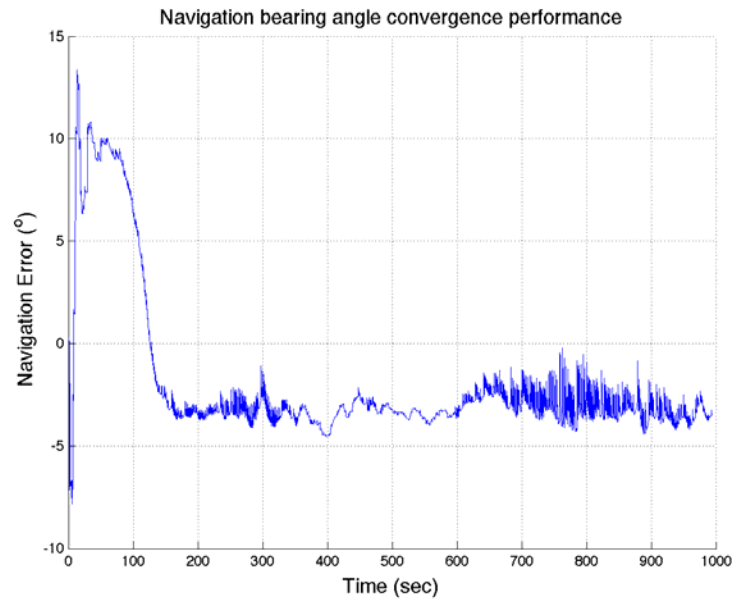
Figure 39.   Constant Gain Control Law HIL Performance $k_1 = 0.3$

Stationary Target Case 4: $k_1 = 0.4$

(a) SUAV & Target Trajectory
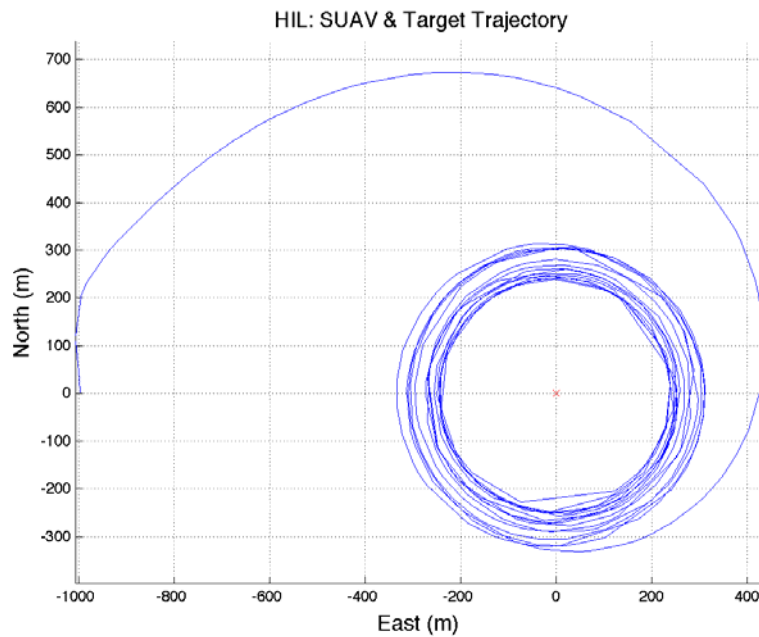
(b) Range Convergence Performance, $\rho_d = 300$
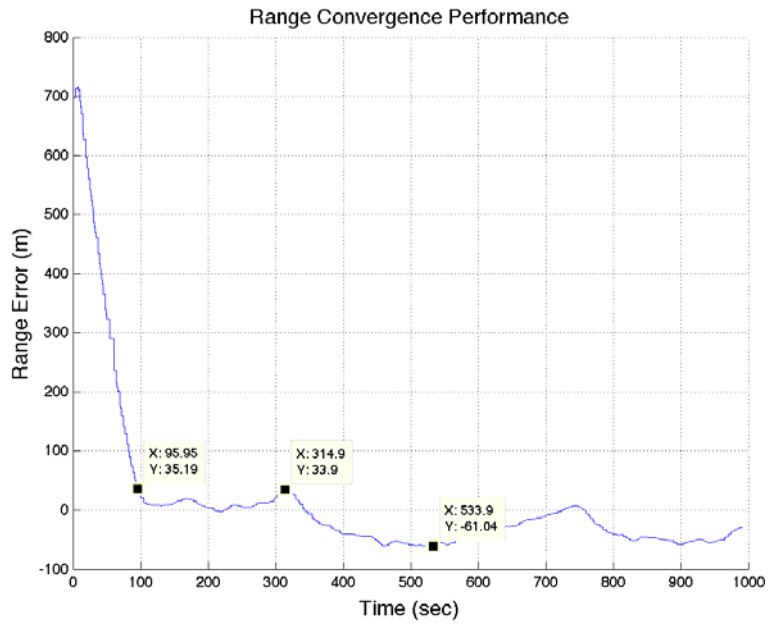
(c) Navigation bearing error Convergence Performance
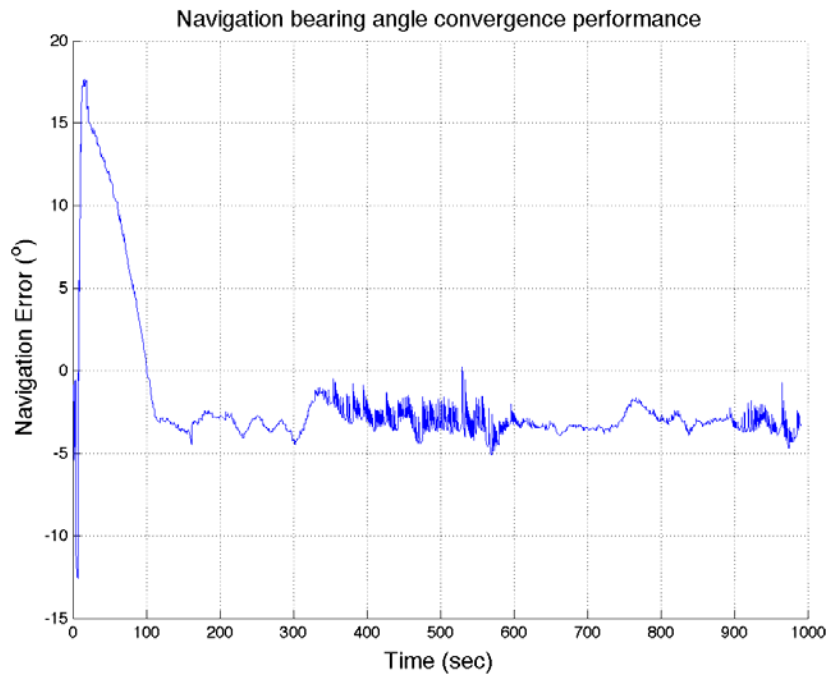
Figure 40.　　Constant Gain Control Law HIL Performance $k_1 = 0.4$

Stationary Target Case 5: $k_1 = 0.05$

(a) SUAV & Target Trajectory
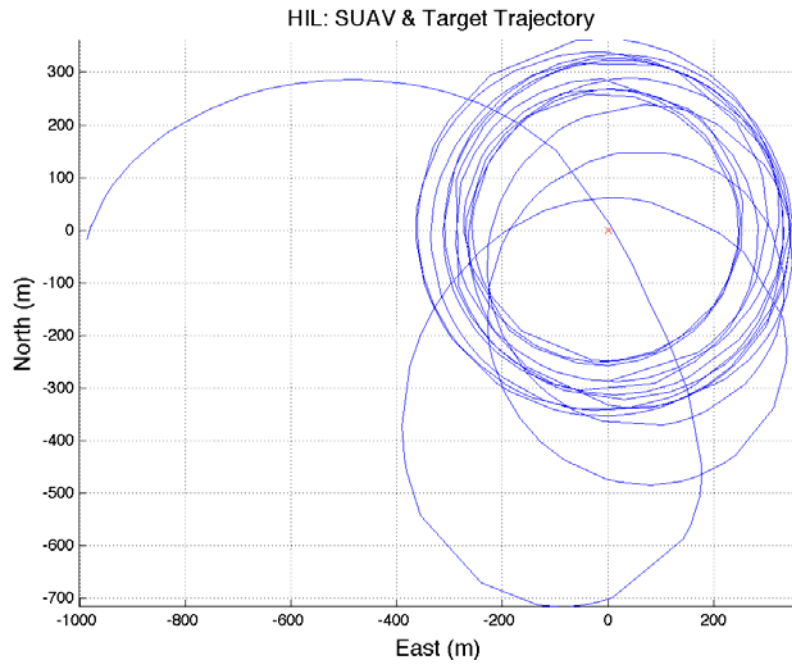
(b) Range Convergence Performance, $\rho_d = 300$
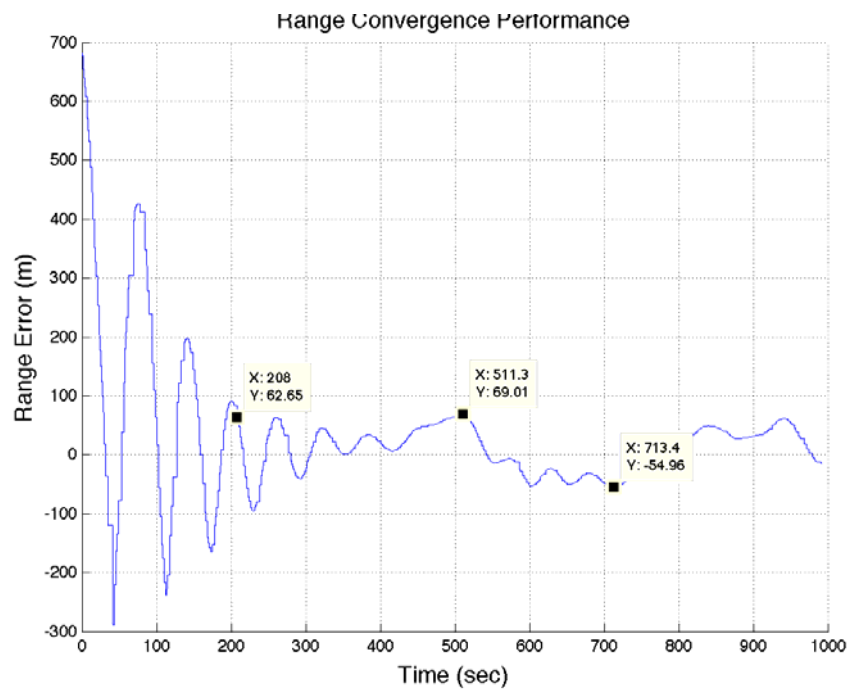
(c) Navigation Error Performance, $\rho_d = 300$

Navigation bearing angle convergence performance
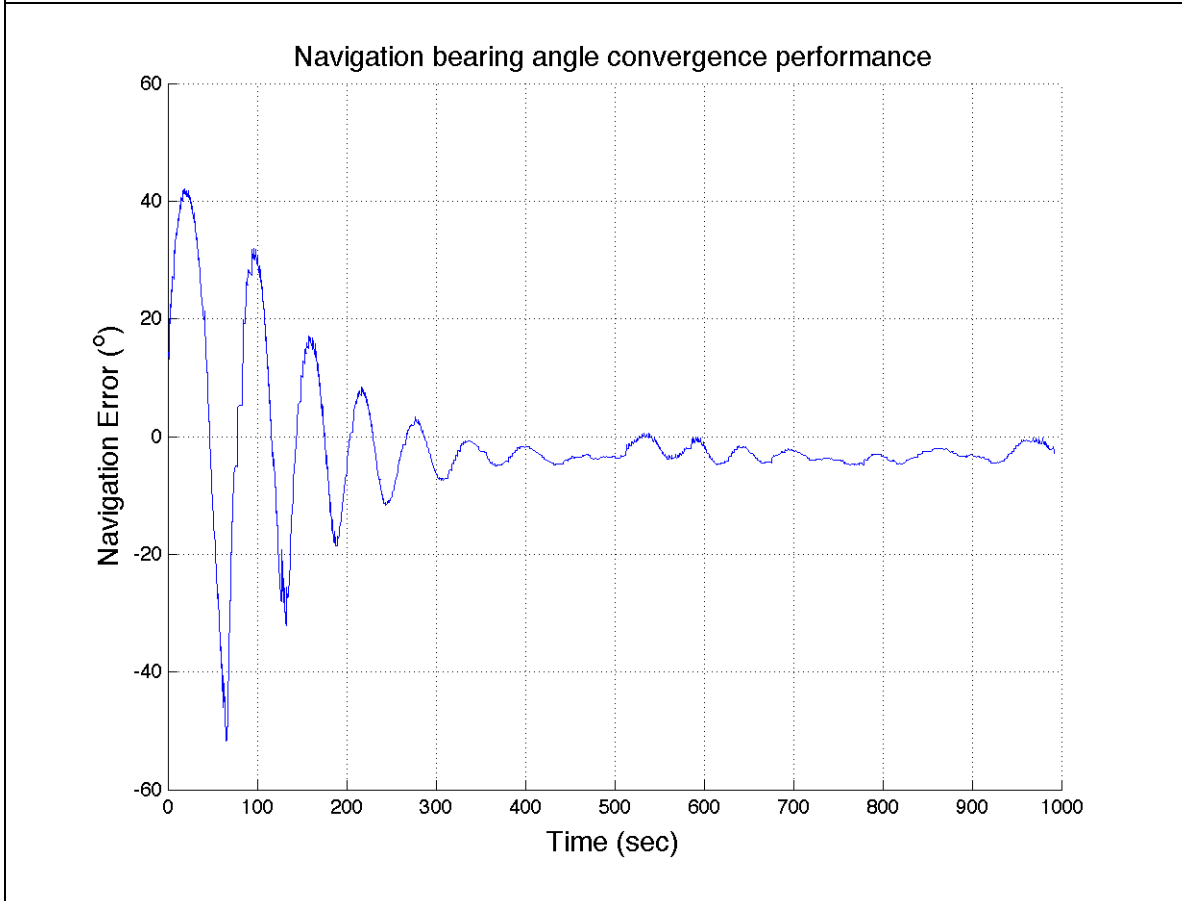
Non-maneuvering Target Case 1: $v_t = 5$

(a) SUAV & Target Trajectory
(b) Range Convergence Performance, $\rho_d = 300$
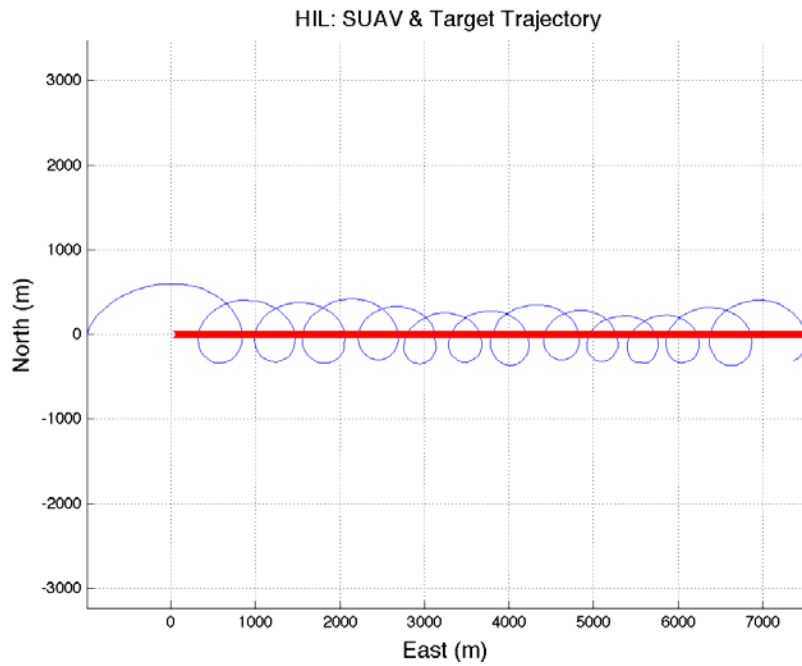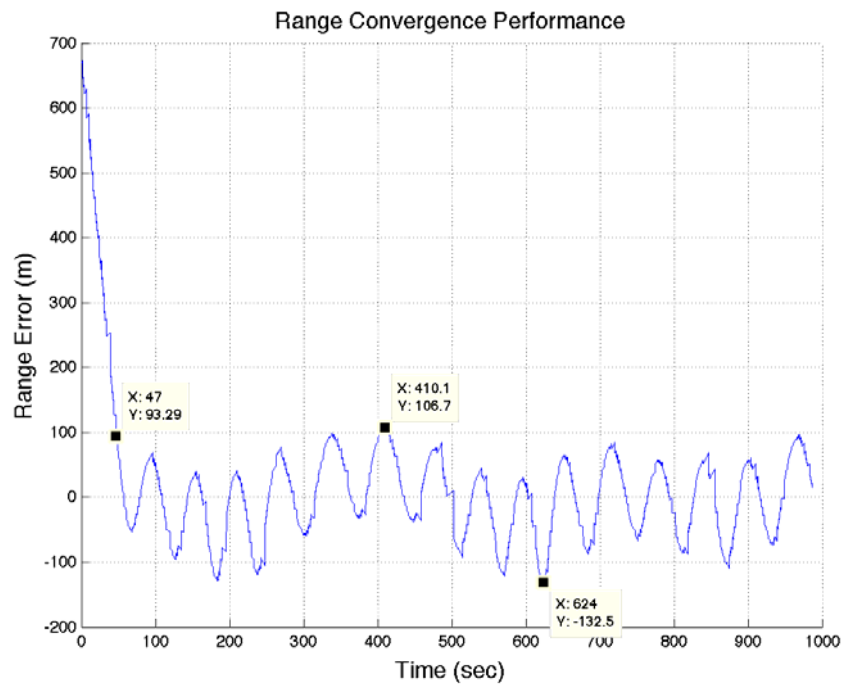
(c) Navigation bearing error Convergence Performance
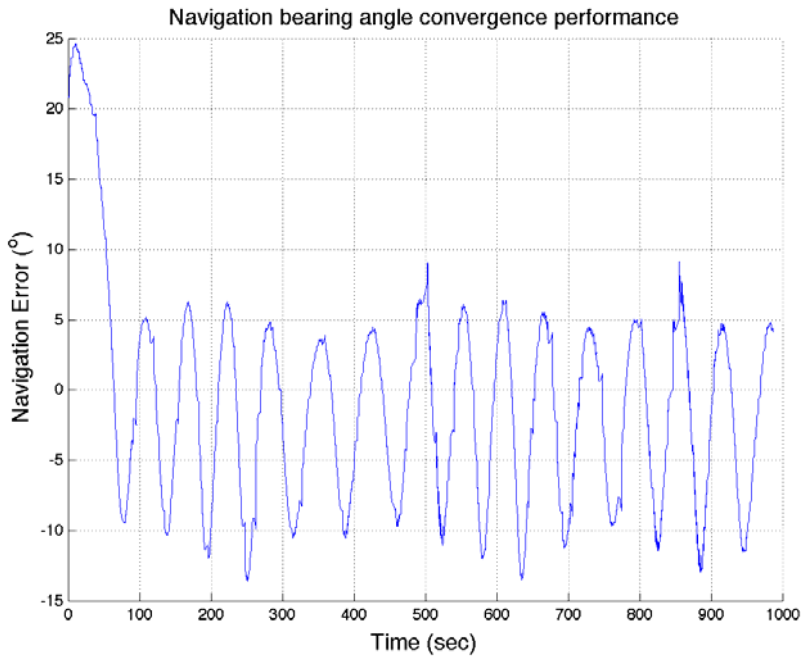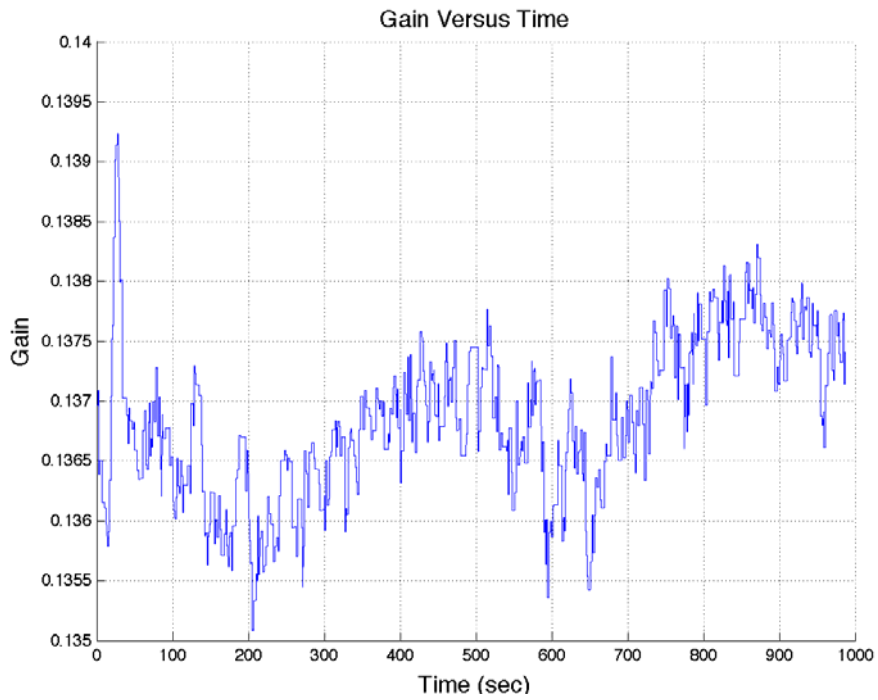
(d) Gain versus Time

Figure 41.　　HIL Performance for Non-maneuvering Target, $v_t = 5$

Non-maneuvering Target Case 2: $v_t = 10$

(a) SUAV & Target Trajectory
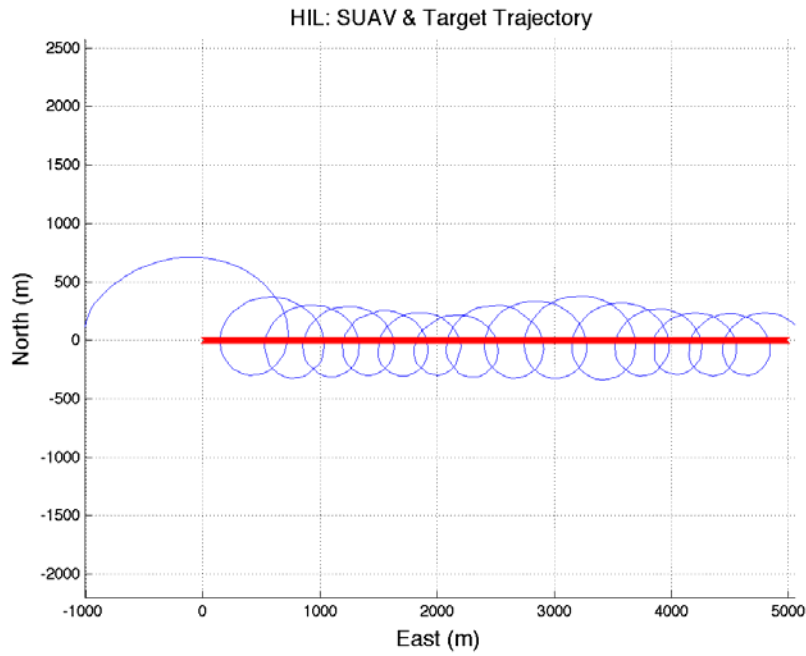
(b) Range Convergence Performance, $\rho_d = 300$

83
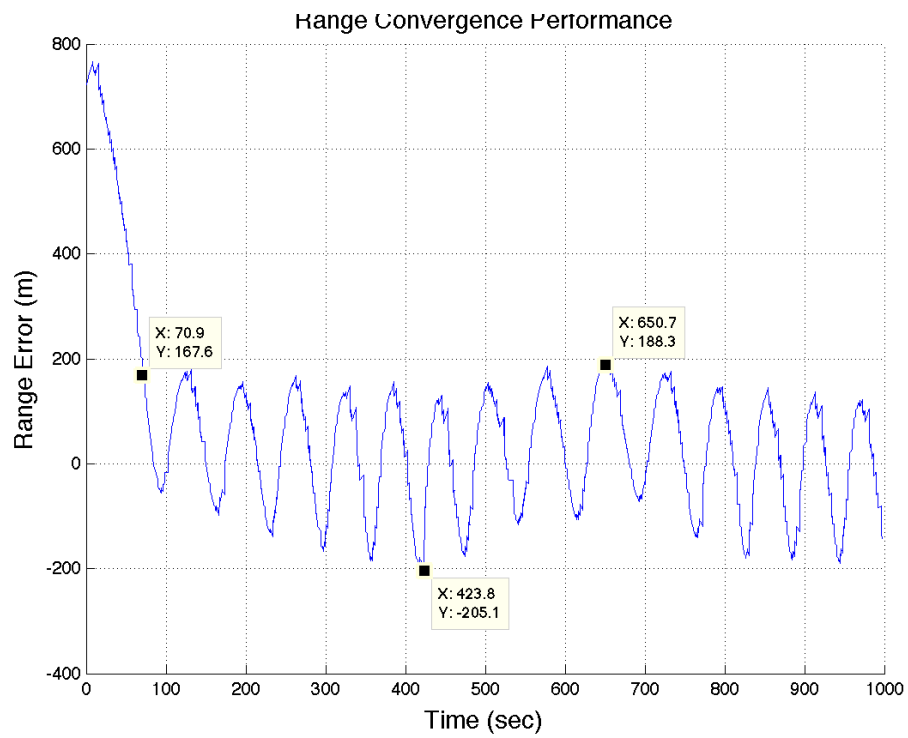
(c) Navigation bearing error Convergence Performance
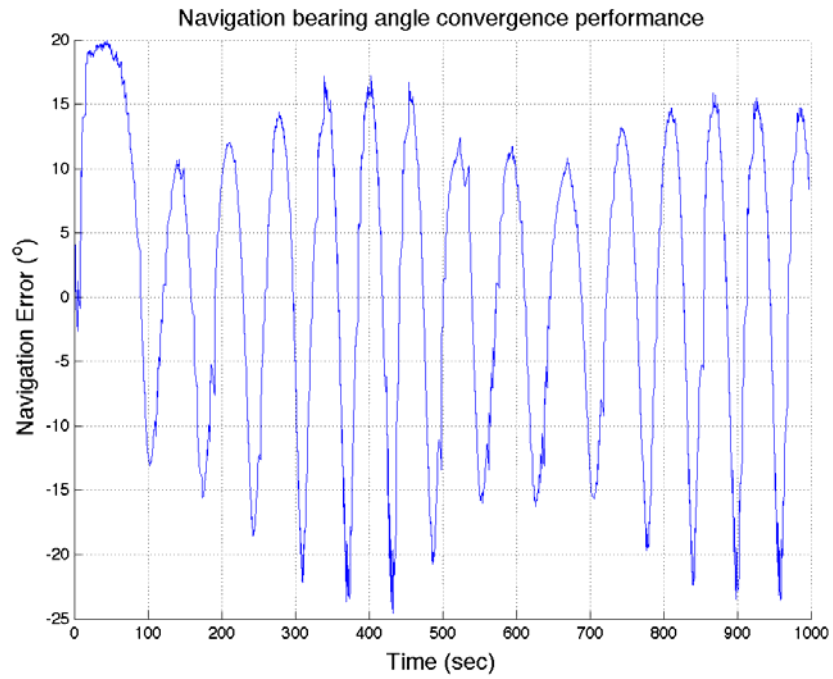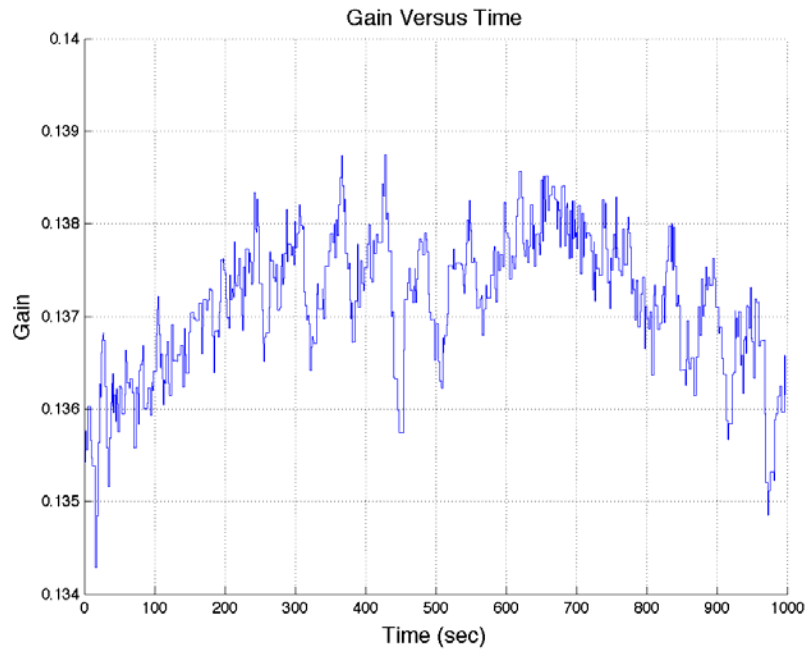
(d) Gain versus Time

Figure 42.   HIL Performance for Non-maneuvering Target, $v_t = 10$

Non-maneuvering Target Case 3: $v_t = 15$

(a) SUAV & Target Trajectory
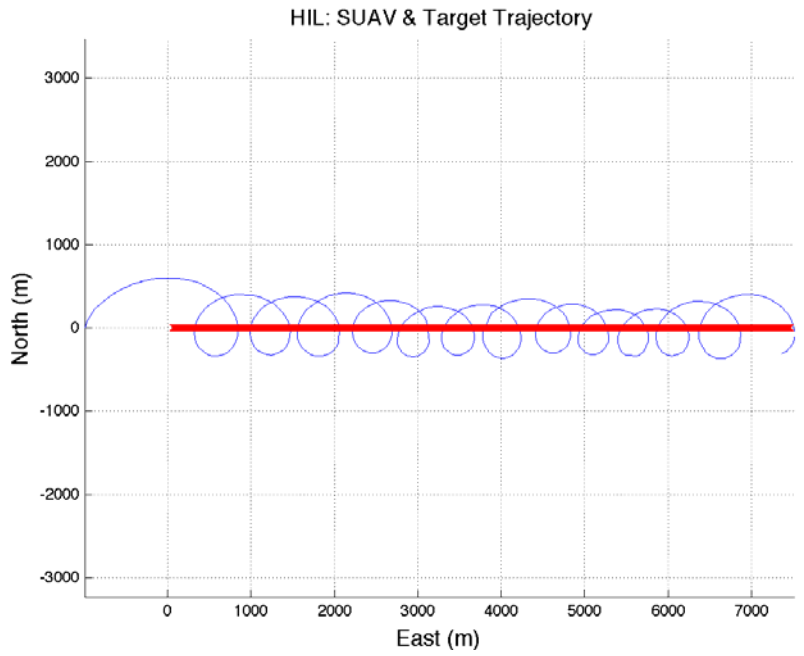
(b) Range Convergence Performance, $\rho_d = 300$
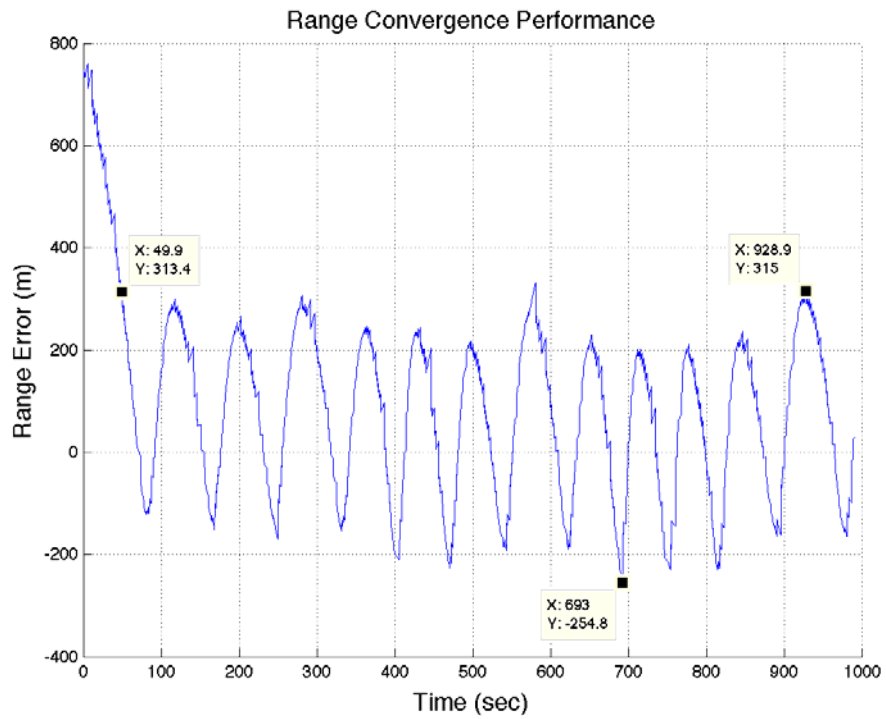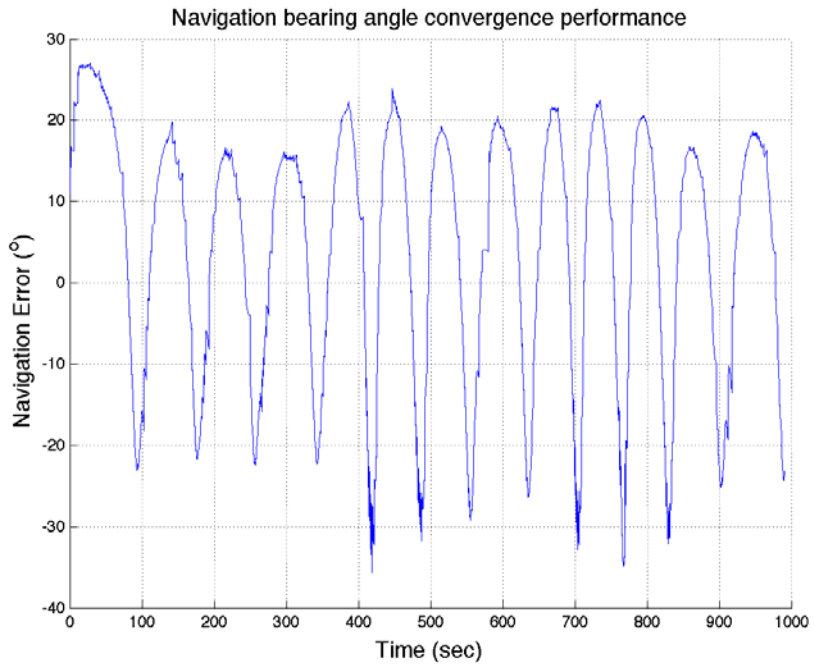
| (c) Navigation bearing error Convergence Performance |
|:---:|
| |
| (d) Gain versus Time |
| |
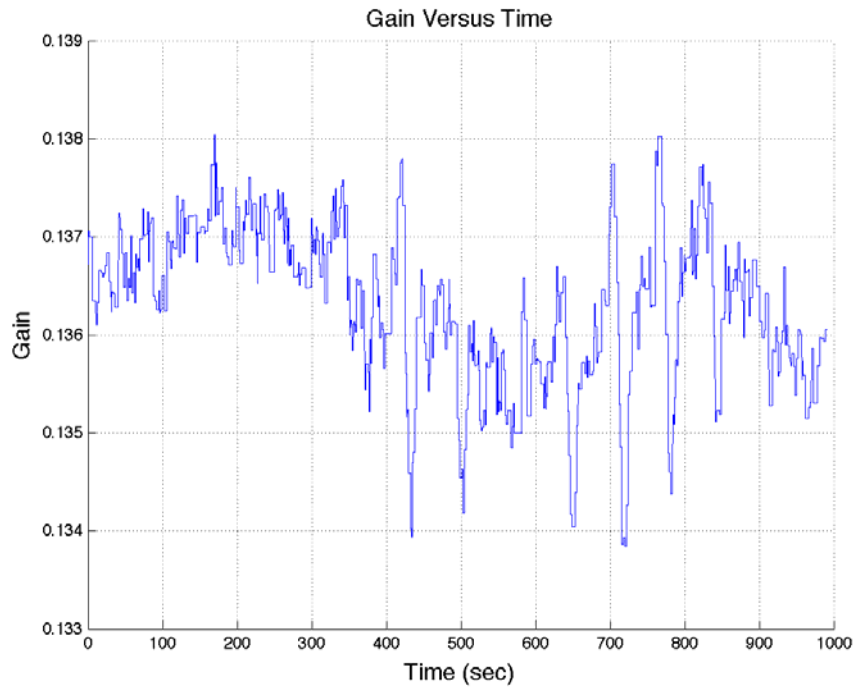
Figure 43. HIL Performance for Non-maneuvering Target, $v_t = 15$

Non-maneuvering Target Case 4: $v_t = 20$

(a) SUAV & Target Trajectory
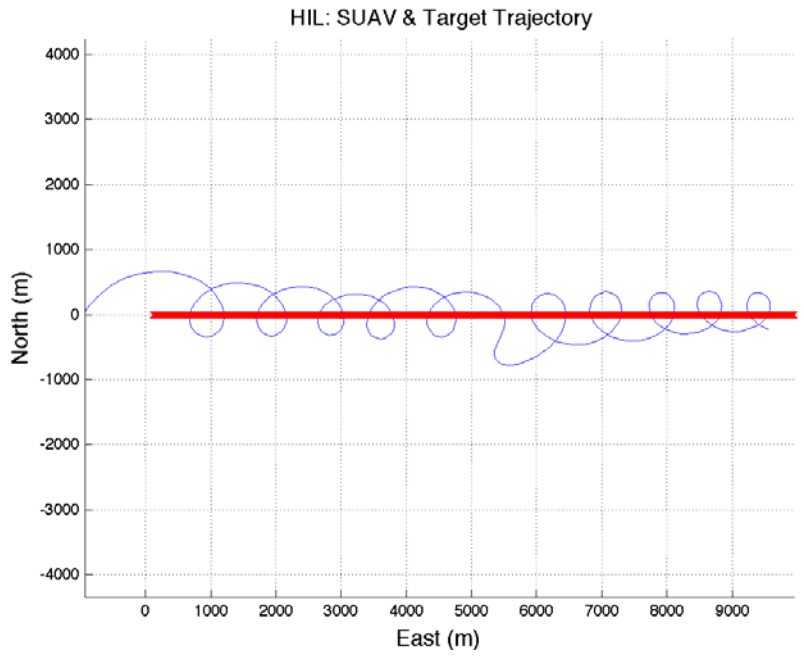
(b) Range Convergence Performance, $\rho_d = 300$
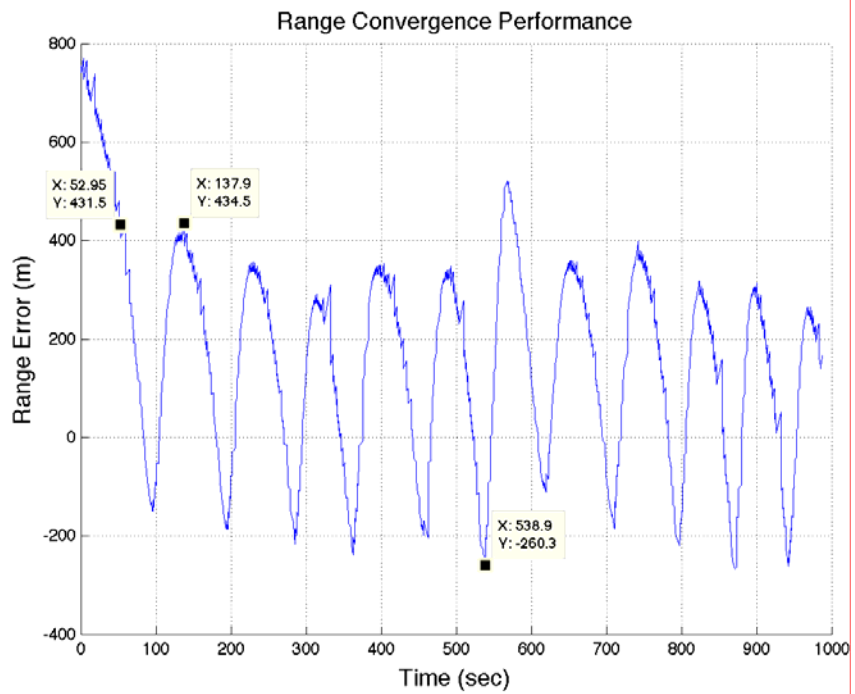
(c) Navigation bearing error Convergence Performance
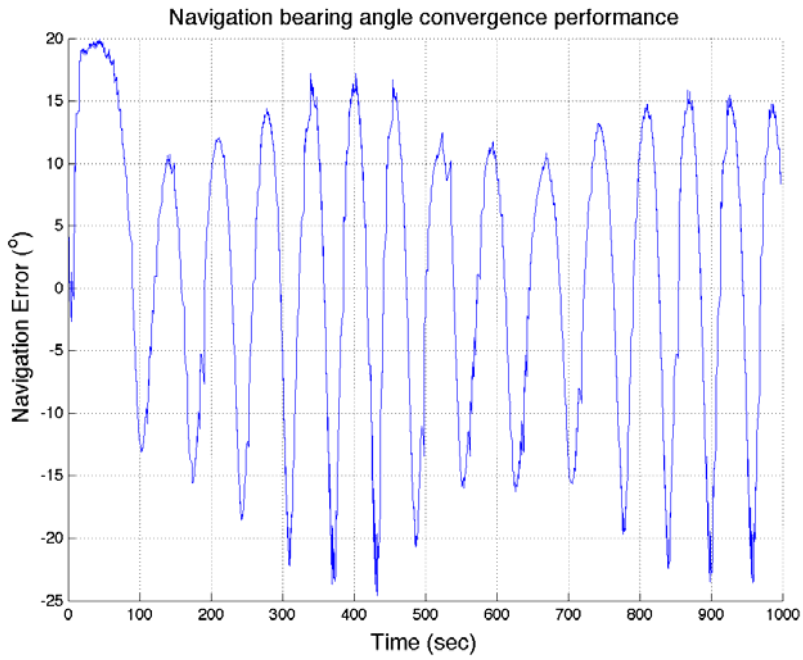
(d) Gain versus Time
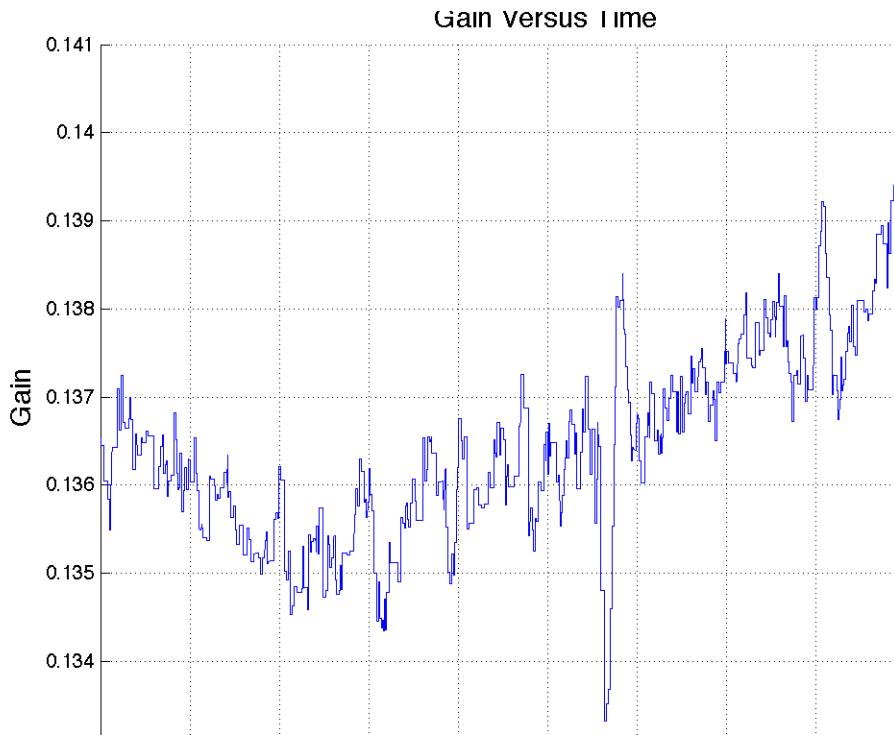

Figure 44.　　HIL Performance for Non-maneuvering Target, $v_t = 20$

APPENDIX V. PROCEDURES FOR HIL SIMULATION

Order	Procedure
1	Set up hardware as described in Chapter III
2	Run Piccolo Simulator software on computer #2. Under the 'file' tab, choose 'open aircraft'. Select Cub.txt from the folder 'Cub Model'. Under 'file' tab, choose 'load state' option. Select initial state desired.
3	On Operator PC, run the Piccolo Operator Software. Using the Futaba controller, attempt to achieve trim flight using manual mode. Once trim flight is achieved, capture trim flight on the Piccolo Operator software and click 'send'. Switch to autopilot mode on the Futaba controller.
4	From the Piccolo Operator Software, design a initial flight plan for the SUAV. The Cartesian coordinates of target and SUAV location are given in NEU coordinates with respect to the ground station. The inputs to the Operator Software have to be given in longitude, latitude and altitude. SIMULINK model in Appendix I converts from the desired longitude, latitude and altitude to NEU coordinates.
5	From the initial location and initial velocity in NEU coordinates, a 3-point flight plan can be designed. From the direction of the velocity, choose a starting point A in NEU such that vector pointing from A to the initial location is in the direction of the velocity. The XPC SIMULINK model sets the initial location as the final point of the of the flight plan. When editing the flight plan, allow the SUAV to pass through initial location i.e. without pre-turn. This can be done by selecting the 'MAP' tab on the operator software and followed by 'Edit' tab.
6	XPC SIMULINK model in Appendix I is the HIL simulation interfacing the operator PC and SUAV. This model also consist of the algorithm loaded onboard SUAV executing the variable gain control law

Order	Procedure
7	Start MATLAB 7.1. Load both XPC model and the GUI model in MATLAB environment. The GUI model for trajectory display is shown by SIMULINK model.
8	To run the XPC model, firstly Crtl+D, followed by Ctrl+B. This compiles and upload the real-time code onto the PC-104 onboard the SUAV. Select "External" and click on "Connect to Target" icon.
9	To initiate the HIL simulation at a desired point of the preset flight plan,
10	Click 'run' icon on the XPC model followed by 'run' icon on the

INITIAL DISTRIBUTION LIST

1. Defense Technical Information Center
   Ft. Belvoir, Virginia

2. Dudley Knox Library
   Naval Postgraduate School
   Monterey, California

3. Professor Vladimir Dobrokhodov
   Naval Postgraduate School
   Monterey, California

4. Professor Richard Harkins
   Naval Postgraduate School
   Monterey, California

5. Professor Anthony Healey
   Chairman, Department of Mechanical and Astronautical Engineering
   Naval Postgraduate School
   Monterey, California

6. Professor James Luscombe
   Chairman, Department of Physics
   Naval Postgraduate School
   Monterey, California

7. Lee Shay Liang
   Defence Science Technology Agency, Singapore
   Singapore